The Pennsylvania State University
The Graduate School
Eberly College of Science

DYNAMICS OF LIFE:
LARGE-SCALE SIMULATIONS
OF THE BEHAVIOR OF SMALL BODIES
IN SYSTEMS OF MULTIPLE LARGE BODIES

A Dissertation in
Astronomy & Astrophysics
by
Rachel J. Worth

Submitted in Partial Fulfillment
of the Requirements
for the Degree of

Doctor of Philosophy

December 2016

The dissertation of Rachel J. Worth was reviewed and approved* by the following:

Steinn Sigurdsson
Professor of Astronomy & Astrophysics
Dissertation Advisor, Chair of Committee

Eric Ford
Professor of Astronomy & Astrophysics

Jason Wright
Associate Professor of Astronomy & Astrophysics

Christopher House
Professor of Geosciences

Michael Eracleous
Graduate Program Chair

*Signatures are on file in the Graduate School.

Abstract

Gravity is of fundamental importance to all astronomical objects: it dictates where matter goes, and therefore what it is able to become, from superclusters of galaxies to dust around a star. While the underlying principles are straightforward, all but the simplest gravitationally bound systems quickly become chaotic and unpredictable. This is where my research resides: I am interested in how orbital dynamics affects life in the universe.

For life to exist, it first needs a place to grow; I study the formation of planetary systems to understand where habitable planets may reside and how common they are. A large fraction of all stars have stellar companions, which implies that most potential planetary systems form in multistellar systems, yet studies and models of planet formation so far have focused on systems with a single star. I study the stability of circumstellar disks and the formation of planets in environments with two or three stars, in order to better constrain which stars are appropriate targets for planet searches, in terms of both the size of planets that may form and their habitability based on location. I also explore an alternative algorithm for simulating the formation of planets from a planetesimal disk, which dramatically reduces the necessary computation time.

In addition, in order to understand how common life may be, I study lithopanspermia, the transfer of life between planets on rock fragments ejected by meteorite impacts. In order to predict how common life is, we must determine how easy it is for life to arise on a planet. This topic is entangled with transfer between planets, and by better understanding the constraints of such transfer we can better understand how common life may be.

Table of Contents

List of Figures vii

List of Tables xi

Acknowledgments xii

Chapter 1
Introduction 1
1.1 Orbital dynamics . . . 2
1.2 Orbital integrators . . . 3
1.2.1 Regular MERCURY . . . 3
1.2.2 Binary MERCURY . . . 6
1.3 Alpha Centauri system . . . 7
1.3.1 Planet Simulations . . . 8
1.3.2 Planet Searches . . . 11
1.4 Requirements for habitability . . . 12
1.5 Overview . . . 14

Chapter 2
Seeding Life on Moons of the Outer Planets via Lithopanspermia 15
2.1 Background . . . 16
2.1.1 Characterizing impacts and ejections . . . 16
2.1.2 Previous dynamical studies . . . 17
2.2 Methods . . . 19
2.2.1 Results . . . 21
2.2.2 Total rates of transfer between planets . . . 21
2.2.3 Timescales of transfers . . . 21
2.2.4 Impacts at 10-30 Myr . . . 22
2.2.5 Moon impact rates . . . 23
2.3 Discussion . . . 25

2.3.1 Correlation with initial conditions . . . 25
2.3.2 Calibrate with Mars-Earth transfer rates . . . 27
2.3.3 Estimated numbers of transfers . . . 27
2.3.4 Effects of returned material . . . 32
2.3.5 Discussion of uncertainties . . . 32
2.3.6 Area for future study . . . 34
2.4 Conclusions . . . 35
2.5 Appendix: Linear modeling . . . 36

Chapter 3
Dynamical Evolution of Alpha Centauri **38**
3.1 Introduction . . . 39
3.2 Simulations . . . 41
3.2.1 Numerical Method . . . 41
3.2.2 Stellar Mass Cases . . . 45
3.2.3 Orbital Parameters . . . 45
3.2.4 Disk Stability . . . 46
3.3 Results and Analysis . . . 47
3.3.1 Stellar System Simulations . . . 47
3.3.2 Disk Simulations . . . 51
3.3.3 Implications for Planet formation . . . 60
3.3.3.1 Planet formation: Jang-Condell Model . . . 60
3.3.3.2 Planet formation: Planetesimal Disk Simulations . 63
3.3.4 Planets around Proxima . . . 65
3.4 Conclusions . . . 65
3.5 Acknowledgments . . . 67

Chapter 4
***Audumbla*: A Semi-Numerical Planet Formation Algorithm** **71**
4.1 Introduction . . . 71
4.2 Current algorithm . . . 73
4.3 Evaluation . . . 75
4.3.1 Comparison with MERCURY planet formation . . . 76
4.3.2 Annulus test case . . . 78
4.3.3 Areas for Further Refinement . . . 79
4.4 Conclusions . . . 82

Chapter 5
Conclusion **84**
5.1 Lithopanspermia . . . 84

5.2 Planet Formation 86
5.2.1 Planets in Alpha Centauri 86
5.2.2 Proxima Centauri b 87
5.2.3 *Audumbla* 88
5.3 Final Thoughts 88

Bibliography **89**

List of Figures

2.1 Histograms showing the distribution in impact time for each location, in million-year bins. 23
2.2 The results of our moon simulations, plotted against different predictors. The lettered plot symbols identify Io, Europa, Ganymede, Callisto, and Titan by their first letter, and Enceladus is represented with an N. (a) The Liouville theorem prediction is represented by the black line. "A" is the cross-section area, "F_g" is focusing factor, and subscripts "m" and "p" indicate moon and planet, respectively. (b) A useful empirical correlation was observed between the moon-planet collision ratio and a combination of the moon and planet parameters. The x axis is the gravitational focusing factor of the moon divided by that of the planet, times the planet's Hill sphere radius divided by the square of the moon's semimajor axis. The black line is a fit to the points, with a slope of 4.8×10^9 and intercept 1.3×10^{-6}. 25
2.3 Cumulative collision rates for transfer (a) from Earth to Mars and (b) from Mars to Earth, separated by ejection velocity. 31
2.4 The percentage of ejected material returned to its planet of origin over the first million years after impact. 34

3.1 Initial (left) and final (right) parameters from 947 simulations using current stellar masses (top) and 575 simulations where all stars have masses of 0.123 $M_\odot$ (bottom). Dots in the left panels represent initial parameters for Alpha Centauri B (red) and C (blue). Large dots show simulations which survived, while small ones were disrupted. On the right, final parameters for surviving simulations are marked with large dots, with lines connecting them back to their original parameters. Faint dotted lines connect the stars to their companion from the same simulation. The shaded region shows "Proxima-like" orbits with apocenter between 10,000 and 20,000 AU, and orange rings mark system with final orbits with this separation or larger. . 48

3.2 The evolution of a representative triple star system. Inner binary system parameters are shown in red, while the outer star's orbital parameters relative to the inner binary's center of mass is shown in blue. **Top:** Points indicate semimajor axis over time, with shading extending from pericenter to apocenter. For the outer star, due to the gas potential the calculated orbit sometimes appears unbound, in which case the area from the pericenter up is shown in gray. **Middle:** System inclinations relative to the binary's initial inclination, and their difference (black). **Bottom:** Eccentricities, using same color convention. 52

3.3 (a) Minimum binary pericenter vs. final pericenter for each disk simulation. The legend indicates the simulation group, where "B2" indicates two-star simulations with a disk centered on star B, "B3" indicates a similar three-star system, etc. (b) Histogram of the inner binary's minimum pericenter in simulations which did (green) and did not (blue) produce Proxima-like systems, as a fraction of the final pericenter. 53

3.4 Disk survival for a typical early-interaction Proxima-like simulation of a disk around Alpha Centauri B, for (top) the binary, and (bottom) the triple. The presence of the third star typically removes about 1-2 AU of the disk in the equal mass case. Disk material within the truncation radius remains undisturbed. 54

3.5 Truncation radius vs. minimum pericenter. As in Fig. 3.3, "A2" indicates a two-star simulation with a disk centered on star A, etc. Red points show disk simulations centered on Alpha Centauri A, while blue are B. Circles show simulations including only the inner binary stars, while triangles contain Proxima as well. The lines show power-law fits to the points of the same color. Outlier points identified in Fig. 3.6 were excluded from this plot and the fits. Large points indicate simulations which resulted in a Proxima-like orbit. The coefficients of the fits are shown in Table 3.4. 55

3.6 (a) Truncation radius vs. minimum pericenter. The red points are considered part of the main trend, while the blue points are outliers. The black line shows the fit to all disk simulations ("Both" in Table 3.4). (b) The above data with truncation radius as a fraction of the minimum pericenter. The dotted lines show the boundaries used to exclude outliers. Two more outlying points, with pericenters close to zero and truncation radii many times larger, lie far off the vertical scale, and another two are unplottable because their p_{min} values round to zero. 56

3.7 Semimajor axis and eccentricity of objects formed in the simulations with current Alpha Centauri binary orbital parameters and $r_{tr} =$ 2.5 AU, representing the system after interactions with Proxima Centauri. The symbol size is proportional to the object's radius, and the bottom left panel shows the inner Solar System for comparison. Planets larger than $3M_{Mars}$ (0.32 $M_\oplus$) are plotted in black, and smaller objects in gray. Blue shaded region indicates the traditional conservative habitable zone. Grey shaded bars along the bottom of each plot show the original extent of the disk. The percentage by mass of the initial disk ejected or accreted onto the stars during planet formation is given on the top right. Each plot is labeled with the disk parameters in the top left, where the disk density scales with σ_0, and $\alpha = 1.5$ is the power law slope. $\alpha = 1.5$ and $\sigma_0 = 1$ is the Minimum Mass Solar Nebula. 68

3.8 Same as Fig. 3.7 but for $r_{tr} = 2.8$ AU, representing the system assuming no interaction with other stars. 69

3.9 Same as Fig. 3.9 but for $r_{tr} = 3.1$ AU. The similarity to Fig. 3.8 in planets formed and the higher ejection rates confirm that material placed beyond the truncation radius of 2.77 AU is quickly removed. 70

4.1 Graph tree representation of hierarachical merging algorithm, with the circles representing objects in the simulation. The leftmost column shows the initial disk, and each interaction moves us one column to the right, as objects are merged. 73
4.2 Direct comparison of output of *Audumbla* with MERCURY on systems with the same initial conditions. Note that the x axis is not a measure of time, but number of interactions. The time metric used by the algorithm would result in more horizontal space between interactions on the right side of the plot, as later interactions take place between increasingly widely-separated bodies. 77
4.3 Two examples of systems formed by integrating an annulus of planetesimals: (top) one with a single large central planet and several smaller ones to either side, and (bottom) one with two larger planets and fewer small ones. 80
4.4 The distributions of mass and semimajor axis of planets produced from an annulus of planetesimals in MERCURY and *Audumbla*, as described in Sect. 4.3.2. 81

List of Tables

2.1 Total Numbers and Rates of Transfer Observed in Our Simulations by Origin and Destination. 22
2.2 Characterization of the Transfer Time Distributions for Each Origin-Destination Pair 24
2.3 Number of Impacts per Object in Moon Simulations. 26
2.4 Probabilities and Estimated Viable Transfers to the Planets in the Solar System 29
2.5 Probabilities and Estimated Viable Transfers over the Past 3.5 Gyr to Some of the Moons in the Outer Solar System. 31
2.6 Probability of no transfer for each destination-origin pair 33

3.1 Simulation Regimes Used 42
3.2 Outcomes of Simulations 49
3.3 Median change in orbital parameters 49
3.4 Truncation radius model coefficients 57
3.5 Total Dust Mass in Truncated Disks (M⊕) 60
3.6 Mean number of planets per simulation 63

4.1 Definitions of the algorithm's input parameters, their default values, and units. 74

Acknowledgments

I would like to thank my advisor, Professor Steinn Sigurdsson, for his guidance throughout the long process of getting my degree. He was willing to take on a student with almost no coding experience for a computational project, which which gave me the chance to grow and was a major turning point in my career. I also thank my committee members, Professors Jason Wright, Eric Ford, and Chris House, for all of the effort they put towards making this work the strongest it could be. I am grateful to my undergraduate advisor, Professor Eric Wilcots, without whose influence I would not have gone into astronomy in the first place. Special thanks go to my parents, who encouraged me to follow my curiosity wherever it took me in life. And finally, I dedicate this work to Jesse, who supported me through all of it.

Chapter 1
Introduction

> If you wish to make an apple pie from scratch, you must first invent the universe.
>
> Carl Sagan, *Cosmos*

For generations, humanity has been asking the question, "Are we alone in the Universe?" Although there may be practical implications, for most people the drive to know is deeper than logic – humans are social animals that desire companionship, both as individuals and as a species. This desire has driven the creation of countless works of science fiction exploring possible repercusions of encounters with beings from another planet, as well as innumerable conspiracy theories from those whose desire has outstripped their need for evidence. However, with the rapid advances in the field of exoplanet detection in the last few decades, humanity is finally at a point to scientifically examine the case for life in Universe.

We are now able to put some limits on how common planets are, and as we improve our instruments and get more information on those planets, we can also constrain the frequency of worlds capable of supporting life as we know it. Size, composition, and irradiation all play significant roles in determining what conditions will be like on a given body, such as the temperature range and chemical compounds available, and whether it could support life. These properties are themselves determined by the formation of the planet and its system, which is governed by dynamics. If matter is the thread making up the fabric of the cosmos, dynamics are the weaver, putting it all into place.

All of the properties required to develop and sustain life are determined by the

dynamics of the planet's system during and after formation. The planet's size and orbit are the result of its interactions with the other mass in the system, during or after the formation of the system. Its composition is decided by that of the material it accretes during formation – different regions of the disk will contain different densities of the various elements in the disk. The composition of the disk itself is determined by that of the molecular cloud from which the star forms, and that in turn is the result of the output of stars drifting nearby, the turning of the galaxy it lies within, tracing all the way back to the cooling of the original plasma into atoms after the Big Bang at the start of the Universe.

1.1 Orbital dynamics

The origins of modern dynamics date back to the foundational works of Kepler (1619) and Newton (1687). The orbits of planets in a stable system follow Kepler's three laws of orbital motion:

1. Every orbit follows an ellipse, and the center of gravity is at one of the foci
2. A planet's motion sweeps out an equal area in equal time intervals
3. A planet's period and semimajor axis follow the Harmonic Law $\frac{P^2}{a^3} = \frac{4\pi^2}{G(M+m)}$

The motion of objects is governed more generally by Newton's Law of Universal Gravitation

$$F_g = \frac{GMm}{r^2} \tag{1.1}$$

where G is the gravitational constant (6.674×10^{-11} N (m/kg)^2). This force can be integrated to give the equation for gravitational energy, $\frac{GMm}{r}$. Orbiting planets are held in place by a balance between their momentum and the gravitational force of the object they are orbiting i.e. by the balance between their kinetic and potential energies.

When studying a system of planets orbiting a central star, we often examine each planet's orbit in the framework of a two-body problem (that planet plus the central, dominant mass), ignoring planet-planet interactions. In this context, an important concept is the specific orbital energy, or energy divided by reduced mass $\frac{Mm_i}{M+m_i}$

$$\epsilon = \frac{v^2}{2} - \frac{\mu}{r} \tag{1.2}$$

where r is the distance between the planet and star, v is their relative velocity, and

μ is $G\sum_i m_i$. The first term is the kinetic energy, second is potential. Between this and the angular momentum $\boldsymbol{h} = \boldsymbol{r} \times \boldsymbol{v}$, we can calculate the orbital properties of objects in a system

$$a = -\frac{\mu}{2\epsilon} \tag{1.3}$$

$$e = \sqrt{1 + \frac{2\epsilon h^2}{\mu^2}} \tag{1.4}$$

$$i = \arccos\left(\frac{h_z}{|\boldsymbol{h}|}\right) \tag{1.5}$$

While not every dynamical situation can be represented in orbital element format, they provide a valuable framework in which many astronomical situations can be examined.

Another frequently-used dynamical concept which will be used frequently in this work is the Hill radius, R_H. This is the radius of the Hill sphere, the region around an orbiting object which is dominated by the gravitational influence of that object, rather than that of the central body. The equation for the Hill radius is

$$R_H = a(1-e)\sqrt[3]{\frac{m}{3M}} \tag{1.6}$$

1.2 Orbital integrators

1.2.1 Regular MERCURY

The simulations presented in Chapters 2 and 3 use the MERCURY hybrid symplectic integrator Chambers (1999, 2012). Symplectic integrators are good for collisionless systems because, as long as objects are well-separated, they exactly conserve energy (on average, within roundoff errors) making them reliable over long times (Sanz-Serna, 1992), and also take much less computational time. MERCURY takes advantage of the fast and energy-conserving nature of symplectic integrators, while alleviating their weakness of inaccuracy in close encounters by employing a slower integrator when needed. MERCURY builds on SWIFT (Levison & Duncan, 1994, 2013) and SYMBA (Duncan et al., 1998), and all of them are grounded in the N-body symplectic mapping of Wisdom & Holman (1991). MERCURY also employs mixed-center or democratic heliocentric coordinates, which combine heliocentric

coordinates with barycentric velocities.

While in hybrid mode, the integrator will proceed using the symplectic integrator, advancing with fixed timestep τ, checking for close encounters between objects at each timestep. A close encounter is defined as two objects approaching within a certain critical distance of one another. If both objects are large, the Hill radius R_H can be used to scale the threshold as $n_1 R_H$, where $n_1 = 3$ is the recommended value. However, for smaller bodies the Hill radius may be small compared to the maximum distance traveled per timestep, τv_{max}, where v_{max} is the object's highest velocity during that timestep. This value will be scaled by some other coefficient n_2, so the critical distance is the larger of $n_1 R_H$ and $n_2 \tau v_{max}$. If two objects come within the critical distance of each other, a close encounter occurs, and the algorithm switches to Bulirsch-Stoer (Stoer & Bulirsch, 1980) to integrate that interaction, which is a slower, variable-timestep method, but it is accurate during close encounters where symplectic integrators are not.

The following is an overview of the symplectic integrator used in MERCURY, based on the more complete derivation given by Chambers (1999). Symplectic integrators take advantage of the symplecticness of the Hamiltonian $\mathcal{H}$. For orbital mechanics problems, $\mathcal{H}$ is the sum of the kinetic ($T(\boldsymbol{p}) = \frac{p^2}{2m}$) and potential ($V(\boldsymbol{x}) = \frac{GMm}{r}$) energies of all N objects in the system at time t. For each object i in the system, m_i is its mass, x_i is its position, p_i is its momentum, and r_{ij} is its separation from object j. The vector $\boldsymbol{x}$ contains all the positions x_i, and $\boldsymbol{p}$ contains the momenta.

$$\mathcal{H} = \mathcal{H}(\boldsymbol{x}, \boldsymbol{p}, t) \tag{1.7}$$

$$\mathcal{H} = \sum_{i=1}^{N} \frac{p_i^2}{2m_i} - G \sum_{i=1}^{N} m_i \sum_{j=1+1}^{N} \frac{m_j}{r_{ij}} \tag{1.8}$$

For a closed system with no friction or other dissipative forces, this quantity will be conserved over time, as energy is passed back and forth among the kinetic and potential terms. In order to calculate the movement of an object in the system as time advantaces, the integrator must solve the system of equations

$$\frac{\mathrm{d}\boldsymbol{p}}{\mathrm{d}t} = -\frac{\mathrm{d}\mathcal{H}}{\mathrm{d}\boldsymbol{x}}, \frac{\mathrm{d}\boldsymbol{x}}{\mathrm{d}t} = +\frac{\mathrm{d}\mathcal{H}}{\mathrm{d}\boldsymbol{p}}. \tag{1.9}$$

That solution will be of the form

$$q(t) = e^{\tau F} q(t - \tau) \tag{1.10}$$

where $q(t)$ is some quantity of the system at time t (can be x, p, or a combination), τ is an earlier time, and F is an operator such that

$$\frac{\mathrm{d}q}{\mathrm{d}t} = Fq \tag{1.11}$$

To simplify the solution of this system, $\mathcal{H}$ and the operator F can be separated into three pieces $\mathcal{H}_A + \mathcal{H}_B + \mathcal{H}_C$ and $A + B + C$. The solution in Eqn. 1.10 then becomes

$$q(t) = e^{\tau(A+B+C)} q(t - \tau). \tag{1.12}$$

which can be approximated to second order as

$$q(t) = e^{\tau B/2} e^{\tau C/2} e^{\tau A} e^{\tau C/2} e^{\tau B/2} q(t - \tau). \tag{1.13}$$

For a case in which the central body with subscript 0 dominates, using democratic heliocentric coordinates allows $\mathcal{H}$ to be separated into pieces as follows:

$$\mathcal{H}_A = \sum_{i=1}^{N} \Big(\frac{p_i^2}{2m_i} - \frac{G m_0 m_i}{r_{i0}} \Big) \tag{1.14}$$

$$\mathcal{H}_B = -G \sum_{i=1}^{N} \sum_{j=1+1}^{N} \frac{m_i m_j}{r_{ij}} \tag{1.15}$$

$$\mathcal{H}_C = \frac{1}{2m_0} \Big(\sum_{i=1}^{N} p_i \Big)^2. \tag{1.16}$$

N indicates all bodies except for the central one. Each of these three terms can now be solved independently of the others. H_A contains the unperturbed Keplerian motion of each of the bodies orbiting the central body. H_B contains the cross-terms, i.e. the non-central bodies' influences on each other. A third term H_C is also necessary, which contains terms arising from the central body's kinetic energy.

As long as all bodies are well-separated, $\mathcal{H}_A \gg \mathcal{H}_B$, $\mathcal{H}_A \gg \mathcal{H}_C$, and the error is $O(\epsilon \tau^3)$, where $\epsilon = \sum m_i / m_\odot$. However, as r_{ij} becomes small, $\mathcal{H}_B$ becomes large. To work around this problem, Chambers (1999) re-partitions the energy in a way

that keeps $H_B \ll H_A$ even during close encounters, by choosing a function $K(r)$ where $K \to 0$ when $r \to 0$ and $K = 1$ when for large r. Then

$$\mathcal{H}_A = \sum_{i=1}^{N} \Big(\frac{p_i^2}{2m_i} - \frac{G m_0 m_i}{r_{i0}} \Big) - G \sum_{i=1}^{N} \sum_{j=1+1}^{N} \frac{m_i m_j}{r_{ij}} \Big[1 - K(r_{ij}) \Big] \tag{1.17}$$

$$\mathcal{H}_B = -G \sum_{i=1}^{N} \sum_{j=1+1}^{N} \frac{m_i m_j}{r_{ij}} K(r_{ij}) \tag{1.18}$$

$$\mathcal{H}_C = \frac{1}{2m_0} \Big(\sum_{i=1}^{N} p_i \Big)^2. \tag{1.19}$$

Now we still have $\mathcal{H} = \mathcal{H}_A + \mathcal{H}_B + \mathcal{H}_C$, but $\mathcal{H}_A \gg \mathcal{H}_B$ remains true during close encounters as well and accuracy is not degraded. When objects are well separated and $K(r)$ goes to zero, the equations are unchanged and remain easy to solve quickly. However, at timesteps where $K(r_{ij})$ is nonzero, $\mathcal{H}$ ceases to be solvable and must be numerically integrated to high accuracy, which is where the Bulirsch-Stoer integrator is used.

1.2.2 Binary MERCURY

For Chapter 3, we are examining a binary system rather than one with a single central body. The above assumptions that $H_A \gg H_B$ and H_C is violated when the summations include the companion in a binary, which will have a mass and momentum similar to that of the central body. Therefore, the standard version of MERCURY cannot be used for binary systems . A modified version of MERCURY exists (Chambers et al., 2002) with two new modes for integrating either close or wide binaries.

In the wide-binary case, two widely separated stars A and B orbit one another while a system of N planets orbits one of the stars. A new coordinate system is defined in which the primary star is at the origin and planetary objects' positions are measured relative to the primary star, while the companion star's position is relative to the center of mass of all objects except itself. The Hamiltonian is partitioned into three pieces $\mathcal{H}_{Kep} + \mathcal{H}_{int} + \mathcal{H}_{jump}$, which represent Keplerian motion of the binary, interactions between planets or from the companion star, and indirect correction terms, respectively. In order to address close encounters, the interaction terms are once again repartitioned between H_{Kep} and H_{int} similar to the $K(r)$

function in Eqn. 1.18. The integrator then advances in five substeps per step, as in Eqn. 1.13. The error is order $O(\epsilon\tau^3)$ where τ is the timestep and ϵ is the larger of $|H_{int}/H_{Kep}|$ or $|H_{jump}/H_{Kep}|$.

For close binaries, in which planetary objects orbit around the binary pair, the same Hamiltonian applies. The coordinate system once again puts the primary star at the origin, but now the planetary orbits are with respect to the center of mass of the binary, and the secondary star's coordinates are relative to the primary. The Hamiltonian is split into basically the same three terms, but partitioned slightly differently: K_{int} includes perturbations on the planets due to the binary's higher order moments as well as the planets' interactions. Also, since the binary's orbit is smaller than that of the planets', each timestep in the planets' integration is subdivided into N_{bin} sub-steps for the binary, where N_{bin} is roughly equal to the ratio of the orbital period of the innermost planet to that of the binary. Each of the Hamiltonian pieces H_{Kep} and H_{int} are split further, into sections that involve the binary (e.g. $H_{B,Kep}$) and those that only involve the planets ($H_{P,Kep}$).

1.3 Alpha Centauri system

In Chapter 3 I will examine the formation of planets within multistellar environments, with the nearby Alpha Centauri triple as an example case. The simulations are broken down into three regimes here: first, examining complex three-body interactions the stars may have had early in their lives; then, the disturbance of test particle disks around the stars while they undergo said interactions; and finally, the formation of planets from disks disturbed in this way.

Because of its proximity at 1.3 pc, as well as the similarities between Alpha Centauri A and B to our own Sun, Alpha Centauri has been a subject of much interest in the exoplanet community. The system consists of a binary of two Sun-like stars, Alpha Centauri A and B. With masses 1.105 and .934 $M_\odot$ respectively (Pourbaix et al., 2002) and ages of approximately 5 Gyr, as well as the increased observing potential given their proximity, these stars have long held special interest as potential habitable planet hosts. However, their orbital parameters ($P = 80$ years, $a = 23.4$ AU, $e = 0.519$) put them near the limit of binary systems able to form inner planets (Jang-Condell, 2015).

The binary is orbited by an extremely distant and much smaller M dwarf

star, Proxima Centauri. Whether Proxima is in fact bound to the system is still somewhat of an open question: Matthews & Gilmore (1993) attempted to explain a positive energy result by claiming the stellar mass measurements were too low, while Anosova et al. (1994) concluded that it was not, in fact, bound. The latter conclusion is unsettling to many, given that it is unlikely for unbound stars to randomly pass so close together and with such low relative velocities – the probability is less than 10^{-6} (Matthews & Gilmore, 1993) – so they conclude the three stars are part of a stellar moving group.

In Wertheimer & Laughlin (2006), the question of stability is examined with Monte Carlo simulations. Observational information on the stars is not perfectly precise, so they calculate the total energy for the system (treating the binary as a single mass) for a suite of configurations with the mass and RVs drawn from the possible values. They perform these calculations first with the data used by Anosova et al. (1994), reaching the same conclusion as that group, then again with the more accurate *Hipparcos* data (Perryman et al., 1997), as well as non-public data, and find that the energy is consistent with zero given the errors, and the probability of being unbound $P = 0.55$. This does not conclusively prove whether the system is bound or not, though combining this information with the probability of this configuration occurring randomly in nature for an unbound system tips the balance in favor of it being bound.

If it is bound, its separation of about 15,000 AU means the system is larger than the molecular cloud cores stellar systems form from. However, a plausible formation scenario was proposed by Reipurth & Mikkola (2012) in which the third star initially formed much closer in (within a few hundred AU), and as the gas cloud dispersed, the three-body interactions resulted in the third star being thrown out to its current distant orbit before it had finished accreting, also explaining its lower mass.

1.3.1 Planet Simulations

Several studies have been performed examining planet stability and formation within the Alpha Centauri binary, ignoring Proxima's ifluence. Wiegert & Holman (1997) located orbits within Alpha Centauri in which a planet could remain stable by simulating test particle stability over about 2.8 Myrs (300,000 orbits) are examined

across a grid of possible semimajor axis and inclination values, using the Wisdom & Holman (1991) N-body symplectic mapping technique. They found stability regions for particles up to a few AU from their star, as long as they were not too strongly inclined to the binary's orbit – the outermost stable orbit was reduced the closer particles got to 90°, and no stability was seen for particles between 75° and 105°. Prograde orbits (i approaching 90°) remained stable to $a \approx 3$ AU, and for retrograde orbits a went up to about 4 AU. Most non-stable objects were removed from the simulation by the end, either by ejection or a close encounter with the companion star.

The same authors then study the more general case of stability regions within binaries in Holman & Wiegert (1999). The simulations this time explore a range of mass ratios and eccentricities, using both the Wisdom & Holman (1991) symplectic mapping method again, as well as a conventional Bulirsch-Stoer integrator in regions where forces from the two stars are comparable. They consider the critical semimajor axis a_c, the outermost stable orbit, as a fraction of the binary's semimajor axis a_b, and for approximately Alpha Centauri's values they predict $a_c = 0.12$. This and a previous work (Rabl & Dvorak, 1988) derived a formula for a_c as a fraction of a_b as a second-order polynomial in eccentricity e and, in the former, mass ratio μ as well. The equation from Holman & Wiegert (1999) (slightly reformatted and with uncertainties omitted for readablity, though they can be found in the original papers) is

$$\frac{a_c}{a_b} = 0.464 - 0.631e + 0.150e^2 - 0.380\mu + 0.586\mu e - 0.198\mu e^2. \tag{1.20}$$

Below we have eqn. 1.20 with $\mu = 0.5$, followed by the comparable equation from Rabl & Dvorak (1988).

$$\frac{a_c}{a_b} = (0.274 \pm 0.008) - (0.338 \pm 0.045)e + (0.051 \pm 0.055)e^2 \tag{1.21}$$

$$\frac{a_c}{a_b} = (0.262 \pm 0.006) - (0.254 \pm 0.017)e - (0.060 \pm 0.027)e^2 \tag{1.22}$$

The two are almost consistent within errors, though the latter paper shows a steeper decline with e. For Alpha Centauri, with $e = 0.519$ and approximating μ as 0.5, the above two equations predict $a_c = 0.112$ and $0.114a_b$ respectively.

Another work (Benest, 1988) examined the same question for the case of a few

specific systems, including Alpha Centauri. He finds significantly higher stability limits of $a_c = 0.23a_b$ and $0.15a_b$ for Alpha Centauri A and B, respectively. The above two studies use simulation lengths of 300 and 10,000 binary orbits (about 24,000 and 800,000 years), while this one uses 100 orbits (8,000 years), so it is the shortest of the three, but based on the lifetimes of the unstable particles in Holman & Wiegert (1999) this does not fully account for the discrepancy.

Two studies of planet formation around Alpha Centauri using MERCURY were published in short succession: Barbieri et al. (2002), using the original version, and Quintana et al. (2002) using the binary version. Both conclude that planetary growth in the final stages, from planetary embryos to planets, can proceed in the inner ~ 2.5 AU nearest the star. Another paper (Guedes et al., 2008) found consistent results and also determines that for planets in the Habitable Zone which are at least 1.8 $M_\oplus$, they should be within RV detectability limits.

Earlier stages of planet formation may be more affected by the presence of a binary companion than the final planetary embryo stage. Marzari & Scholl (2000) examined the accretion of smaller (~ 1 km) planetesimals with one another to form planetary embryos. The interaction of dynamic stirring from the companion with damping from the gas disk results in orbital phasing, with higher-mass objects grouped in higher-eccentricity orbits at a given semimajor axis, resulting in relative velocities Δv which depend strongly on how similar the mass of two colliding objects are. This phasing results in particularly low Δv and enhanced accretion for equal-mass objects such as those used in Marzari & Scholl (2000). However, Thébault et al. (2008) and Thébault et al. (2009), which examine Alpha Centauri A and B respectively, find that when collisions between objects with a range of sizes are considered, orbital phasing instead increases the relative velocities for all but equal-sized objects and ultimately results in more erosive than accretional impacts in the region beyond ~ 0.5 AU from the star. This remains important for objects of ~ 10 km or less, where the impacts are more likely to be destructive because small planetesimals are more easily damaged and the objects' lower escape velocities make it easier for them to loser material during impact.

However, since many planets have been discovered in binary systems, there must be a way for accretion to continue in spite of these effects. (Rafikov & Silsbee, 2015b) assert that planet formation in tight binaries is possible if the disk is sufficiently massive and non-eccentric. The total mass that can be expected in protoplanetary

disks is still uncertain, making it unclear how common a pathway to formation this might be. Thébault et al. (2008) and Thébault et al. (2009) discuss a few possible explanations, one of which is that the planetesimals are re-phased during the dispersal of the gas disk, and objects of all sizes are driven towards orbits with the same eccentricity at a given semimajor axis, lowering their relative velocities. Thébault et al. (2008) concluded that planetary embryo formation was still unlikely. Close to the star, inward drag during this period would be significant enough to remove most small planetesimals (< 4 km) from the system, and further away small planetesimals could remain but the rephasing effect would only be partial, and the objects would first have to survive a hostile, eroding period during the dispersal. Xie et al. (2010) explore this effect, and find that in 1-2 AU range, the planetesimal collision timescale increases with inclination, from $\sim 10^3$ to 10^6 yrs. They conclude that accretion of terrestrial planets is possible on slow timescales, after the dissipation of the gas disk. This of course makes gaseous planets unlikely, but allows for terrestrial planets.

A possible route to planetary embryo formation which is particularly relevant to my work is a wider past orbit for the binary due to multistellar interactions. Thébault et al. (2009) determine that, with Alpha Centauri's semimajor axis of 23.4 AU, an eccentricity of roughly 0.25 or less would allow for perturbed accretion in the Habitable Zone. Large objects are able to remain in stable orbits around the binary in its current configuration, so if Alpha Centauri's orbit was initially wide, and stayed that large for long enough enough to form planetary embryos, planet formation could still proceed from those embryos even after the binary orbit shrank.

1.3.2 Planet Searches

Alpha Centauri has been the focus of numerous planet searches (e.g. Endl et al. (2015)) which have been sensitive enough to conclusively rule out the presence of any giant planets in the system. A terrestrial planet around Alpha Centauri B was claimed (Dumusque et al., 2012) but subsequent studies refute its existence (Hatzes, 2013; Rajpaul et al., 2016). It is still possible that undetected terrestrial planets exist around Alpha Centauri A or B, given current observational sensitivity.

Recently, Anglada-Escudé et al. (2016) reported a planet in orbit around

Proxima Centauri. Discovered via radial velocity (RV) observations, the planet has a minimum mass of 1.3 $M_\oplus$ and a period of approximately 11.2 days which, based on the low insolation from its M dwarf host, puts it at a distance from its star such that it may be able to sustain liquid water on the surface. The discovery is based on a combination of HARPS and UVES observations, particularly HARPS observations obtained during the recent *Pale Red Dot* campaign.

As Proxima is the closest star to our Solar System, Proxima b is the closest planet we can ever expect to find, making this a historically significant discovery. As such, it has aroused considerable interest from the science community. Already discussion is underway about the possibility of directy detecting atmospheric signatures from the planet (Lovis et al., 2016). There is also considerable speculation regarding the potential habitability of the planet (Barnes et al., 2016; Meadows et al., 2016; Ribas et al., 2016; Turbet et al., 2016) and formation (Coleman et al., 2016).

1.4 Requirements for habitability

Along with fiction and speculation about life beyond Earth, we now have substantial and ever-increasing scientific knowledge about the subject. Thanks to NASA's Kepler mission and the rest of the exoplanet observation field, we know of thousands of planets; however, in most cases we have very little information characterizing individual planets. We may know the size of the planet – either mass, radius or, if we're lucky, both – and commonly have a sense of its irradiation level. But this is still a long way from understanding actual surface conditions like temperature, availability of water and nourishment, and protection from harm such as damaging radiation. As we know from our experiences on Earth, lifeforms are strongly affected by subtle changes to their planet that often come from terrestrial sources, rather than astronomical ones. Atmospheric and surface conditions are interconnected in a complex feedback loop, so the state on the surface cannot be predicted in detail based on only the major external characteristics.

What we believe about habitability comes primarily from observations of our own planet, and to a lesser extent those of our Solar System. Our planet shows us one example of life and its requirements. In the absence of a larger dataset, we extrapolate to other planets with the assumption that our particular case is representative. Below is a brief overview of life's requirements as we understand

them.

We expect that life requires liquid water, thus putting limits on the allowed temperature and pressure conditions and setting boundaries on the Habitable Zone (HZ), the region around a star where a terrestrial planet may be habitable (Kasting et al., 1993). The outer edge of the habitable zone is where a planet becomes too far from its star and freezes, possibly locking into a state like Snowball Earth, in which the ice covering the surface raises the planet's albedo, further lowering the temperature and making it harder for the planet to escape this state once reached (Hoffman et al., 1998). At the inner edge of the HZ, the oceans evaporate. Since water also acts as a greenhouse gas, preventing heat from escaping back into space, a runaway greenhouse effect occurs, heating a planet above habitable temperatures. Thus, the requirement for liquid water determines the orbits around a star where a habitable planet may be found.

The mass of a planet is also important. Life on Earth seems to depend on either a solid or liquid medium to live on or in, which we expect means a planet must be terrestrial to have a physically stable enough environment for organisms to develop, putting an upper bound on allowable planet size – large planets accrete more atmosphere and become gaseous giant planets. A planet which is too small, on the other hand, would make it difficult to develop life as well. Smaller planets cool more quickly because of a higher surface area to volume ratio, resulting in cold, static interiors. With no rotating iron core, they lack magnetic fields to protect the atmosphere from being driven off by solar winds. This atmospheric loss is further hastened by the planet's lower escape velocity.

All life on Earth has genetic material which controls how it grows and evolves. This material comes in the form of large, complex DNA or RNA molecules, and their structural integrity can be damaged by UV or higher-energy radiation. Although some damage can be repaired, and the process of evolution takes advantage of some amount of mutation, too much will kill an organism quickly. Earth's Sun produces significant amounts of UV radiation, but most of it is blocked by Earth's atmosphere before reaching the ground. The surface is also protected from damaging cosmic rays by our magnetic field, generated by a rotating iron core.

1.5 Overview

In order to understand the likelihood of life beyond our planet, we must understand which conditions allow for it, and where those conditions can be found. In this work, I examine the planetary formation processes which lead to the creation of habitable environments (Chapters 3 and 4) as well as processes which can spread life from one habitable environment to another (Chapter 2). Both have important implications for the abundance of life in our Universe, as well as in how best we should search for it.

Chapter 2
Seeding Life on Moons of the Outer Planets via Lithopanspermia

[Note: this chapter is an expanded version of Worth et al. (2013). The primary difference is the addition of Table 2.6 and some discussion of recent discoveries of water plumes on Europa. As first author, I ran the simulations, analyzed the data, and wrote the paper, with feedback and editing from my co-authors Profs. Sigurdsson and House.]

Material from the surface of a planet can be ejected into space by a large impact and could carry primitive lifeforms with it. We performed N-body simulations of such ejecta to determine where in the Solar System rock from Earth and Mars may end up. We found that, in addition to frequent transfer of material among the terrestrial planets, transfer of material from Earth and Mars to the moons of Jupiter and Saturn is also possible, but rare. We expect that such transfers were most likely to occur during the Late Heavy Bombardment or during the ensuing 1-2 billion years. At this time, the icy moons were warmer and likely had little or no ice shell to prevent meteorites from reaching their liquid interiors. We also note significant rates of reimpact in the first million years after ejection. This could reseed life on a planet after partial or complete sterilization by a large impact, which would aid the survival of early life during the Late Heavy Bombardment.

2.1 Background

Panspermia is the hypothesis that life can be spread between planets and planetary systems. One class of panspermia is lithopanspermia, in which pieces of rock are the mechanism for dispersal (Melosh, 1988; Tobias & Todd, 1974). Rock fragments can be ejected from an inhabited planet's surface via large meteor impact. This ejected material can then travel through space and may land on another planet or moon, as we have seen in identified meteorites from Mars found on Earth (Bogard & Johnson, 1983; Carr et al., 1985) . If an ejected rock encases sufficiently resilient organisms, life could be seeded on its destination planet or moon.

2.1.1 Characterizing impacts and ejections

Of the over 53,000 meteorites found on Earth, 105 have been identified as martian in origin (The Meteoritical Society, 2012*). The oldest of these observed falling to Earth is dated from 1815, though many have been discovered after falling. Some of our samples are compositionally similar and may have come from a common impact. The entire collection of martian meteorites represents at least four impacts on Mars (Nyquist et al., 2001).

One of these meteorites, Allan Hills 84001 (ALH 84001), was initially claimed to contain evidence of life in the form of polyaromatic hydrocarbons, carbon globules, magnetite crystals, and fossilized nanobacteria (McKay et al., 1996). This claim sparked recent investigation into quantifying and characterizing lithopanspermia. Each of the claimed biomarkers has been shown to be reproducible inorganically (see Martel et al. (2012), for a review and references therein for specific counterarguments, e.g., Benzerara et al. (2003); Cisar et al. (2000); Golden et al. (2004). Despite the lack of hard evidence for life existing in any of the transferred rocks, the debate motivated a number of important studies of the process of lithopanspermia, which will be discussed below.

It is known that rock can be exchanged between planets; therefore, if life can survive the transfer, it is probable that life from Earth has already been brought to other planets. Also, it is theorized that Mars may have been habitable during the Noachian period, when the young planet is thought to have been warm and wet (McKay et al., 1992). Carbonates in the Allan Hills meteorite mentioned above

precipitated in a fluid of 18°C about 4 billion years (Gyr) ago, when the planets were only 500 million years (Myr) old (Halevy et al., 2011). Early Mars appears to have been warm and wet, which would have provided prime conditions for the development of life. Thus, life from Earth or Mars could have been brought to other planets in the Solar System, and any habitable niches may continue to harbor descendants of such life. It is even possible that life on Earth originated on Mars (McKay et al., 1996).

2.1.2 Previous dynamical studies

For decades, astronomers have been attempting to model the dynamics of ejected rocks migrating about the Solar System, but technological limitations have always restricted the scope of such simulations. Early studies used Arnold-Öpik integrators (Melosh & Tonks, 1993). These methods underestimated the amount of interplanetary exchange and overestimated the timescale of transfer because they did not include secular effects, in which the resonance of precession frequencies causes increases in eccentricity and inclination in small bodies on timescales of millions of years. Without these effects, transfer between Earth and Mars was still observed, but it took place very slowly, transferring only a few percent of ejecta over 150 Myr.

Subsequent studies were conducted by Gladman & Burns (1996), Gladman et al. (1996), and Gladman (1997). Their use of symplectic integrators improves accuracy and greatly increases the speed at which interplanetary transfer occurs in the simulations. The difference between methods is discussed in more detail in the work of Dones et al. (1999), but in brief, the inclusion of secular effects results in gradual eccentricity increases, which causes objects initially originating from and orbiting near one planet to eventually cross the orbit of another within timescales of a few million years.

At this point, the meteoroid may impact the other planet or be scattered into many possible new orbits. Comparing transfer times at different ejection velocities with the ages of collected meteorites, Gladman et al. (1996) determined that most rocks are ejected at velocities just above the escape velocity. Additionally, they found that most transfer between planets occurs on the timescale of < 10 Myr, after which most remaining meteoroids ultimately fall into the Sun. The Gladman

studies included all the planets from Venus through Neptune, and particles were considered ejected from the Solar System if they went beyond 100 AU from the Sun. No collisions with the outer planets or moons were observed, due to the relatively small number of objects in the simulations.

Gladman (1997) found that some objects were held within the asteroid belt between Mars and Jupiter by secular resonances for millions of years. This timescale is sufficient for these objects to be collisionally destroyed, which reduces interplanetary transfer by a small amount. However, most rocks subjected to this fate were long-lived (>10 Myr) objects that would have ultimately ended up in the Sun and thus are not significant to our study.

A comprehensive, multidisciplinary study of transfer between Earth and Mars (Mileikowsky et al., 2000) combined studies of ejection rates, dynamical transfer, biological survival requirements, and impact physics to determine the amount of viable biological material transferred between Earth and Mars. Survivability constraints are based on the microbe species *Bacillus subtilis* and *Deinococcus radiodurans R1*. The authors calculated the number of rock fragments ejected that satisfy two survivability criteria: remaining below 100°C through the ejection and being large enough to shield microbes from the harms of a space environment for the duration of travel. They estimate that a rock of 3 m across shields D. radiodurans for 10 Myr and B. subtilis for 3.3 Myr.

Mileikowsky et al. (2000) estimated the total number of ejected fragments from Earth and Mars over the roughly 4 Gyr since life arose on Earth. To update these values, we repeated their calculations using updated cratering rates (Ivanov & Hartmann, 2007) to estimate the numbers of viable fragments ejected. We found that, over the last 3.5 Gyr, approximately 3×10^8 suitable fragments have been ejected from Earth and 6×10^8 from Mars. Gladman et al. (2005) performed simulations in which 36,000 particles were ejected from Earth with v_∞ (residual velocity, or velocity when the object is an infinite distance from other bodies) from 0.67 to 12.41 km/s and integrated over 30 thousand years (30 kyr). Residual velocity is defined as

$$v_\infty^2 = v_{ej}^2 - v_{esc}^2 \tag{2.1}$$

where v_{ej} is the ejection velocity relative to the planet, and v_{esc} is the escape velocity $v_{esc}^2 = 2GM_{planet}/r$.

The authors found transfer to Venus (0.1%), back to Earth (1%), and to Mars

(0.001%) in the 30 kyr of this study, which represents only the very beginning of our time frame. Gladman et al. (2006) made use of technological improvements to expand the scope of their simulations. Using 18,000 particles in orbits evolved over 5 Myr, with v_∞ of 5-10 km/s, they used the number of flybys to extrapolate the number of collisions that might occur on Titan and Europa and conclude that the rate of transfer would be on order of 10 objects per 600 million ejected, or roughly 10^{-6}%.

A more recent study (Reyes-Ruiz et al., 2012) built on the foundations of Gladman et al. (2005), again studying high-velocity ejections from Earth on shorter timescales (30 kyr). They found some transfer to Jupiter but only at very high ejection velocities ($v_\infty = 9.64$ and 12.1 km/s). The velocities used here and by Gladman et al. (2006) are significantly higher than what Gladman et al. (1996) predicted to be typical but result in faster transfer and thus less expensive simulations.

2.2 Methods

Using the hybrid symplectic integrator in MERCURY (Chambers, 1999), we simulated the ejection of tens of thousands of meteoroids from both Earth and Mars. Because they are so much smaller than the other bodies, the meteoroids were treated as test particles with no gravitational influence on one another or on the planets in the system. The program integrated over 10 Myr, with one-day time steps. All eight planets were included in the simulations. The inputs for the simulations were the positions and motions of the planets of the Solar System – taken from the Jet Propulsion Laboratory (2013) online ephemerides system HORIZONS (JPL) – and positions and motions of the meteoroids. The meteoroids were placed at a distance near one Hill radius R_H away from their planet of origin at randomly generated angles, thus covering the surface of the Hill sphere centered on the planet, where $R_H \approx a(\frac{M_{planet}}{3M_\odot})^{1/3}$. For Earth, objects were placed at 2×10^{11} cm or 360 Earth radii $R_\oplus$, while for Mars the distance was 1×10^{11} cm or 300 Mars radii R_{Mars}.

To simulate ejection, the ejected rocks were given the origin planet's orbital velocity, plus a strictly radial ejection velocity vector varying randomly between 1 and 3 times the escape velocity from the planet at that location.

$$v_{ej} = v_{orb,pl} + [1,3] * v_{esc,pl} \tag{2.2}$$

At these distances, escape velocities are 0.58 km/s for Earth and 0.28 km/s for Mars. The residual velocity v_∞ ranges from almost zero to a maximum of 1.6 km/s for Earth and 0.78 km/s for Mars. The flat distribution of velocities over this range does not represent a natural distribution that would result from a given impact but allows us to explore potential dependencies of impacts on the initial velocity across a range of energies. Moons were not included in the main simulations, as they are near enough to their host planets to be considered close encounters by the integrator, thus continuously triggering the switch to the non-symplectic integrator, which is an order of magnitude slower. To estimate impact on moons for ejecta on orbits with essentially random orbital phases, rates can be estimated from the geometric projected area of the target moon, corrected for gravitational focusing, an effective application of Liouville's theorem, as noted by Melosh (2003). It is possible that impact rates can be enhanced by ejecta being captured into orbits bound to the planet and going through multiple passes through the system of moons on chaotically resonant orbits, a phenomenon well known in 3-body dynamics (Hut & Bahcall, 1983). The only way to test whether this is a significant effect is through numerical simulations.

To calculate the probability that an object may hit a moon instead of a planet, we performed many short simulations of meteoroids approaching Jupiter and Saturn with the moons included and counted the number of times they hit either the planet or one of the moons. These simulations were again performed with MERCURY, including all the Solar System bodies as well as the moons of interest as "big" objects and the meteoroids as "small" ones. Since the moons are within the close-encounter cutoff radius, the simulation proceeds by using a slower but more precise variable-timestep integrator. For the meteoroids' trajectories, we put them near the planet's orbit at a random orbital phase, adding random variations of position up to 10^{11} cm and of velocity up to 100 cm/s. This procedure was repeated hundreds of times, with different random orbital positions of the moons, until we could estimate a ratio of moon-to-planet impacts to apply to the planet-to-planet transfer rates.

Calculating a 10 Myr trajectory took approximately 1000 CPU seconds per ejected object, or roughly 1000 CPU days for the entire population of about 100,000 objects. Most of the simulations were performed with 2.6 GHz Intel Xeon cores. This only counts the time used on the main simulations, not the smaller moon-impact simulations. The absolute amount of CPU time used was substantial, as

each trajectory must be modeled for many dynamical times, and the code requires a dedicated processor over long periods of time. However, this amount of time is modest by modern standards, and breaking the population of small objects up into several simulations allows us to run in parallel on multiple processors, which greatly reduces the wall time.

We noted a problem with the selection criteria for collisions with the central body when satellite bodies were involved. Additional criteria were needed to allow stable moon orbits. For details, visit `www.personal.psu.edu/rjw274/Code.html`.

2.2.1 Results

2.2.2 Total rates of transfer between planets

The majority of collisions by far were onto the planet of origin for the simulation (see Table 2.1). Large numbers also impacted the planets inward from the origin planet, and many meteoroids were either captured by the Sun or ejected from the system entirely. Small numbers were gradually perturbed into orbits that allowed them to impact planets outward from their origin, namely from Earth to Mars, Jupiter, and Saturn, and from Mars to Jupiter. In general, the number of impacts decreased with distance from planet of origin, except for the Sun and ejections from the system, which serve as outer boundaries and catch large numbers of objects. In general, the planet of origin influences the rate of transfer most strongly for collisions on Venus, Earth, and Mars, while for more distant destinations, the importance of which planet the object was ejected from is reduced.

2.2.3 Timescales of transfers

The distribution of impact times can be seen in Fig. 2.1. The majority of collisions occurred as ejected meteoroids reimpacted their planet of origin on short (< 0.5 Myr) timescales. These impacts drop off exponentially with time, while impacts on more distant bodies occur later and less frequently, with peaks at later times for destinations more distant from the planet of origin, as shown below in Table 2.2. The distributions for some bodies appear to be truncated by our simulations' lengths of 10 Myr, indicating that extending the length of simulation would increase the proportions of impacts on these planets.

Table 2.1: Total Numbers and Rates of Transfer Observed in Our Simulations by Origin and Destination.

	Earth	Earth (%)	Mars	Mars (%)
Orbit	17,484	40 ± 0.3	30,384	75 ± 0.4
Sun	659	1.5 ± 0.06	508	1.3 ± 0.06
Mercury	159	0.37 ± 0.03	12	0.03 ± 0.009
Venus	5,713	13 ± 0.2	617	1.5 ± 0.06
Earth	17,201	40 ± 0.3	1,048	2.6 ± 0.08
Mars	79	0.18 ± 0.02	6,362	16 ± 0.2
Jupiter	18	0.41 ± 0.01	16	0.04 ± 0.01
Saturn	3	0.0069 ± 0.004	0	< 0.0025*
Ejected	2,184	5 ± 0.1	1,553	3.8 ± 0.1
Total	43,500	100	40,500	100

*No Mars-to-Saturn transfers were seen in the simulations, so we show the upper limit on the probability. The value is the probability for a single simulation transfer.

2.2.4 Impacts at 10-30 Myr

Our primary interest for these simulations is in whether ejected material could carry life between Solar System bodies. Based on the estimates of Mileikowsky et al. (2000) that moderately sized ejecta could shield organisms on timescales of millions of years, and the findings of Gladman et al. (1996) that most transfer occurs in the first 10 Myr of their simulations, we set 10 Myr as the length of most of our simulations. However, for a small number of objects (9,000 from Earth, 6,000 from Mars), we extended the simulations to 30 Myr to see how transfer rates might change on longer timescales. The small number of objects in these simulations means that the results are noisy, especially for transfer to the outer planets where the numbers are low to begin with. We found that impact rates after 10 Myr decline for most destinations, with a few exceptions: rates of collision with the Sun or ejection from the Solar System peak between 10 and 15 Myr from initial ejection; transfer rates from Earth to Jupiter continue until about 15 Myr from ejection and from Mars to Jupiter until nearly 25 Myr; and transfer from Mars to Mercury and Venus increases after the first 10 Myr. However, the numbers for Jupiter, Mercury, and Venus are particularly small and subject to large amounts of noise, so the significance of these results is uncertain. The median transfer times for these simulations can be found in Table 2.2.

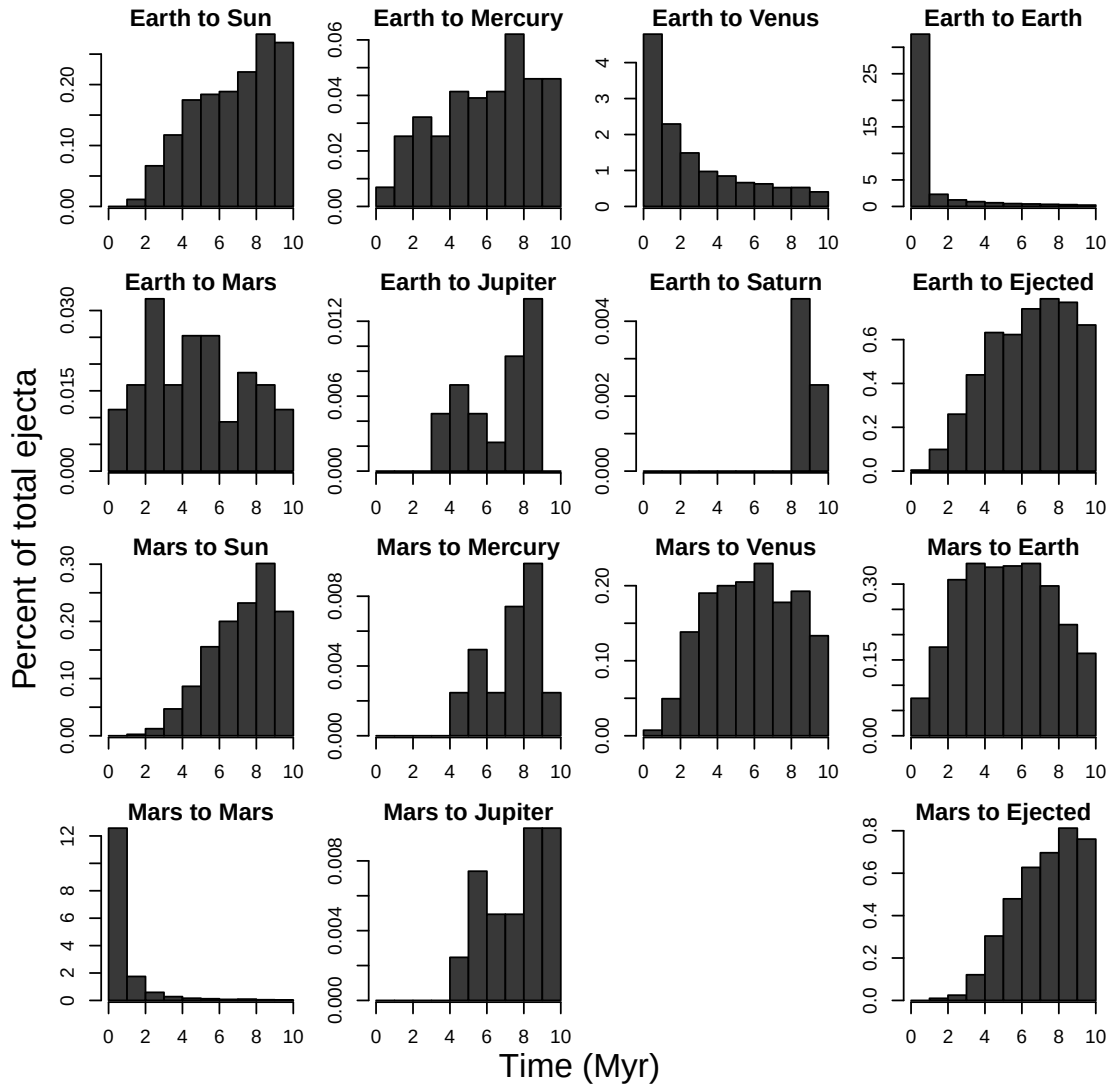

Figure 2.1: Histograms showing the distribution in impact time for each location, in million-year bins.

2.2.5 Moon impact rates

We performed additional simulations of meteoroids approaching Jupiter and Saturn with the moons included, as described in Section 2.2. These simulations included either two of Saturn's moons (Titan and Enceladus) or Jupiter's four Galilean moons (Io, Europa, Ganymede, and Callisto), as well as a set of randomized meteoroids already near the giant planet. We ran these small simulations many thousands of

Table 2.2: Characterization of the Transfer Time Distributions for Each Origin-Destination Pair

	Destination	Time of first impact (yr)	10 Myr Median (Myr)	30 Myr Median (Myr)
	Sun	1,014,612	7.1	12
	Mercury	482,101	6.3	9.9
	Venus	8,338	1.7	2.4
from	Earth	0.303	0.096	0.095
Earth	Mars	112,689	4.7	6.4
	Jupiter	3,852,399	7.6	9.4
	Saturn	8,008,387	8.8	8.8
	Ejected	670,965	6.6	12
	Sun	1,737,473	7.5	15
	Mercury	4,949,372	7.7	18
	Venus	456,864	5.8	13
from	Earth	281,754	5.2	9.3
Mars	Mars	0.575	0.21	0.23
	Jupiter	4,831,160	7.9	19
	Saturn	-	-	-
	Ejected	1,570,842	7.5	15

Time of first impact shows the minimum amount of time that was needed for an object to reach this destination after being ejected. Median impact times are given for both the 10 and 30 Myr simulations. The former is representative of the typical transfer time for possible viable organisms, while the latter more closely describes the overall distribution of ejecta.

times to calculate the ratio between the number of meteoroids that hit the planet to the number that hit each moon. We then used this to estimate how many of the planet impactors from the main simulations would actually hit the moons instead, had they been present. We found that many of the moons were hit more often than the Liouville theorem (discussed in Section 2) would predict, as shown in Fig. 2.2a. The exceptions to this were Titan and Callisto, which both received fewer impacts than expected. The impacts recorded in these simulations can be found in Table 2.3. We observed a correlation between the moons' impact ratios and a combination of their parameters, as illustrated in Fig. 2.2b. The moons and planets in our study indicate that the collision ratio between a satellite and parent body is proportional to the ratios of their gravitational focusing factors, times the

planet's Hill sphere radius divided by the square of the moon's semimajor axis. If the correlation proves applicable over a wide range of satellite systems, it could prove a useful tool.

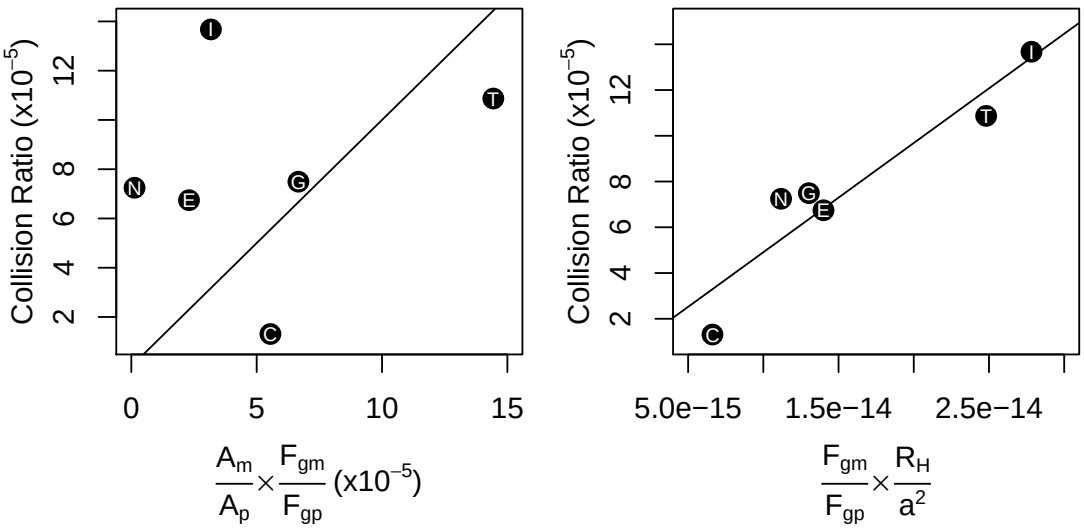

(a) . (b) .

Figure 2.2: The results of our moon simulations, plotted against different predictors. The lettered plot symbols identify Io, Europa, Ganymede, Callisto, and Titan by their first letter, and Enceladus is represented with an N. (a) The Liouville theorem prediction is represented by the black line. "A" is the cross-section area, "F_g" is focusing factor, and subscripts "m" and "p" indicate moon and planet, respectively. (b) A useful empirical correlation was observed between the moon-planet collision ratio and a combination of the moon and planet parameters. The x axis is the gravitational focusing factor of the moon divided by that of the planet, times the planet's Hill sphere radius divided by the square of the moon's semimajor axis. The black line is a fit to the points, with a slope of 4.8×10^9 and intercept 1.3×10^{-6}.

2.3 Discussion

2.3.1 Correlation with initial conditions

Using the statistical program R (Team et al., 2013), we attempted to quantify which parameters were significant in a determining the destination and timescale of the meteoroids' collisions. We used the function *glm*, which calculates a general

Table 2.3: Number of Impacts per Object in Moon Simulations.

Body	Number	Body	Number
Jupiter	533,776	Saturn	27,597
Io	73	Enceladus	2
Europa	36	Titan	3
Ganymede	40		
Callisto	7		

linear model for a data set. The user chooses a response variable Y (the parameter we are trying to fit) and one or more predictor variables X_i (the parameters to which we want to fit the response variable). The program uses maximum likelihood estimates to fit the response as a function of the predictors, as described in more detail in the Appendix. It also determines the significance of each parameter based on a false-alarm probability P, the probability that the given results could occur randomly. Convention dictates that $P < 0.05$ indicates significance.

Below, we discuss two fits: destination as a function of planet of origin, initial velocity v_0 , and two ejection angle parameters (ϕ indicates the direction within the ecliptic plane, while θ indicates the direction above or below the plane); and collision time as a function of destination, origin, initial velocity, and ejection angle.

We fit the destination by using it as the response variable in the model, with the initial conditions of ejection (planet of origin, initial velocity, and two angles parameterizing the direction of ejection from the planet) as predictors. The false-alarm probability for the origin parameter is smaller than the program can calculate (i.e., less than the minimum nonzero double-precision floating point value, $2.225074 \times 10^{-308}$), indicating (unsurprisingly) that the planet of origin is extremely important in determining which planet an ejected object will collide with. The initial ejection velocity is also quite important in determining whether an object will collide with its planet of origin but otherwise is not statistically significant. The direction of ejection is insignificant except for one case: a high polar angle has a small but statistically significant influence on the chances of re-impact. This seems to indicate that ejection angle and velocity are randomized before most objects impact a planet.

Using the same program, we then fit the impact time as a function of destination and the same four initial properties used above. We found that the destination is

the most significant predictor of impact time, and origin is once again also very significant. The initial velocity is also statistically significant, but this is likely due to the correlation between velocity and likelihood of re-impacting, which occurs at far earlier times than other impacts. The ejection angle parameters are both insignificant.

Thus, overall we found that the fate of an ejected rock depends on the planet it is ejected from and to some extent the velocity with which it is ejected, but otherwise it is largely due to chance. Once an object gets beyond the influence of its origin body, its ejection parameters are no longer important.

2.3.2 Calibrate with Mars-Earth transfer rates

The rates of transfer from Mars to Earth and Earth to Mars found by Mileikowsky et al. (2000) are

$$f_{M2E} = 0.6\% \times T \tag{2.3}$$

$$f_{E2M} = 0.016\% \times T \tag{2.4}$$

for T up to 10 Myr, or 6% and 0.16% for the full length of our simulations. This is in reasonable agreement with our results of 0.2% for Earth-to-Mars transfer, but our 3% Mars-to-Earth transfer rate is only half their value. Figure 2.3 shows a stronger velocity dependence in this transfer, so these results appear consistent with our lower ejection velocities.

2.3.3 Estimated numbers of transfers

Mileikowsky et al. (2000) went into detail estimating the number of rocks ejected from Earth and Mars with favorable conditions for propagating life. The fragments of ejecta must be of sufficient size to protect life for a journey through space of millions of years. They must also receive low enough shock pressures that the entire rock is not sterilized in ejection. We repeat the calculations described in Sections 3.1 and 3.2 of Mileikowsky et al. (2000) but use the martian cratering rates from Table 1 of Ivanov & Hartmann (2007). We scaled the ejected fragments by the transfer probabilities we found, giving us estimates of the total number of viable fragments that may have reached each destination. These results are presented in Tables 4 and 5.

The rates are provided for logarithmic bins of crater size, and we obtain a conservative estimate by using the minimum size in a given bin for subsequent calculations. We derived the impactor size L for each crater diameter D. For Earth, we scaled the martian impact rate by the relative rates for Earth and Mars given in Table 4 of Ivanov & Hartmann (2007). Additionally, since the rates are given per square kilometer, we multiplied by the land surface area of the planet to obtain the whole-planet impact rates.

Mileikowsky et al. (2000) found that the approximate number of unsterilized fragments n (i.e., heated to no more than 100°C and subjected to pressures no more than 1 GPa) is independent of L. For Mars impacts, $n = 2 \times 10^7$, and for Earth, $n = 6 \times 10^8$. We then calculated the fraction of unsterilized fragments that are at least 3 m in diameter, the minimum size able to shield organisms from the damages of space for up to 10 Myr. [1]

For each size L, we multiplied the impact rate over 3.5 Gyr by the number of unsterilized fragments of sufficient size. As stated by Mileikowsky et al. (2000), an impactor with a relatively high velocity (> 15 km/s on Mars or > 30 km/s on Earth) is needed to eject a substantial number of fragments. They estimated that only about one-third of incoming objects are fast enough, so we reduced the impact rates accordingly. Finally, we summed over all values of L to obtain the estimates for total viable fragments from each planet. Very large impactors with less than one expected high-velocity impact on land over 3.5 Gyr were excluded from the sum. We estimate roughly 2×10^8 qualifying meteoroids have been ejected from Earth and 8×10^8 from Mars over 3.5 Gyr. This time span is both roughly the time since the Late Heavy Bombardment (LHB) and the period that Earth is known to have contained life.

As noted by Ivanov & Hartmann (2007), the eccentricity of Mars varies significantly, and the impact rates on its surface vary as a result. They show in Table 2.4 that the variance is within a factor of 2 over the known eccentricity range. We note that this effect could cause a moderate change in our estimation for Mars ejecta rates.

Due to Earth's high surface gravity and impact velocity compared to that of

[1] For the benefit of readers who may wish to reproduce these calculations, we note that the paper mistakenly states that F(2l) = 0.04, when it is actually 0.4. Additionally, the equation relating transient to final diameter for Earth craters has 3 km as the first transition point, while the values in Table II imply that it should be 30 km.

Table 2.4: Probabilities and Estimated Viable Transfers to the Planets in the Solar System

		Probability (%)	3.5 Gyr Total	Mass (kg) transferred
	Orbit	40 ± 0.3	$80,000,000 \pm 600,000$	2.7×10^{13}
	Sun	1.5 ± 0.06	$3,000,000 \pm 100,000$	1.0×10^{12}
	Mercury	0.37 ± 0.03	$730,000 \pm 60,000$	2.5×10^{11}
from	Venus	13 ± 0.2	$26,000,000 \pm 300,000$	8.9×10^{12}
Earth	Earth	40 ± 0.3	$79,000,000 \pm 600,000$	2.7×10^{13}
	Mars	0.18 ± 0.02	$360,000 \pm 40,000$	1.2×10^{11}
	Jupiter	0.041 ± 0.01	$83,000 \pm 20,000$	2.8×10^{10}
	Saturn	0.0069 ± 0.004	$14,000 \pm 8,000$	4.7×10^{9}
	Ejected	5 ± 0.1	$10,000,000 \pm 200,000$	3.4×10^{12}
	Orbit	75 ± 0.4	$600,000,000 \pm 3,000,000$	2.0×10^{14}
	Sun	1.3 ± 0.06	$10,000,000 \pm 300,000$	3.4×10^{12}
	Mercury	0.03 ± 0.009	$240,000 \pm 50,000$	8.1×10^{10}
from	Venus	1.5 ± 0.06	$12,000,000 \pm 400,000$	4.1×10^{12}
Mars	Earth	2.6 ± 0.08	$21,000,000 \pm 500,000$	7.0×10^{12}
	Mars	16 ± 0.2	$130,000,000 \pm 1,000,000$	4.3×10^{13}
	Jupiter	0.04 ± 0.01	$320,000 \pm 60,000$	1.1×10^{11}
	Saturn	< 0.0025	$< 20,000$	$< 6.8 \times 10^{9}$
	Ejected	3.8 ± 0.1	$31,000,000 \pm 600,000$	1.0×10^{13}

The 3.5 Gyr total is the number of transferred objects we expect. Mass transferred assumes each object is ≈340,000 kg (i.e., a 3 m sphere with density of 3 g/cm^3). No Mars-to-Saturn transfers were seen in the simulations, so we show the upper limits.

Mars, an impactor of a given size ejects a smaller amount of mass on Earth in smaller but more numerous fragments. On Earth, a few very large impacts will eject huge numbers of viable fragments, while on Mars the same fragment size will be primarily produced by smaller impactors, in small but more frequent batches. Over 3.5 Gyr, the largest portion of the ejecta from Earth come from impactors approximately 19 km in size, which will eject 1.6×10^8 viable fragments from a single impact over the course of 3.5 Gyr. On Mars, the most ejecta come from roughly 5 km impactors, which eject 2.7×10^8 such fragments, around 8 million each from approximately 35 impacts.

For the impacts under discussion, Mileikowsky et al. (2000) estimated that the mass ejected is 5.3×10^{-4} of the impactor mass on Mars and 2.3×10^{-4} on

Earth, although the fraction of it that would be in > 3 m objects varies from none for small impactors to nearly all for the largest. The ejected mass would then be distributed between destinations of the Solar System in accordance with our calculated probabilities, as in Tables 4 and 5. The impactor that created the Chicxulub crater and caused mass extinction on Earth roughly 65 Myr ago (Schulte et al., 2010) likely launched about 7×10^{11} kg of rock into orbit, of which about 20,000 kg (7×10^{-10} of the impactor's mass) could have reached Europa. For a single impact of this size, the probability of a fragment > 3 m reaching Europa is 0.6, and over 3.5 Gyr we can expect one or two rocks to have made the journey due to impacts of this size.

Combining the above ejection rates with the rates of transfer, we estimate some tens of thousands of meteoroids from each planet should have been transferred to Jupiter, and several thousand from Earth should have hit Saturn. The transfer to these and the other planets is shown in Table 4. Based on the simulations described above, we can approximate the likelihood of hitting Europa as a scaling factor times the probability of hitting Jupiter, where the scaling factor is derived from the shorter simulations described in the previous section. The expected transfer rates to the moons of the outer Solar System are shown in Table 5. We find expectation values of one to a few objects reaching Io, Europa, Ganymede, Callisto, Enceladus, and Titan from Earth since the LHB, and slightly higher numbers for Jupiter's moons from Mars. Transfer from Mars to the moons of Saturn is less likely, but the upper limits we calculated do not completely rule out the possibility.

The above values are based on post-LHB impact rates. The LHB was a period of intense meteor impacts on the inner Solar System from 4.1 to 3.8 Gyr ago. Chapman et al. (2007) found that more than half of large impact craters date from the LHB, and Ivanov & Hartmann (2007) implied that LHB impacts may have been even more numerous. This indicates that we can expect at least as many impacts to have occurred during the LHB as in the period of time since. Whether life was already present during this period is unknown, but if so, that could substantially raise the number of potentially life-bearing rock transfers between planets.

We can also calculate the probability of any transfer for each origin-destination pair. For transfer with a probability of p per ejected fragment, and n total fragments ejected in 3.5 Gyr, the probability that no fragments will make that transfer is $(1 - p)^n$. Table 2.6 lists the probability that at least one fragment from the given

Table 2.5: Probabilities and Estimated Viable Transfers over the Past 3.5 Gyr to Some of the Moons in the Outer Solar System.

	Destination	Impact Ratio	Probability (%)	3.5 Gyr Total	Mass Transfer (kg)
	Io	$7,300 \pm 900$	5.7e−6 ± 7.0e−7	10 ± 1	3,800,000
	Europa	$15,000 \pm 2,000$	2.8e−6 ± 5.0e−7	6 ± 0.9	1,900,000
from	Ganymede	$13,000 \pm 2,000$	3.1e−6 ± 5.0e−7	6 ± 1	2,100,000
Earth	Callisto	$76,000 \pm 30,000$	5.4e−7 ± 2.0e−7	1 ± 0.4	370,000
	Enceladus	$14,000 \pm 10,000$	5.0e−7 ± 4.0e−7	3 ± 2	1,000,000
	Titan	$9,200 \pm 5,000$	7.5e−7 ± 4.0e−7	4 ± 3	1,500,000
	Io	$7,300 \pm 900$	5.4e−6 ± 6.0e−7	10 ± 1	3,700,000
	Europa	$15,000 \pm 2,000$	2.7e−6 ± 4.0e−7	5 ± 0.9	1,800,000
from	Ganymede	$13,000 \pm 2,000$	3.0e−6 ± 5.0e−7	6 ± 0.9	2,000,000
Mars	Callisto	$76,000 \pm 30,000$	5.2e−7 ± 2.0e−7	1 ± 0.4	350,000
	Enceladus	$14,000 \pm 10,000$	$<$ 1.8e−7	< 1.4	$<$ 490,000
	Titan	$9,200 \pm 5,000$	$<$ 2.7e−7	< 2.1	$<$ 730,000

The impact ratio is the number of meteoroids that hit the planet (Jupiter or Saturn) for each one that hits the moon. For transfer from Mars to Saturn's moons, upper limits are used. The mass transfer rates are estimated by assuming that each transferred fragment is a sphere 3 m in diameter, with a density of 3 g/cm^3 , i.e., a mass of 340,000 kg each.

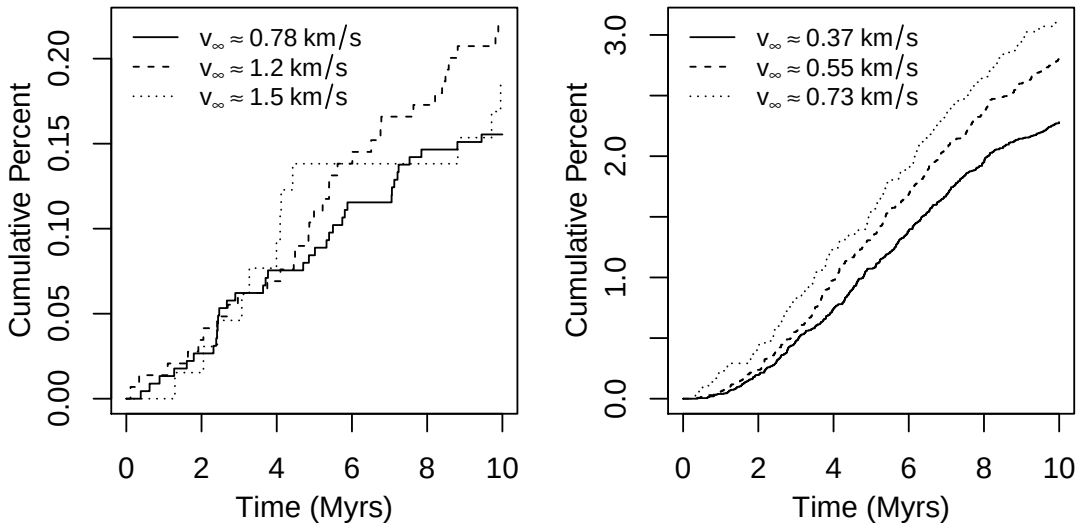

(a) . (b) .

Figure 2.3: Cumulative collision rates for transfer (a) from Earth to Mars and (b) from Mars to Earth, separated by ejection velocity.

origin planet has reached the destination planet.

2.3.4 Effects of returned material

We observed that a large portion of material ejected returns to the planet of origin on short timescales of ≤ 1 Myr. Wells et al. (2003) studied the effect of returned material on restoring life after sterilizing impacts during the LHB. If life had arisen by this time, it may have been present on some of the many fragments ejected by the bombardment. The ejected fragments could have served as a refuge for life while the surface cooled enough to permit survival, then fallen back to re-seed life (Maher & Stevenson, 1988; Sleep & Zahnle, 1998). The fallback rates in the first 3000 years after impact were characterized by Wells et al. (2003). Our results show these rates over a longer timescale but with a coarser grid; our data were written in 1000-year time steps.

We find that the cumulative probability of re-impact continues to increase substantially through the first few 10^5 years, as shown in Fig. 2.4. We also note that Earth's higher gravity allows it to recapture far more of its ejecta than Mars can. This is despite the fact that we scaled our ejection velocities to the planet's escape velocity, resulting in Mars' ejecta having lower residual velocities than that from Earth.

2.3.5 Discussion of uncertainties

We are able to include estimates of the Poisson errors in the counts of meteoroids in the simulations, but we cannot quantify the possibility of systematic errors. Due to the chaotic nature of complex dynamics simulations, effects may have unexpected consequences – for example, strong unsampled resonances could exist that would result in skewed collision rates. We are aiming for simply an order-of-magnitude estimate of the transfer rates.

Additionally, if future studies revise the numbers on which our assumptions are based, our probabilities for transfer can be applied to the updated values. For a different estimate of the number of viable rocks ejected, the final numbers scale linearly. If the timescales for organism viability are found to be higher or lower than estimated here, then the number of viable rocks delivered within this time frame will respectively be higher or lower as well. However, due to the varying

Table 2.6: Probability of no transfer for each destination-origin pair

Origin	Destination	Transfer Probability per Ejection	Probability of No Transfer
Earth	Orbit	4.02×10^{-1}	0.0
	Sun	1.51×10^{-2}	0.0
	Mercury	3.66×10^{-3}	0.0
	Venus	1.31×10^{-1}	0.0
	Earth	3.95×10^{-1}	0.0
	Mars	1.82×10^{-3}	0.0
	Jupiter	4.14×10^{-4}	0.0
	Io	5.66×10^{-8}	1.22×10^{-5}
	Europa	2.79×10^{-8}	3.77×10^{-3}
	Callisto	5.42×10^{-9}	3.38×10^{-1}
	Ganymede	3.1×10^{-8}	2.03×10^{-3}
	Saturn	6.9×10^{-5}	0.0
	Titan	7.5×10^{-9}	2.23×10^{-1}
	Enceladus	5.0×10^{-9}	3.68×10^{-1}
	Ejected	5.02×10^{-2}	0.0
Mars	Orbit	7.5×10^{-1}	0.0
	Sun	1.25×10^{-2}	0.0
	Mercury	2.96×10^{-4}	0.0
	Venus	1.52×10^{-2}	0.0
	Earth	2.59×10^{-2}	0.0
	Mars	1.57×10^{-1}	0.0
	Jupiter	3.95×10^{-4}	0.0
	Io	5.4×10^{-8}	1.71×10^{-19}
	Europa	2.66×10^{-8}	5.56×10^{-10}
	Callisto	5.18×10^{-9}	1.59×10^{-2}
	Ganymede	2.96×10^{-8}	5.21×10^{-11}
	Saturn	$< 2.47 \times 10^{-5}$	> 0.0
	Titan	$< 2.68 \times 10^{-9}$	$> 1.17 \times 10^{-1}$
	Enceladus	$< 1.79 \times 10^{-9}$	$> 2.39 \times 10^{-1}$
	Ejected	3.83×10^{-2}	0.0

The probability of no transfer to a particular destination is $(1-p)^n$, where p is the probability of transfer for a single particle and n is the total number of ejections from the planet in 3.5 Gyr (2×10^8 fragments from Earth and 8×10^8 from Mars). For non-zero p and finite n, the values in the second column are never actually mathematically zero; entries that read "0.0" indicate those for which the probability is smaller than 2.225×10^{-308}, the smallest positive float value allowed. Also, once again upper limits for Mars-Saturn transfers are used, resulting in lower limits on the probability of no transfer.

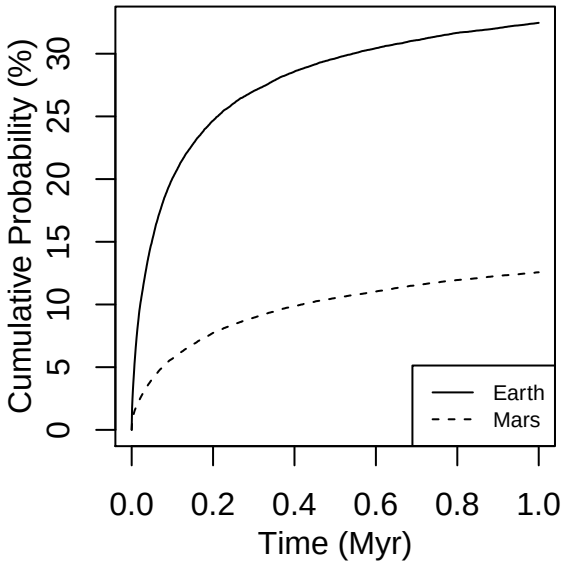

Figure 2.4: The percentage of ejected material returned to its planet of origin over the first million years after impact.

rates of transfer over time, the amount of variation is less predictable.

2.3.6 Area for future study

One additional aspect of physics that was not included in this study is the Yarkovsky effect (Bottke et al., 2006). Objects from approximately 10 cm to 10 km will receive an extra propulsive force due to asymmetrically radiating more energy from the warm "afternoon" side of the object. The magnitude of this force will depend on the speed and angle of the object's rotation, and a population of ejected rocks will likely have a wide distribution of rotations. For many ejected objects, it will likely have a negligible effect, but for some subset, it may be significant and lead to faster inward decay or outward transfer, depending on the direction of rotation. This could be a fruitful area for future study, and we are composing a module to include this effect in MERCURY.

2.4 Conclusions

We find that transfer of rock capable of carrying life has likely occurred from both Earth and Mars to all the terrestrial planets in the Solar System and Jupiter, and transfer from Earth to Saturn is also probable. Additionally, we find smaller but significant probabilities of transfer to the moons of Jupiter and Saturn from Earth and to the moons of Jupiter from Mars. These estimates are dependent on the number of rocks assumed ejected from the planets of origin. Our results indicate that transfer of life to these moons cannot be ruled out, and searches for life on these objects should keep in mind the necessity of determining whether life arose independently or descended from common ancestors to Earth life. Any life found there cannot be assumed to be of independent origin.

The probability of life surviving such a journey or finding a tenable environment on arrival is beyond the scope of our research. However, we note that studies of Titan, Europa, and Callisto all indicate significant liquid water oceans beneath the surface (Khurana et al., 1998; Lorenz et al., 2008). Europa currently presents the thinnest surface ice layer, which provides less of a barrier for life to eventually find its way through. Plumes of apparent water vapor have been detected erupting from the surface near the south pole (Roth et al., 2014), indicating that water from the interior can reach the surface. Whether material from the surface can in turn make it to the interior ocean is still unknown, but the surface contains "chaos regions" that indicate recent partial melting. It appears that regions of the ice sheet sometimes break into large chunks separated by liquid water, which later refreezes. Any meteorites lying on top of the ice sheet in a region when this occurs would stand a chance of falling through. Additionally, the moons are thought to have been significantly warmer in the not-too-distant past. Titan currently has a roughly 50 km thick crust, but the moon only cooled enough to form this shell after 4 Gyr (Tobie et al., 2006), before which it had only a few kilometers of methane clathrate over the surface, allowing a significant time in which life could have more easily penetrated into the liquid water ocean. Jupiter's moons are also believed to have been significantly warmer in the past, due to both residual heat of formation and their slow outward migration, making them previously subjected to stronger tidal heating from Jupiter.

Ultimately, we conclude that the possibility of transfer of life from the inner

Solar System to outer moons cannot be ruled out based on current knowledge. Any planned missions to search for life on Titan or the moons of Jupiter will have to consider whether any biological material found represents an independent origin, rather than another branch in the family tree populated by Earth life.

2.5 Appendix: Linear modeling

Our data include both continuous (numerical) and categorical (non-numerical) variables, which require different treatments when fitting. When both predictor and response are continuous, we fit a line of the form $Y = \beta_1 X + \beta_0$, where β_0 is the intercept of the line, and X and β_1 are the predictor variable and its corresponding slope. In the case of multiple predictors, X is replaced with the predictors X_1, X_2, and so on, each of which will have its own slope β_1, β_2, and so on. If the predictor is categorical, β simply becomes the difference between the average response values for the two categories.

For a categorical response variable such as destination (where the value may be collision with the Sun or other planets, ejection from the system, or remaining in orbit), the meaning of the actual fit parameters is somewhat less straightforward. In this case, β represents the change in the natural log of the odds when the predictor changes from one category to the other. The model treats the first category as the baseline and uses a binomial model for each of the other categories paired with the baseline. For example, remaining in orbit (i.e., destination = orbit) is the baseline, and each of the other destinations is evaluated against the baseline. For the case of comparing "destination = Earth" versus "destination = orbit", the baseline value (orbit) is designated a negative result, with a value of 0, and Earth is positive and has a value of 1. The probability of impacting Earth compared to that of staying in orbit, when the planet of origin is Earth, is then

$$P_{01} = \frac{N_{E2E}}{N_{E2E} + N_{E2O}} \tag{2.5}$$

where N_{E2E} and N_{E2O} are the number of objects from Earth that hit Earth or stay in orbit, respectively. Similarly, for the probability of staying in orbit,

$$P_{00} = \frac{N_{E2O}}{N_{E2E} + N_{E2O}} \tag{2.6}$$

Correspondingly, the probability for objects from Mars of impacting Earth compared to staying in orbit is

$$P_{11} = \frac{N_{M2O}}{N_{M2E} + N_{M2O}} \tag{2.7}$$

and so on. The odds are defined as the ratio of probabilities of a positive result over a negative one, so the odds of hitting Earth for an object from Earth, when comparing the destinations of Earth versus orbit, would be P_{01}/P_{00}, which reduces to N_{E2E}/N_{E2O}, and the odds for an object from Mars would be $P_{11}/P_{10} = N_{M2E}/N_{M2O}$. The parameter being fit by the model, β_1, is the change in the natural log of the odds when the predictor's value increases by one or, for a categorical variable like planet of origin, changes from the first to the second category, that is,

$$\beta_1 = \ln(N_{M2E}/N_{M2O}) - \ln(N_{E2E}/N_{E2O}) \tag{2.8}$$

$$\beta_1 = \ln[(N_{M2E}/N_{M2O})/(N_{E2E}/N_{E2O})] \tag{2.9}$$

Equivalently, the odds of hitting Earth for an object from Mars would be e^{β_1} times the odds for an object from Earth.

$$(N_{M2E}/N_{M2O}) = (N_{E2E}/N_{E2O})e^{\beta_1} \tag{2.10}$$

Thus, a positive b implies the odds increase as you go from the first to the second category, and negative implies a decrease.

Chapter 3
Dynamical Evolution of Alpha Centauri

[Note: this chapter has been accepted for publication as an article in The Astrophysical Journal, and can currently be found on arXiv as Worth & Sigurdsson (2016). As first author, I ran the simulations, analyzed the data, and wrote the paper, with feedback and editing from my co-author Prof. Sigurdsson.]

Proxima Centauri is an M dwarf approximately 15,000 AU from the Alpha Centauri binary, comoving and likely in a loosely bound orbit. Dynamic simulations show this configuration can form from a more tightly bound triple system. As our nearest neighbors, these stars command great interest as potential planet hosts, and the dynamics of the stars govern the formation of any planets within the system. Here we present a scenario for the evolution of Alpha Centauri A and B and Proxima Centauri as a triple system. Based on N-body simulations, we determine this pathway to formation is plausible, and we quantify the implications for planet formation in the Alpha Centauri binary. We expect this formation scenario may have truncated the circumstellar disk slightly more than a system that formed in the current configuration, but that it most likely does not prevent terrestrial planet formation. We simulate planet formation in this system and find that in most scenarios, two or more terrestrial planets can be expected around either Alpha Centauri A or B, orbiting in a region out to approximately 2 AU, assuming planetesimals and planetary embryos are able to first form in the system. Additionally, terrestrial planet formation and stability in Proxima Centauri's habitable zone is also plausible. However, an absence of planets around these stars may be indicative of highly disruptive stellar dynamics in the past.

3.1 Introduction

Our nearest neighbor, the M-dwarf Proxima Centauri, is thought to be tenuously bound to the Alpha Centauri binary, forming an extremely wide triple system; although measurements are not precise enough to constrain the orbit, its proximity to Alpha Centauri along with its comoving velocity would be very unlikely in a passing, unconnected star (Wertheimer & Laughlin, 2006). A detailed study of triple system dynamics (Reipurth & Mikkola, 2012) hypothesized that the three stars could have formed closer together, as part of a single system, and that dynamical interactions between them could then have led to Proxima's near-ejection onto its current highly eccentric path.

There has also been significant interest in the possibility of planets in the Alpha Centauri system. As our nearest neighbors, these stars represent the best candidates for in-depth study, as well as the most likely target for a search for biomarkers or any distant future interstellar contact if habitable planets were to be found there. A hot Earth-sized planet has been reported around Alpha Centauri B (Dumusque et al., 2012), although the detection has been disputed (Hatzes, 2013; Rajpaul et al., 2016). Other observational studies have ruled out the possibility of giant planets in the system (Demory et al., 2015; Endl et al., 2001) and put constraints on the detectability of planets within the system (Eggl et al., 2013; Endl et al., 2015; Guedes et al., 2008).

The gravitational forces of multiple stars introduce additional complications for planetary formation; however, the prevalence of stellar multiplicity means it is critical to understand such systems if we are to understand planet formation in the Universe as a whole (Thebault & Haghighipour, 2014). Although planet searches initially avoided binaries due to their additional complications as observational targets as well as the reduced likelihood of planet formation in their more turbulent dynamical environments (Eggenberger & Udry, 2010), many planets have now been discovered in binary systems, including a multiplanet system in the binary 55 Cancri (Fischer et al., 2008). In some cases, planet searches discovered both a planet and a previously unknown companion star (Mugrauer & Neuhäuser, 2009). A planet has also been detected in 16 Cygni, a triple system consisting of two Sun-like stars and a red dwarf, similar to Alpha Centauri except that here the smaller star is part of the inner binary (Cochran et al., 1997).

In addition to the multiple systems we see today, it is likely that even more stars were members of such systems when they formed. There is evidence to suggest many, if not most, stars form in bound multistellar systems which then eject members until they reach stable configurations, resulting mostly in singles and binaries but occasionally in higher-multiplicity systems (Goodwin et al., 2007; Reipurth et al., 2014, 2010). This is consistent with the lower multiplicity rates of smaller stars, as they are more easily ejected than massive stars. The consequences of "fly-by" interactions between stars have been studied (Li & Adams, 2015), but multiple bound stars have different outcomes, as they repeatedly interact over multiple orbits. The protoplanetary disks around these stars, from which planets will eventually form, may be truncated or disturbed during these stellar interactions (Quintana et al., 2007).

Several groups have made theoretical studies of the disk or planet stability (Artymowicz & Lubow, 1994; Jang-Condell, 2015; Müller & Kley, 2012; Payne et al., 2009; Popova & Shevchenko, 2012b; Rafikov & Silsbee, 2015a,b) and formation environment (Barbieri et al., 2002; Guedes et al., 2008; Quintana et al., 2002; Thébault et al., 2008, 2009; Wiegert & Holman, 1997; Xie et al., 2010) in Alpha Centauri. However, most of these studies assume the stars were in their current orbits. If Alpha Centauri exchanged energy with Proxima Centauri to allow the latter to reach its current orbit, the Alpha Centauri binary would have lost energy in the process, altering its own orbit as well. These interactions typically take place soon after the stars' formation, as does the formation of any circumstellar disks and protoplanets within them. Therefore, such interactions could have significant consequences for our assumptions about planet formation in this system. In Thébault et al. (2009), the possibility of wider initial orbits was examined in the context of formation in a cluster, finding that initially wider orbits could improve the ease of formation of planetesimals.

In this work, we seek to characterize the limits of the dynamical history of the Alpha Centauri star system, with particular interest in how it may affect any planet formation within that system. We will assume Proxima Centauri is on an eccentric, bound orbit, and that its current position at around 15,000 AU from the Alpha Centauri binary is likely in the long, slow, portion of its orbit relatively near apocenter. We constructed a large population of triple systems that could evolve into the current arrangement and simulate their interactions, looking

for examples of Proxima (a.k.a. Alpha Centauri C) ending up on a wide, highly eccentric orbit. We examine two limiting cases: all stars at their present masses, so that A and B significantly outweigh C, thus minimizing the effects any energy exchanges have on the binary; and an equal-mass case which assumes that all three stars initially grew at similar rates, but that C was ejected when mass was still accreting and all three stars were its size (0.123 $M_{\odot}$), maximizing the effects on the binary system. This puts bounds on the amount by which the binary orbit could possibly change. Ultimately, we seek to understand whether planets may be present in Alpha Centauri, at what locations, and with what mass. The evolution of Proxima Centauri can affect this, but the effect could range from trivial to quite substantial depending on timing, so we bracket the range of possibilities to consider the range of outcomes.

3.2 Simulations

3.2.1 Numerical Method

We performed suites of simulations in three different regimes to explore different stages of the system's evolution: three-body simulations of just the stars, simulations of two or three stars with a disk of test particles, and planetary formation simulations within a stellar binary system. These regimes are laid out in Table 3.1 for clarity. For all three, we used the hybrid symplectic N-body code MERCURY (Chambers, 1999), which was designed for use on systems with a single, dominant central mass object. In some cases, a binary system will break the assumptions underlying the integration scheme and cause errors. By design, the first two regimes explored avoid these issues, in the first case due to the well-separated hierarchical nature of the systems, and in the second by the use of test particles. In order to correctly simulate planetary formation in a binary, however, we used a version of the hybrid symplectic integrator that has been modified for wide binary systems, as described in Chambers et al. (2002) and used in Quintana et al. (2002).

Our first regime follows the methods of Reipurth & Mikkola (2012) to examine the three-body interactions of Alpha Centauri A and B and Proxima Centauri in 1,522 randomized simulations. We added physics to MERCURY's user module that includes the gravitational potential of the nascent molecular cloud core from which

Table 3.1: Simulation Regimes Used

Regime	Simulations	Algorithm	Cases	Features
Stars	1522	hybrid	Early	Three stars (all 0.123 $M_{\odot}$)
			Late	Three stars (1.103, 0.934, and 0.123 $M_{\odot}$)
Disk	224	hybrid	Binary	Stars A and B plus disk particles,
			Triple	Stars A, B, and C plus disk particles
Planets	36	wb	various parameter combinations	$\sigma_0 = \{2.8, 3.1\}$ AU, $r_{tr} = \{0.3, 1, 3\}$

the stars form, as in Reipurth & Mikkola (2012). We omit accretion of gas directly onto the stars, but otherwise use parameters similar to theirs: 10 $M_\odot$ cloud core mass with a Plummer sphere potential of $M/(r^2 + R^2)^{1/2}$, where M is the cloud mass in $M_\odot$, R is the cloud core radius, 7,500 AU, and r is the distance of the object in question from the cloud center. The cloud mass disperses linearly over 440,000 years. In addition, because of the very large spatial separations involved, we included Galactic tidal forces using code provided by Dimitri Veras, as described in Veras & Evans (2013). The modification described in Worth et al. (2013), which improves the criteria for determining when an object impacts the central body, was also included but is generally not significant for simulations which do not involve satellites.

Simulations were initially run for 10^3 years, then checked for ejections. If none were found, the stop time was increased by an order of magnitude and the simulation was resumed. This process was repeated up to a simulation length of 10^9 years. Systems surviving the full length were then counted as "surviving" if the eccentricities of each object were less than 1.0, i.e. the stars were on bound ellipsoidal orbits. The simulation does not count stars as "ejected" until they go beyond some outer bound, which was set to 100,000 AU to allow for the large orbits desired, so it is possible for objects to be on ejection orbits but not yet counted as "ejected." It was also possible for stars to have orbits with apocenters greater than 100,000 AU, in which case they were falsely counted as ejected while still stable; however, at this scale we expect the orbit would be quickly destabilized by Galactic tides if it were integrated further.

Also note, the orbital parameters output by MERCURY assume all orbits are with respect to the designated "central" object, which is not the case here. Semimajor axis, eccentricity, and inclination were calculated separately for the binary orbit and for C's orbit with respect to the binary's center of momentum, treating the inner binary as a single companion mass. This does not account for the gas cloud potential; because of this, calculations of initial orbital parameters give seemingly unphysical results such as eccentricities greater than one.

In the second regime, we took systems which had ended resembling the Alpha/Proxima Centauri system today and repeated them, adding in a disk of test particles around Alpha Centauri B. This simulation was also repeated with the third star removed, so that Proxima's effects could be isolated. The parameters

used were the same as for the first regime, except that the larger number of particles meant it was infeasible to continue the simulations beyond 10 Myrs. By this point most of the interactions have already taken place and the systems are fairly stable. A total of 224 simulations of this type were performed.

The third regime consists of planet formation simulations in a disk around Alpha Centauri B. Thirty-six simulations were performed over several discrete values of truncation radius, disk slope, and disk density. These simulations represent a later time period, when the three stars have become well-separated and the gas cloud has dispersed, so the third star and the user module forces were omitted, and the wide-binary algorithm was used (Chambers et al., 2002). These integrations have shorter time steps (one day) due to the closer object spacing. In MERCURY's hybrid symplectic mode (as used here), whenever two objects approach each other within a few Hill radii, the algorithm switches to a slower mode which more accurately calculates whether the objects collide. Collisions are simple, perfect accretion. As the detailed physics of collisions are still a rapidly developing field with significant uncertainty, and we are interested in the end state of how the mass groups up rather than intermediary details, we consider this simple scheme appropriate for the scope of this study.

As our computational resources are limited and our interest in planet formation is motivated largely by claims of planets around Alpha Centauri B, our simulations focused on planet formation around B and not A. However, although the two stars are not the same mass, their masses are similar enough relative to the range of masses for planet-hosting stars ($< 0.1 M\odot$ to $> 2.5 M\odot$). It is plausible that planet formation processes around Alpha Cen A and B are closely symmetric and any systematic differences due to the stellar mass differences in the underlying planet formation processes are likely to be small (less than a factor of 2) compared to variations in outcomes due to the variation in disk parameters explored. Therefore, we expect simulations for formation around one star to be fair predictors of the distribution of likely planets around the other star, within the scope of this study and given the uncertainties in the assumptions.

3.2.2 Stellar Mass Cases

Two different sets of masses were used for the simulations, representing two different scenarios: interactions at early or late times. In the later scenario, the stars have already achieved their current masses, with the binary stars being near a solar mass and Proxima much smaller. The early interaction scenario is following that presented by Reipurth & Mikkola (2012), in which the stars are still accreting mass when Proxima is ejected, preventing it from accreting as much as its companions. In this case, all three stars have masses of 0.123 $M_{\odot}$. Neither case is intended a perfect representation of the true physical situation, but they provide outer bounds on the strength of the interactions, with the reality likely lying closer to the early case.

3.2.3 Orbital Parameters

Alpha Centauri A and B and Proxima Centauri are represented as Alpha Centauri A, B, and C in the simulations, and may be referred to as such in this paper when talking about the stars in the simulations, as opposed to the actual physical system.

In MERCURY's default mode, a single central body is chosen, and the other objects are listed as "big" objects with orbital parameters relative to the central body, although internal calculations are carried out in center-of-momentum coordinates. Star A is the largest, and was used as the central object, with Alpha Centauri B in an orbit around A with parameters randomly generated within specified ranges: semimajor axis (a) in the range 23.4-28.1 AU, eccentricity (e) between 0 and 0.52, and zero inclination (i). Parameters were then generated for C so that it had a pericenter between one and ten times the apocenter of B. C could have an initial eccentricity between 0 and 0.75, and any inclination. Both stars were also given random values for the argument of pericenter (g), longitude of the ascending node (n), and mean anomaly (M). These parameter ranges were chosen based on the assumption that the interactions we are interested in would cause the binary to become tighter while Proxima receded, and that both orbits would likely become more eccentric in the process. When close encounters between two objects occur, the simulation switches to a variable-time step regime with slower processing time but greater accuracy, and when objects are far apart it uses a fixed time step, which we set to 10 days. The close-encounter radius used was three Hill radii.

The binary parameters used are based on Pourbaix et al. (2002) ($M_A = 1.105$, $M_B = 0.934$) and Pourbaix et al. (1999) ($a_{AB} = 17.57$", $e = 0.5179$). Proxima's expected orbital parameters of a near 10,000 AU or above and e just below 1 are based on the arguments in (Wertheimer & Laughlin, 2006) that it is unlikely for Proxima to be seen so near Alpha Centauri in both position and velocity unless it is bound, and that given that, it is most likely eccentric and near apocenter, when it moves most slowly along its orbit.

Calculation of orbital parameters from the simulations is done instantaneously based on the system's energy and momentum. To calculate the outer third star's orbit, the inner binary is treated as a single mass at the binary's center of momentum. The equations used are as follows:

$$a = \frac{-\mu}{2\epsilon} \tag{3.1}$$

$$e = \sqrt{1 + \frac{2\epsilon \bar{h}^2}{\mu^2}} \tag{3.2}$$

$$i = arccos(\frac{h_z}{\bar{h}}). \tag{3.3}$$

The gravitational parameter μ is the sum of the masses involved (M_A and M_B for calculations of the binary parameters, and all three stars' masses for the outer star's orbit). The specific orbital energy is

$$\epsilon = \frac{v^2}{2} - \frac{\mu}{r}. \tag{3.4}$$

The angular momentum h is the cross product of the stars' separation r and relative velocity v, where h_z is the angular momentum in the z direction, and $\bar{h}$ is the magnitude of the angular momentum.

3.2.4 Disk Stability

By adding disks around each of the stars in the inner binary, we were able to see the influence of the triple-system interactions on protoplanetary disks in Alpha Centauri. Each disk consisted of 100 massless test particles on circular orbits, coplanar with the binary, spaced evenly from 0.1 AU to half of the binary's semimajor axis a_{bin}

(typically around 10 AU). We ran pairs of simulations, in which one contained only the inner binary and the other included the third star, to separate out the effect of the third star on the disks.

At each timestep, we tracked whether each particle was still stable (orbit's eccentricity is less than 1 and semimajor axis is within 20% of initial value) as well as whether it had been removed from the system (i.e. collided with a star or traveled beyond the 100,000 AU ejection radius) and found that stability is a very reliable predictor of removal: objects with orbits outside the above bounds almost always suffered an ejection or collision before the end of the simulation. Due to the large ejection radius used for the simulations, the destabilization time appears to more accurately track when changes to the system happen than the removal time.

Based on this, we define the truncation radius as the distance from the star which best defines an inner section closest to completely filled and outer section closest to completely depleted. That is, for each particle's orbital radius, we calculate the stable fraction inward (f_{in}) and outward (f_{out}) of this point, and the truncation radius r_{tr} is defined as the radius at which $|1 - f_{in}| + f_{out}$ is minimized. On timescales shorter than 1,000 years, particles in the outer disk oscillate between stable and unstable, making the truncation radius not especially meaningful until after this time, at which point it tracks the disk shape well.

3.3 Results and Analysis

3.3.1 Stellar System Simulations

The results from suites of simulations of the stars' dynamical interactions can be seen in Fig. 3.1. The left panels show the initial semimajor axis and eccentricity for both B and C. On the right, the final parameters of surviving systems are shown, along with a colored line connecting the points back to their initial parameters, and thin black dotted lines connecting B and C from the same simulation. The shaded region indicates the orbits with an apocenter of between 10,000 and 20,000 AU, which is our criterion for a system to be dubbed "Proxima-like." Systems with an orbit this size or larger are marked on the plot with orange rings. This population is examined with further simulations in the next section.

The majority of systems are disrupted (small dots in left hand panel). In most

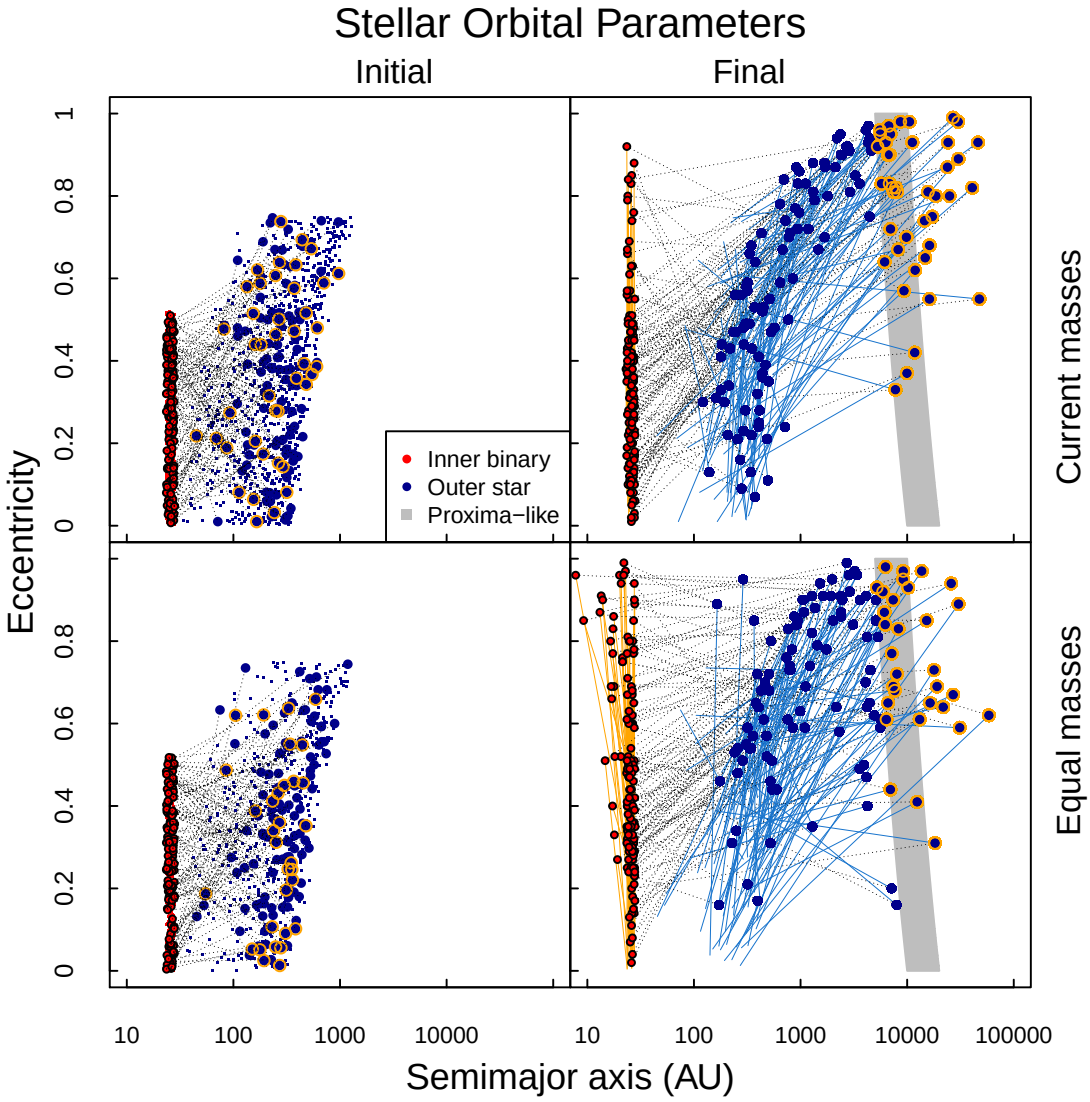

Figure 3.1: Initial (left) and final (right) parameters from 947 simulations using current stellar masses (top) and 575 simulations where all stars have masses of 0.123 $M_\odot$ (bottom). Dots in the left panels represent initial parameters for Alpha Centauri B (red) and C (blue). Large dots show simulations which survived, while small ones were disrupted. On the right, final parameters for surviving simulations are marked with large dots, with lines connecting them back to their original parameters. Faint dotted lines connect the stars to their companion from the same simulation. The shaded region shows "Proxima-like" orbits with apocenter between 10,000 and 20,000 AU, and orange rings mark system with final orbits with this separation or larger.

Table 3.2: Outcomes of Simulations

	Late	Early
Total Number	947	575
Survived (%)	14.4	24.3
Expanded (%)	13.3	22.6
Proxima-like (%)	4.44	5.94
Huge orbit (%)	0.634	2.64
A Ejected (%)	0.739	13.8
B Ejected (%)	0.211	8.2
C Ejected (%)	84.5	52.6
Collision (%)	0.211	0.696
Broken* (%)	1.9	16

Table 3.3: Median change in orbital parameters

	Late	Early
a_B	-0.045	-0.035
e_B	0.027	0.354
i_B	13.0	37.25
a_C	9695.87	8852.03
e_C	0.4	0.4805
i_C	-9.8	-4.7

of the surviving systems, star B's semimajor axis decreases a small amount and the eccentricities of both B and C increase. The initial orbital conditions do not appear to predict whether a system will survive or become Proxima-like.

Table 3.2 shows the types of outcomes as percentages of the total number of simulations of each type. Comparing the two stellar mass cases, the rate of surviving systems and Proxima-like systems are similar for both the current and equal mass cases, but the fates of disrupted systems differ. In the case where all three stars had small masses, it was far more likely for one of the central stars (A or B) to be ejected, whereas in the other mass case, the outer star's smaller mass made its ejection much more likely. In addition, an error in MERCURY's output caused by a very high kinetic/potential energy ratio occurred far more often in equal-mass cases, indicating higher-energy ejections. MERCURY does not save orbital parameters directly, but stores the value $f_v = \frac{1}{1+2(K/U)^2}$ (where K is

the kinetic energy and U is the binding energy) in a condensed format of eight 224-bit characters, from which ELEMENT can later calculate them. This allows for a precision of $224^{8-1} = 2.83 \times 10^{-10}$ in f_v, so for K/U ratios of $\gtrsim 42,000$ it experiences underflow error and may output $f_v = 0.0$, despite this never being correct for a physical system. This causes the calculations for orbital parameters to return infinity, NaN, or 0. Although the internal values remain unaffected and the integration continues successfully, some time-series information can be lost in cases where the ratio of the star's kinetic to potential energies is particularly large. This only affects stars which are being rapidly ejected, and thus is not significant for the results of our study, which is primarily concerned with the bound systems.

It seems that for most systems with the current stellar masses, the inner stars' orbit was only slightly altered; a decreased by only a fraction of an AU in most cases, while eccentricities and inclinations sometimes remained similar and sometimes increased significantly. For the case in which all three stars have small, equal masses, the changes in orbital parameters are more pronounced, particularly in eccentricity increases. The median changes in orbital parameters are shown in Table 3.3.

Typically, the triple system remains clearly hierarchical as intended, with the outer star well-separated from the inner system. In a few cases this assumption did not hold, which brings the system into a regime where the integrator used is not accurate. These systems were ignored. This implies that the region of parameter space in which the stars do not remain well separated is unexplored, but this appears to be an unlikely way to form the system in question and does not significantly skew our results.

The evolution of the system to a Proxima-like structure generally followed one of two paths. Most commonly, the system began in a state that quickly moved in and out of stability as the gas cloud dispersed, then froze in at a large stable orbit as the gas potential finally disappeared after 440,000 years, consistent with the scenario in which interactions occur early on; an example system is shown in Fig. 3.2. (Because of the gas cloud potential, initial calculations of the outer binary's eccentricity are incomplete, which is why the eccentricity sometimes appears to be greater than zero initially.) Less commonly, the system remained tightly bound but subject to significant Kozai-Lidov oscillations or general three-body interactions which pushed it into a large orbit at late times (10-100 Myr). We also observe slow (≈ 1 Gyr) Kozai-Lidov oscillations between the eccentricities and inclinations of the inner

binary and outer star, causing a gradual oscillation in their pericenters, which may be significant for disk and planet stability.

3.3.2 Disk Simulations

We performed simulations of coplanar test particle disks around Alpha Centauri A and B, in pairs of simulations using the same initial conditions in all ways except that one included Proxima Centauri while the other did not. These simulations indicate the region of stability around each star in which protoplanetary disk material can remain throughout the star's lifetime, allowing for later planet formation. The initial conditions for these systems were copied from the simulations that produced Proxima-like systems in the previous section. Due to the extremely sensitive, chaotic nature of dynamics and the finite precision of floating point number computation, sometimes the simulations resulted in different final orbits from the original version. Therefore, the following analysis will make a distinction between when all simulations are being discussed, or only those which resulted in Proxima-like final configurations.

Generally, we find that the disk particles are truncated at some distance from the star, which we call the truncation radius r_{tr}. The edge is clean, in that almost all particles' orbits within this radius remain stable, while almost all particles beyond this point are removed from the simulation through ejection or collision with a star. The behavior of disks around the two stars in the binary is very similar, with a slightly larger disk remaining around the slightly larger primary star (companion mass ratio = 0.85). Typically, in simulations without the third star, the outer portion of the disk was destabilized within about 10,000 years, while disk material within a certain truncation radius (r_{tr}) remained stable for the 10 Myr duration of the simulations. The presence of the third star induced additional truncation of one or two AU at around 100,000 years, as the binary's pericenter shrinks (see Fig. 3.4).

Although previous literature commonly discusses disk extent as a fraction of the binary's semimajor axis, we find the minimum pericenter p_{min} (the smallest observed pericenter over the course of the simulation, or $\min(a(1-e))$ where a and e are the binary's instantaneous semimajor axis and eccentricity), to be the most relevant parameter and will primarily discuss the disk extent in relation to it.

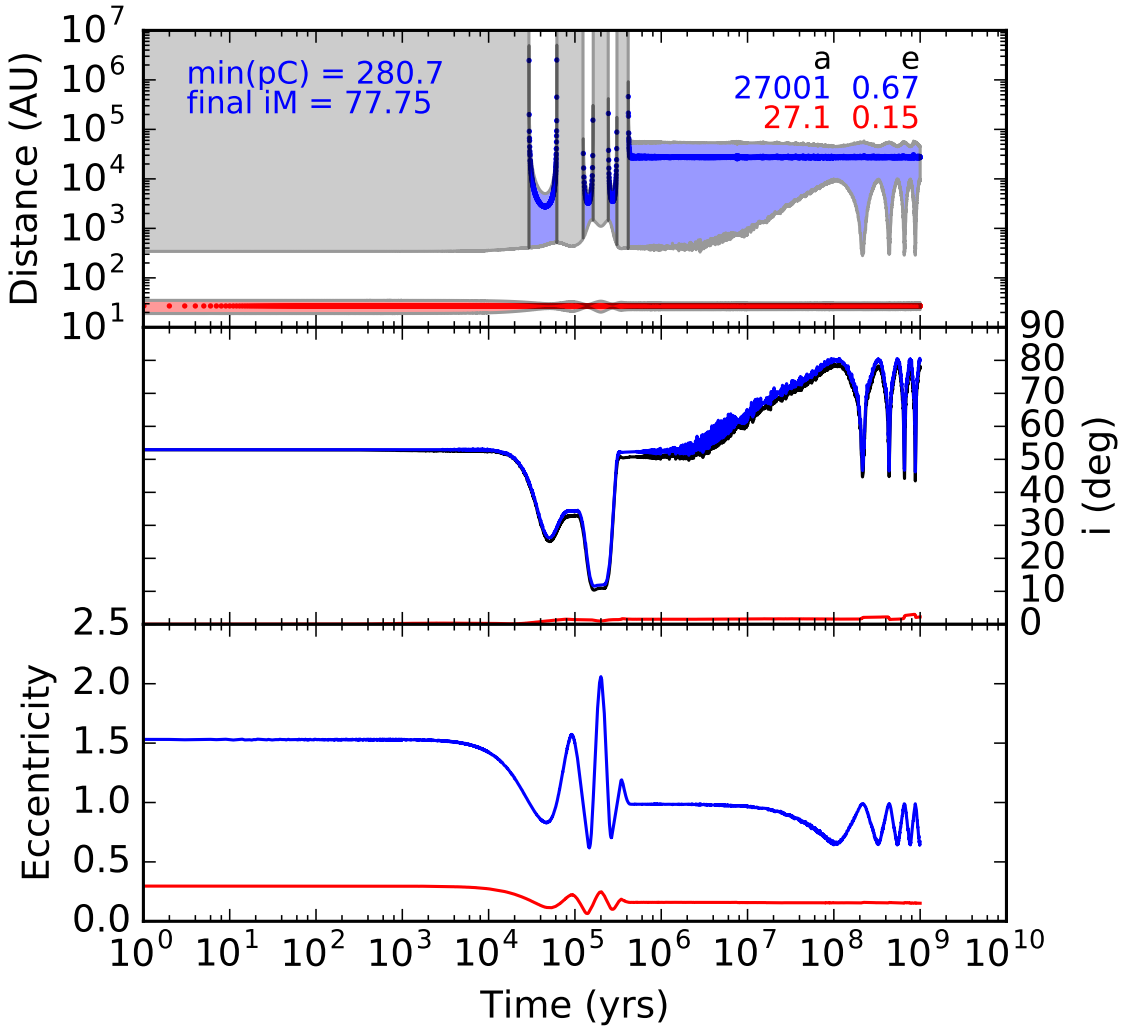

Figure 3.2: The evolution of a representative triple star system. Inner binary system parameters are shown in red, while the outer star's orbital parameters relative to the inner binary's center of mass is shown in blue. **Top:** Points indicate semimajor axis over time, with shading extending from pericenter to apocenter. For the outer star, due to the gas potential the calculated orbit sometimes appears unbound, in which case the area from the pericenter up is shown in gray. **Middle:** System inclinations relative to the binary's initial inclination, and their difference (black). **Bottom:** Eccentricities, using same color convention.

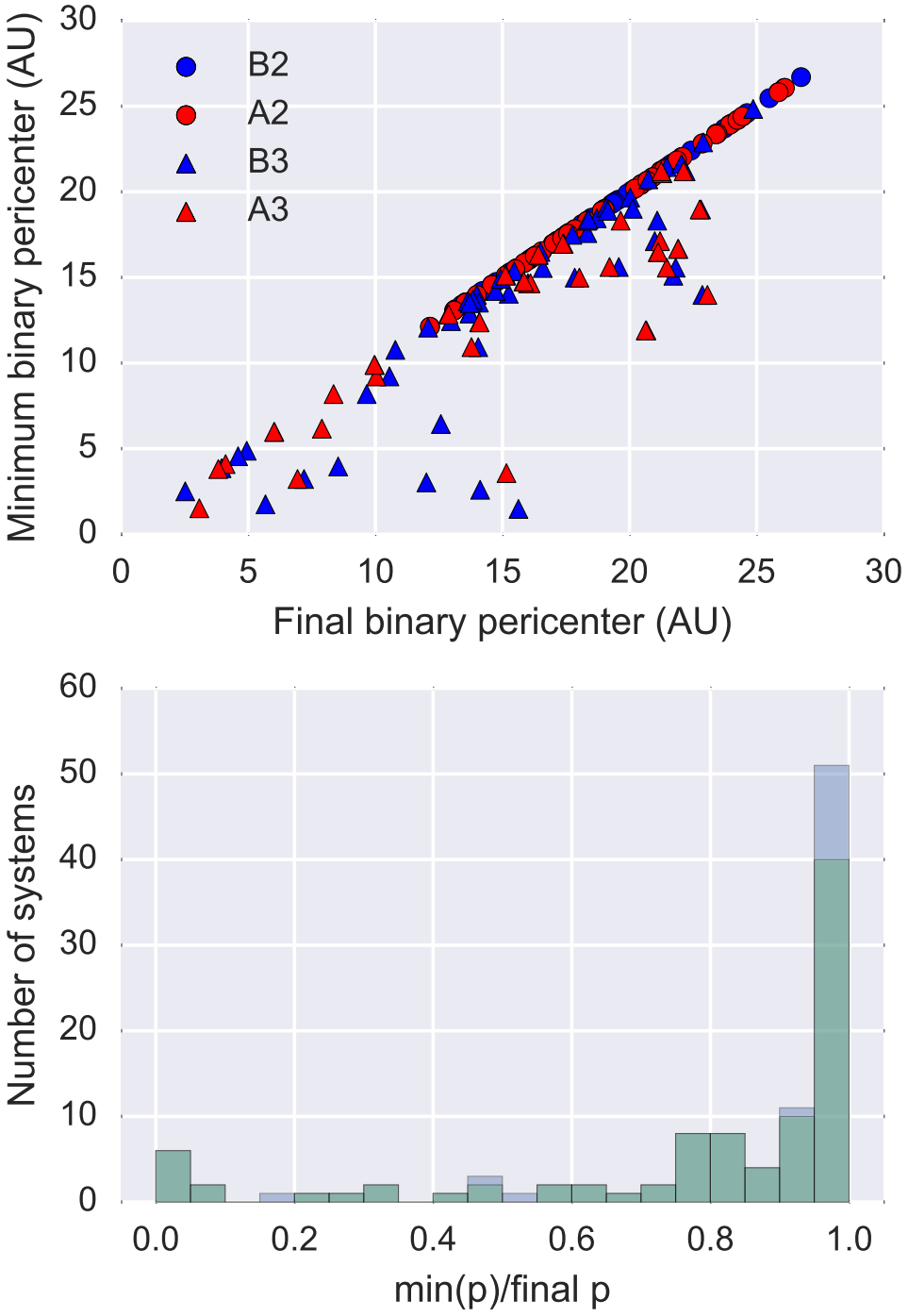

Figure 3.3: (a) Minimum binary pericenter vs. final pericenter for each disk simulation. The legend indicates the simulation group, where "B2" indicates two-star simulations with a disk centered on star B, "B3" indicates a similar three-star system, etc. (b) Histogram of the inner binary's minimum pericenter in simulations which did (green) and did not (blue) produce Proxima-like systems, as a fraction of the final pericenter.

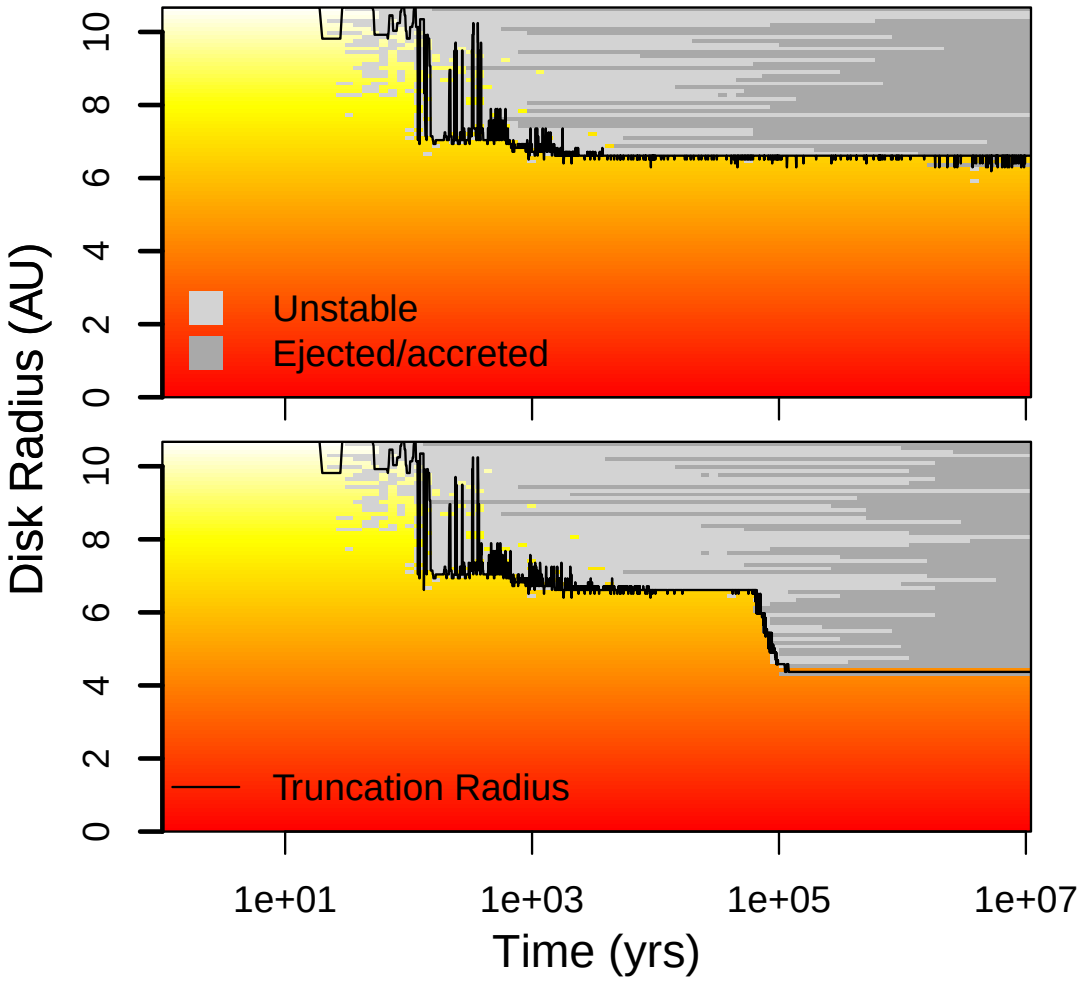

Figure 3.4: Disk survival for a typical early-interaction Proxima-like simulation of a disk around Alpha Centauri B, for (top) the binary, and (bottom) the triple. The presence of the third star typically removes about 1-2 AU of the disk in the equal mass case. Disk material within the truncation radius remains undisturbed.

The binary's closest approach, while probably an even better predictor, cannot be reliably measured because the orbital parameters are output at a finite number of timesteps which often miss the closest approach. In most cases, minimum pericenter closely tracks closest approach, but because it is based on instantaneous parameters, it sometimes gives odd results in quickly-evolving systems (see the discussion of outliers below).

Ultimately, the binary's minimum pericenter over the course of the simulation is the best predictor we have of the final disk truncation radius, with a Pearson

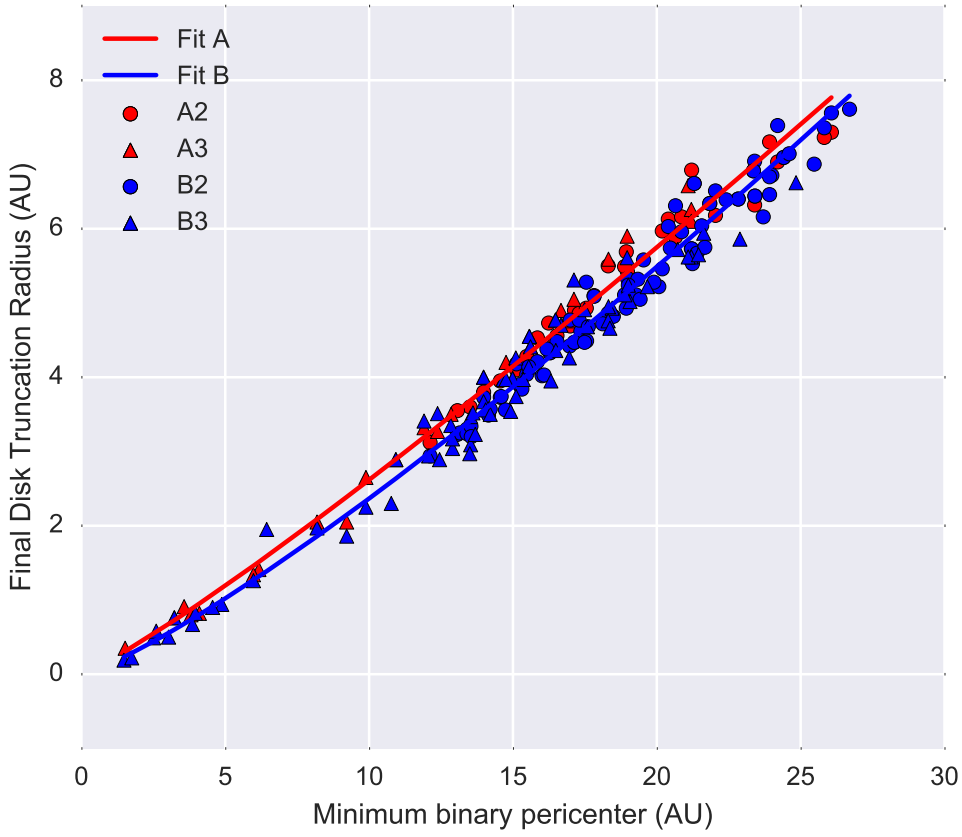

Figure 3.5: Truncation radius vs. minimum pericenter. As in Fig. 3.3, "A2" indicates a two-star simulation with a disk centered on star A, etc. Red points show disk simulations centered on Alpha Centauri A, while blue are B. Circles show simulations including only the inner binary stars, while triangles contain Proxima as well. The lines show power-law fits to the points of the same color. Outlier points identified in Fig. 3.6 were excluded from this plot and the fits. Large points indicate simulations which resulted in a Proxima-like orbit. The coefficients of the fits are shown in Table 3.4.

correlation coefficient $R = 0.95$. Exclusion of the seven outlier points, discussed more below, improves this correlation to 0.987. Of the directly observable system properties, final binary pericenter p_f (instantaneous pericenter at the end of the simulation) is also a good predictor ($R = 0.91$), as the final and minimum pericenters are themselves strongly correlated ($R = 0.90$).

The distributions in these simulations are non-Gaussian, so rather than using

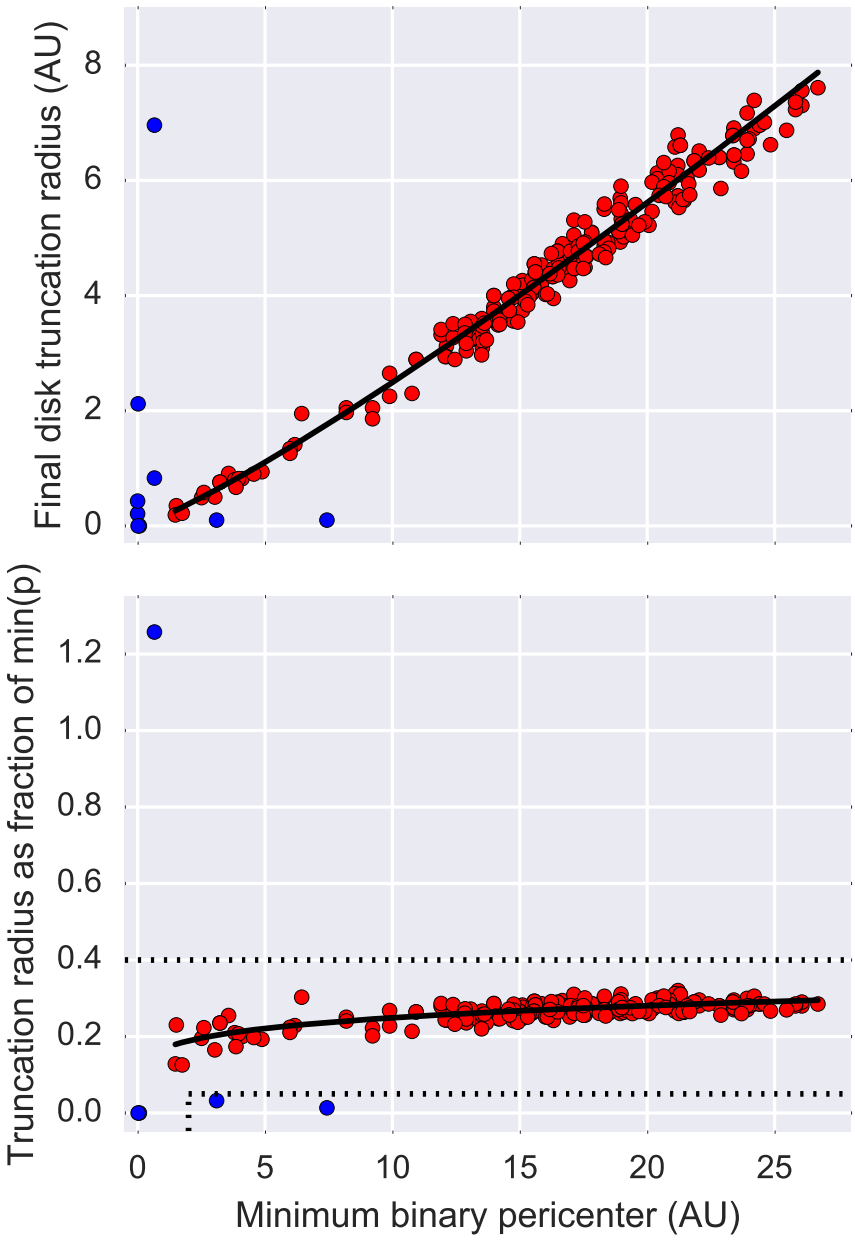

Figure 3.6: (a) Truncation radius vs. minimum pericenter. The red points are considered part of the main trend, while the blue points are outliers. The black line shows the fit to all disk simulations ("Both" in Table 3.4). (b) The above data with truncation radius as a fraction of the minimum pericenter. The dotted lines show the boundaries used to exclude outliers. Two more outlying points, with pericenters close to zero and truncation radii many times larger, lie far off the vertical scale, and another two are unplottable because their p_{min} values round to zero.

Table 3.4: Truncation radius model coefficients

Subset	a	b	R^2
A	1.14	0.192	0.9926
B	1.21	0.145	0.9862
Both	1.17	0.168	0.9839

Coefficients for a power law model predicting disk truncation radius r_{tr} as a function of minimum binary pericenter p_{min}, of the form $r_{tr} = b \times (p_{min})^a$. The leftmost column indicates which subset of the data the model was fit to: disks centered around Alpha Centauri A or B, or both sets combined. The fits are shown in Fig. 3.5. The score column shows the model's coefficient of determination.

the mean and standard deviation to characterize ranges of values, we use the more robust median and median absolute deviation (MAD). The median radius at which the disk was truncated in simulations with the Alpha Centauri binary alone, in units of the minimum binary pericenter p_{min}, was $0.281 p_{min} \pm 0.014$ for disks around Alpha Centauri A, and $0.267 p_{min} \pm 0.016$ for B. The minimum pericenter in simulations with a third star was a median of $18.3\% \pm 26.5\%$ smaller than binary simulations with the same initial orbits, resulting in a corresponding reduction in disk radius. The outcomes for r_{tr} in triple systems covered the full possible range, from disks the same size as the binary-only simulation, to 100% loss of disk material. The relationship between minimum and final pericenter is shown in Fig. 3.3a and the distribution in Fig. 3.3b. The fractional truncation radius in triple systems is similar to the binary case, but slightly smaller and with a larger spread: $0.274 p_{min} \pm 0.030$ and $0.264 p_{min} \pm 0.027$ for disks around Alpha Centauri A and B respectively.

The main trend between truncation radius and minimum pericenter can be fit very well with a power law using an exponent slightly above 1, as shown in Fig. 3.5. Coefficients for a power law model fit to disks centered on Alpha Centauri A or B, and on the combined dataset, are shown in Table 3.4. There were 150 simulations around Alpha Centauri B and only 74 around A due to logistical limits on computation time and greater observational interest in B, so in the combined fit the A samples were weighted proportionally higher. A similar trend is seen around each star, with slightly larger disks remaining around the more massive one, as is expected.

This is consistent with previous studies by Holman & Wiegert (1999), which

examined stability in coplanar binary disks for varying eccentricities. According to their Table 4, they found "critical semimajor axes" (equivalent to our "truncation radius") of 2.79 and 2.54 AU around Alpha Centauri A and B, respectively. Our estimates of 3.0 and 2.7 AU for the current pericenter of 11.2 AU are roughly similar, though somewhat higher; the differences are likely due to their assumption that the truncation radius as a fraction of semimajor axis does not vary with semimajor axis, where in our model it does, and possibly also due to the different integrators used.

Although the power law model fits the data very well in the studied parameter range, because the exponent is larger than one, the predicted disk radius as a fraction of the pericenter can become arbitrarily large as the binary orbit grows in size, and could eventually surpass the binary orbit itself, which is clearly unphysical. Therefore, we expect the relationship must become linear or otherwise change at large separations; further study is needed before extrapolating to larger binary orbits. Additionally, the model coefficients' apparent dependence on mass should be studied at more stellar masses and mass ratios.

All but nine of the 224 stable disk simulations have a r_{tr}/p_{min} value lying between 0.05 and 0.4. These outlying points are identified in blue in Fig. 3.6a and b. Seven points appear to be outliers from the main trend, and are omitted based on the cuts shown in the dotted lines of Fig. 3.6b, which were chosen by eye. The five systems lying above this limit do so because their binary pericenters drop to nearly zero for a very brief time (less than an orbit) while the gas cloud is dispersing, and the stars do not actually pass this close to each other before continuing to be perturbed into another orbit, so the disk is not significantly perturbed. Two points also lie below the trend, with truncation radii of 0.1 AU but minimum pericenters of several AU; these disks contain gaps at small radii that confuse the disk fitting algorithm. The other two blue points lie close to the origin, and are likely a continuation of the downward curve seen for small-pericenter systems. However, because their r_{tr} values round to zero, they are excluded along with the outliers because they must be omitted from the fitting algorithm, which requires taking log_{10} of all r_{tr} and p_{min} values. These nine simulations represent 4% of the three-star systems. When discussing the overall trend of disk survival these special cases are omitted. However, they are possible, though rare, outcomes of multistellar systems, and readers should remain aware that exceptions to the general trend

exist.

The minimum binary pericenter is the most important factor in determining the amount of disk material available for planet formation. When we observe a stellar system, we can only observe the pericenter it has now, without knowing how much smaller it might have been in the past and thus how much additional truncation may have occurred. However, most systems had minimum pericenters which were similar to or only slightly smaller than their final pericenters – the median minimum pericenter was 0.932 times the final pericenter. For the Alpha Centauri binary, with a current pericenter of 11.4 AU, this means we could expect the minimum pericenter the system has experienced to be around 10.6 AU. In our model for truncation radius as a function of pericenter, these values would imply disk truncation radii of 2.8 and 2.5 AU, respectively. Obviously, the possible values for minimum pericenter and truncation radius extend down to zero, and properties from the past are no longer observable. Our goal is to find the most probable values.

The final truncation radius for the disk is closely correlated with the pericenter of the inner binary, and since the change in semimajor axis is generally small, the degree of truncation is primarily a tracer for the amount by which the third star increases the eccentricity of the inner binary. Systems in which the binary's size was considerably reduced necessarily had smaller disks, but those with larger semi major axes could have disks that are either large or small, depending on their eccentricity.

For systems which end up similar to Proxima Centauri, the precise parameters of the outer star were not predictive of any other simulation parameters, including inner binary orbit or disk stability. The two systems with particularly large a_C did see less truncation, but there was no statistically significant correlation. It appears Proxima does not directly interact with the stability of disks in the system, but rather induces changes in the binary, which acts as an intermediary.

The above numbers assume the more likely situation, in which triple-system interactions take place early in the stars' lifetimes (that is, when all three stars are still small). This means that Proxima's influence on the binary stars is larger compared to late-stage interactions in which they have accreted more mass. In this less physically plausible case, the inner binary's orbit changes by a relatively small amount; the median pericenter reduction from the two- to three-star case

Table 3.5: Total Dust Mass in Truncated Disks (M⊕)

	r_{tr}	2.5			2.8			AU
α	r_{ice} / σ_0	2.5	2.7	3.0	2.5	2.7	3.0	AU
	0.3	0.39	0.37	0.37	0.56	0.45	0.41	
1	1	1.17	1.11	1.11	1.67	1.34	1.23	
	3	3.52	3.33	3.33	5.00	4.02	3.68	
	0.3	1.16	1.12	1.12	1.49	1.27	1.20	
3/2	1	3.49	3.35	3.35	4.48	3.81	3.59	
	3	10.46	10.05	10.05	13.45	11.44	10.76	

was $3.7\% \pm 4.9\%$.

3.3.3 Implications for Planet formation

The effects of any potential past interactions between Alpha and Proxima Centauri will have resulted in the orbital parameters we see today. The most likely interaction based on our simulations was an increase in eccentricity in the binary, resulting in a smaller pericenter and removal of an outer portion of the protoplanetary disk. This means that at one time there likely was more material in the disk, but it would have been removed well before the epoch of planet formation. The only clear signature we predict would be a slightly smaller disk than if the binary had formed in isolation. Assuming disks of these sizes, we consider expected planet formation in each case, first through an analytic method, then with N-body simulations of planet formation.

3.3.3.1 Planet formation: Jang-Condell Model

Jang-Condell (2015) proposes an analytic method to predict the ease of planet formation in binary star systems based on the amount of disk material remaining, with additional background found in Jang-Condell (2007); Jang-Condell et al. (2008). The system is based on the number of simulations (out of a set of 18 total) retaining sufficient mass to form giant planets via the disk instability or core accretion methods (N_{DI} and N_{CA}). An equation is then fit to the cases explicitly simulated, which allows one to predict how many simulations would allow planet

formation based on the masses (μ and M_*) and orbital parameters (a and e) of the system. This equation is reproduced here:

$$N = \sum_{i,j,k,l} c_{ijkl} \left(\frac{a}{1AU}\right)^i e^j \mu^k \left(\frac{M_*}{M_\odot}\right)^l \tag{3.5}$$

where the values of c_{ijkl} are found in Table 3 of Jang-Condell (2015).

For Alpha Centauri, out of 18 simulations with a variety of disk parameters, three retained enough dust to form a solid giant planet core (i.e. $N_{CA} = 3$), compared with seven or higher for systems with confirmed planets. This puts the Alpha Centauri binary at the lower edge of the parameter space which allows for planet formation. Inferring the most likely initial parameters for Alpha Centauri by subtracting the median change in a and e in our simulations from its current parameters (giving $a_0 = 23.5$ AU, $e_0 = 0.16$) gives an analytic N_{CA} estimate of 11.2 based on Eqn. 1, implying giant planets would form easily in the pre-truncation disk; however, truncation occurs at approximately 100,000 years, significantly before core accretion is believed to occur. The pre-truncation disk instability parameter N_{DI} remains unfeasibly low at 1.89.

For the sake of estimating the likelihood of terrestrial planet formation, we follow the method of Jang-Condell (2015) in calculating the total dust mass likely to remain in the extent of the stable disks. Using the Minimum Mass Solar Nebula (MMSN) (Hayashi, 1981) as a point of comparison, we assume a power law density profile

$$\Sigma(r) = \Sigma_0 \left(\frac{r}{r_0}\right)^{-\alpha} \tag{3.6}$$

where $\Sigma(r)$ is the surface density at r, the distance from the central star; α is some exponent determining the slope; Σ_0 is a density normalization parameter; and $r_0 = 1$ AU. We can find the total disk mass M_{tot} for a given set of disk parameters (surface density normalization σ_0, exponent α, and ice line r_{ice}) by integrating from the inner disk edge r_i to the truncation radius r_{tr}.

$$M_{tot} = \int_{r_i}^{r_{tr}} \Sigma(r) 2\pi r dr \tag{3.7}$$

For $\alpha = 3/2$ and constant Σ_0, this simplifies to

$$M_{tot}(r_{tr}) = 4\pi \Sigma_0 {r_0}^{3/2} (r_{tr}^{1/2} - r_i^{1/2}) \tag{3.8}$$

while for $\alpha = 1$ it comes to

$$M_{tot}(r_{tr}) = 2\pi\Sigma_0 r_0(r_{tr} - r_i). \tag{3.9}$$

The disk density changes significantly at the system's ice line, r_{ice}, and each section must be integrated separately. Water inside this distance is photo-evaporated, while further out it remains frozen and contributes to the solid mass of the disk. The Hayashi values for Σ_0 inside and outside of the ice line are 7.1 and 30 g/cm^2 respectively.

The physical parameters of protoplanetary disks are still uncertain, so we consider a range of plausible values in four different parameters: r_{tr}, α, σ_0, and r_{ice}. The values of r_{tr} represent disks formed in systems with and without three-star interactions, as described in the previous section. The potential range of disk densities is not yet well understood, so we multiply the density normalization Σ_0 by a scale factor σ_0 between 0.3 and 3, scaling the total density relative to the MMSN. Canonically, $\alpha = 3/2$ and $r_i = 0.35$ AU. Although the 3/2 slope value is favored in theoretical disk calculations, observations tend to favor $\alpha = 1$; we use both values here. For $\alpha = 1$ cases, we scale the density Σ_0 such that the total mass in disks out to 36 AU would be equal. The location of the ice line is not precisely determined, and so we use a range of values (2.5, 2.7, and 3.0 AU) that encompass commonly used Solar values. Alpha Centauri B is slightly smaller and cooler than the Sun, while A is slightly larger and hotter, so we assume that the variation in ice line location with stellar mass is small compared to the uncertainty in location we have already included. Additionally, we assume that the stars' separation is sufficiently large that they do not strongly affect each others' ice line locations.

Using these values, we calculate the total dust mass of the disk that will remain stable after interactions remove the outer mass. The values are shown in Table 3.5. The total dust mass values range from less than 0.1 to more than 10 $M_\oplus$. Assuming canonical physical properties and efficient accretion, we expect Alpha Centauri B to have formed several terrestrial planets within a few AU, indicating a significant probability for planets in the habitable zone. The density normalization σ_0 is the most significant parameter for determining the likelihood of planet formation,, followed by the slope α. The other parameters (r_{tr} and r_{ice}) have relatively minor effects.

3.3.3.2 Planet formation: Planetesimal Disk Simulations

We performed simple planet formation simulations to estimate the types and locations of planets that could exist in the Alpha Centauri system, similar to those in Quintana et al. (2002) etc. We begin from the planetesimal stage and simulate collisional accretion for 100 Myrs, until a stable population results. Extensive studies of planet formation in the modern Alpha Centauri system and other binaries have been done (e.g. see Quintana et al. (2007)), and our goal here is not to supersede or recreate them, but rather to test the strength of the influence of uncertainty in the initial disk model's physical parameters in comparison with small differences in truncation radius. Collisional modeling has also advanced significantly, e.g. Leinhardt & Stewart (2012), but such models are computationally expensive and introduce many new parameters, and as such are beyond the scope of this study, though would be appropriate for follow up studies. We focus in this section on planets around Alpha Centauri B as it has been the focus of more planet detection activity, but the above disk simulations show the environment around Alpha Centauri A to be qualitatively similar.

Table 3.6: Mean number of planets per simulation

	All		**HZ**	
$\boldsymbol{\alpha}$ / $\boldsymbol{\sigma_0}$	1	3/2	1	3/2
3	3.2	3.5	1.5	0.8
1	1.2	4.2	0.5	1.3
0.3	0.0	0.8	0.0	0.0

The initial configuration is a planetesimal disk around Alpha Centauri B with half the mass in Moon-sized objects and the other half in Mars-sized objects. All planetesimals initially have zero eccentricity and inclination, and are spaced such that the density of the disk follows Eqn. 3.6 out to some truncation radius r_{tr}. Alpha Centauri A orbits the system at its current distance and eccentricity. This configuration represents the system after it has interacted with Proxima Centauri – the stars have attained their current orbital configuration and the truncated disk has evolved into planetesimals and planetary embryos. Proxima is by this point too distant to have a noticeable effect and is therefore omitted.

We vary three parameters to compare their relative significance to planet formation: α takes the values 1 or 3/2; Σ_0 is multiplied by either 3, 1, or 0.3; and r_{tr} values of 2.5, 2.8, and 3.1 AU were tested. The first two r_{tr} values are those predicted for the Alpha Centauri system with and without Proxima interactions in Section 3.2, above. The set of simulations using the third value, $r_{tr} = 3.1$ AU, was created based on preliminary calculations, but is included because it further reinforces the truncation radius relationship found in the disk simulations above: a significantly higher fraction of the disk mass was ejected from disks containing material beyond the expected outer radius, leaving systems otherwise broadly similar to those of the $r_{tr} = 2.8$ AU set. For each combination of parameters, two simulations were run, all of which can be seen in Figs. 3.7–3.9.

We are using the arbitrarily-chosen mass cutoff of at least 3 M_{Mars} as the threshold to consider objects planets, to separate out unprocessed disk material; the number of planets per simulation based on this metric can be seen in Table 3.6. Simulations with at least the density of the MMSN resulted in systems of multiple terrestrial planets, frequently including planets in the habitable zone, while low-density simulations might form only one object large enough to be considered a planet by our definition. We defined the HZ boundaries as 0.693 to 1.241 AU, based on the conservative limits from Ravi Kopparapu's habitable zone calculator (Kopparapu et al., 2014, 2013) using Alpha Cen B's parameters. For a planet in this region, at closest approach, Alpha Cen A would contribute no more than 5% the flux of B, which would move the bounds of the HZ inward by a small amount. Therefore, we use the single-star HZ as an approximation for this study; however, for further discussion of the binary's influence see Forgan (2012).

The characteristics of the final system were most strongly dependent on the disk model parameters, particularly density. The small difference in truncation radius is unimportant in comparison. In systems with 0.3 times the MMSN, the debris remained in many small objects, and all of the final bodies were smaller than one $M_\oplus$. Systems with 1 or 3 MMSN formed several Earth or super-Earth sized planets, but in fewer numbers. Little disk material survives beyond the ice line, so the planets may be lower in volatiles and will likely resemble terrestrial planets rather than mini-Neptunes. However, the water fraction for a planet like the Earth is quite low compared to that of material beyond the ice line, so we do not consider this a barrier to habitability.

3.3.4 Planets around Proxima

Although we did not explicitly perform simulations of disks or planet formation around Proxima Centauri, we can make some predictions in this regime. Proxima's closest approach during its interaction with the binary ranges from several hundred AU to within the binary's orbit, though it tends to be on the larger end. If we assume that the trend in disk truncation relative to minimum pericenter continues linearly at larger separations with $r_{tr} \approx 0.3 p_{min}$, then in the typical case where Proxima remained several hundred AU from Alpha Centauri, it could retain disk material within several tens of AU, sufficient to form planetary systems though possibly tending towards somewhat smaller planets than it would otherwise have. If, however, the star made a close pass of the inner binary, it likely would have lost most or all of its disk material. If future observations are able to rule out planetary companions to Proxima Centauri, this may be an indicator of past close interactions within the triple star system. Detection of planets could be used to put a lower limit on close approach, in degeneracy with outward migration.

3.4 Conclusions

In a large suite of N-body simulations, we recreate possible pathways to the formation of the Alpha Centauri-Proxima Centauri system according to the method described in Reipurth & Mikkola (2012), and explore the effects this would have on planet formation around the individual stars. In typical scenarios, assuming a debris disk at least as dense as the Minimum Mass Solar Nebula, we expect several terrestrial planets to form within a few AU of the central star, with a high probability of a planet in the habitable zone.

We find it is plausible that Proxima formed at a distance of a few hundred AU from Alpha Centauri and was thrown out to the current (presumed) orbit at tens of thousands of AU while the stars were still accreting mass. In the process, it most likely caused the Alpha Centauri binary to see a decrease in semi major axis and increase in eccentricity, reducing the pericenter. This would cause truncation of the outer protoplanetary disk to a radius that scales with the binary's pericenter. Binaries which have undergone this type of three-body interaction in the past may have gone through a phase with a tighter orbit than it is now; the minimum

pericenter could take any value up to the present one, but is typically no more than 20% smaller). This additional truncation strips additional outer material from the disk, but in most simulations, enough material remains to form systems of terrestrial planets. Although the process of planetesimal formation, especially in binaries, is not yet fully understood, we make the assumption that the system was able to form planetesimals and planetary embryos, and then examine how planet formation would proceed from that point.

In our simulations of the Alpha Centauri system, the disk was typically truncated to near the ice line, likely preventing formation of gas giants and even Neptunes or mini-Neptunes. See Chiang & Laughlin (2013), Raymond & Cossou (2014), and Chatterjee & Tan (2014) for discussions of in situ versus migration formation pathways of close-in mini-Neptunes. Unless the initial disk had a much higher density than expected, high mass, close-in planets such as some found by Kepler (Fabrycky et al., 2014) are not expected here, with neither an outer region to form planets that migrate in, nor an outer well of material to feed an inner region while planets form in situ.

In addition, these interactions do not necessarily rule out the possibility of planets around Proxima, although an absence of planets may indicate a past close encounter and serve as a confirmation of triple system interactions involving a close pass.

Finally, we predict that if Proxima is orbiting at high inclinations, it may be inducing Kozai-Lidov oscillations in Alpha Centauri which will change its eccentricity on a Gyr timescale. It is uncertain whether this would increase or decrease the pericenter from the present value, but it most likely will not decrease it further than the minimum pericenter it has experienced previously, and so should not cause significant disturbance beyond the previous truncation. If, however, the outer star is perturbed enough by external forces such as passing stars, it could end up on a new orbit, essentially randomizing the system.

Overall, significant uncertainties remain, but our simulations indicate that, despite the possibility of a turbulent past, Alpha Centauri B and its companions are still likely terrestrial planet hosts. Missions capable of detecting or conclusively ruling out such planets would yield great insights into the formation of planets within multistellar environments. Any planets found would provide targets for detailed characterization, while a non-detection would be a good indicator of the

system having undergone disruptive stellar interactions, which helps constrain the fitness of multistellar systems as planet hosts. Therefore, we look forward to results from current and future searches of this system.

3.5 Acknowledgments

The authors thank the The Pennsylvania State University, NASA Astrobiology Institute (NNA09DA76A), and the Penn State Astrobiology Research Center for their support. Portions of this research were conducted with Advanced CyberInfrastructure computational resources provided by The Institute for CyberScience at The Pennsylvania State University (http://ics.psu.edu). Special thanks go to Prof. Eric Ford for directing us to Dimitri Veras' work on including Galactic tides in MERCURY. In addition, we thank the anonymous referee for thorough and helpful comments which contributed to the content and clarity of this work.

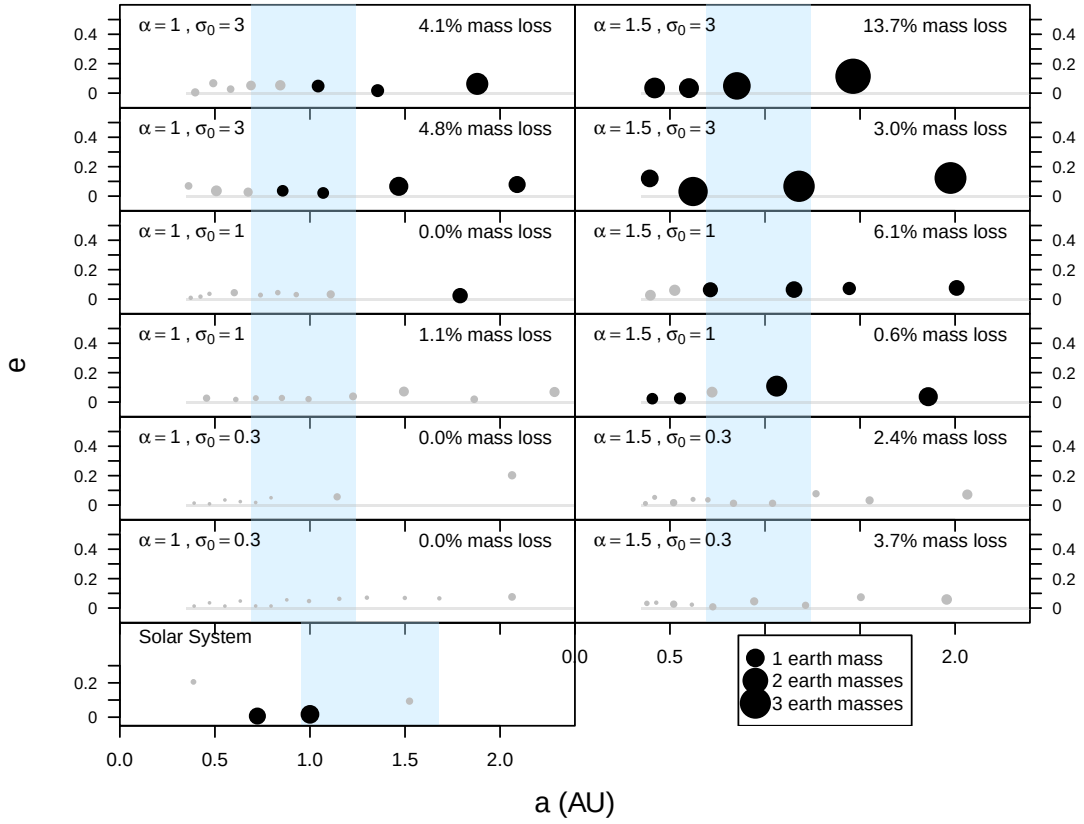

Figure 3.7: Semimajor axis and eccentricity of objects formed in the simulations with current Alpha Centauri binary orbital parameters and $r_{tr} = 2.5$ AU, representing the system after interactions with Proxima Centauri. The symbol size is proportional to the object's radius, and the bottom left panel shows the inner Solar System for comparison. Planets larger than $3M_{Mars}$ (0.32 $M_{\oplus}$) are plotted in black, and smaller objects in gray. Blue shaded region indicates the traditional conservative habitable zone. Grey shaded bars along the bottom of each plot show the original extent of the disk. The percentage by mass of the initial disk ejected or accreted onto the stars during planet formation is given on the top right. Each plot is labeled with the disk parameters in the top left, where the disk density scales with σ_0, and $\alpha = 1.5$ is the power law slope. $\alpha = 1.5$ and $\sigma_0 = 1$ is the Minimum Mass Solar Nebula.

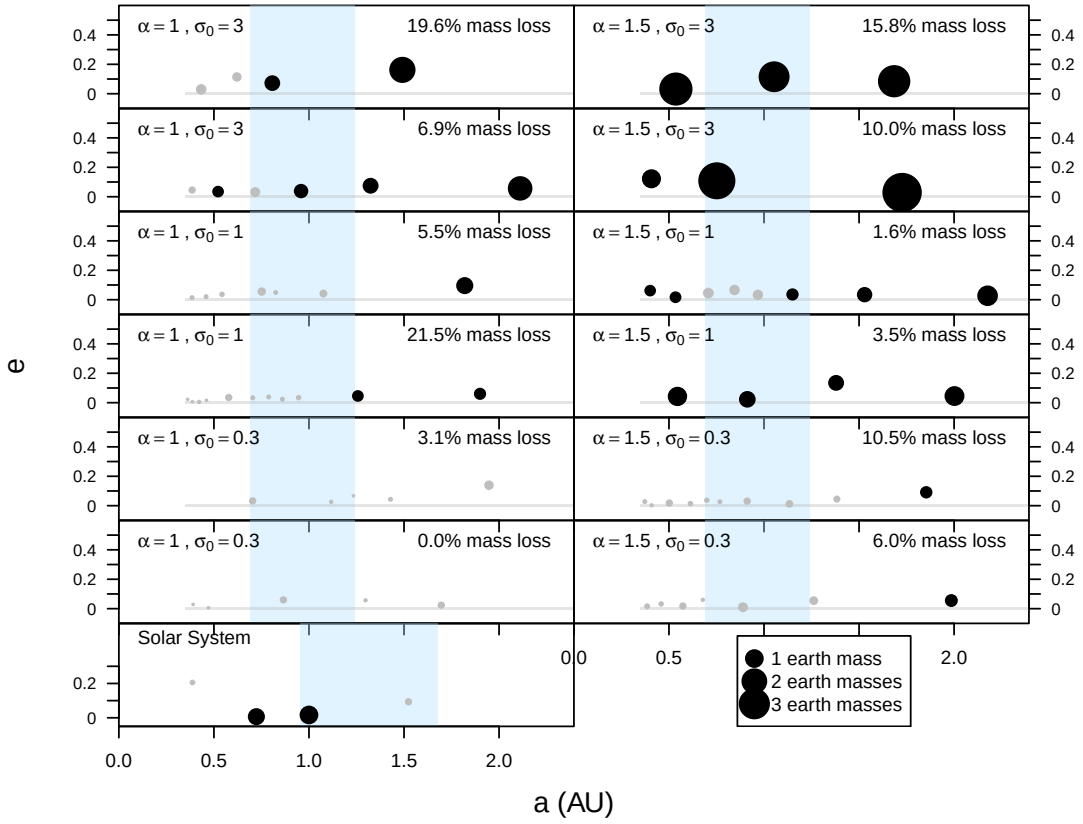

Figure 3.8: Same as Fig. 3.7 but for $r_{tr} = 2.8$ AU, representing the system assuming no interaction with other stars.

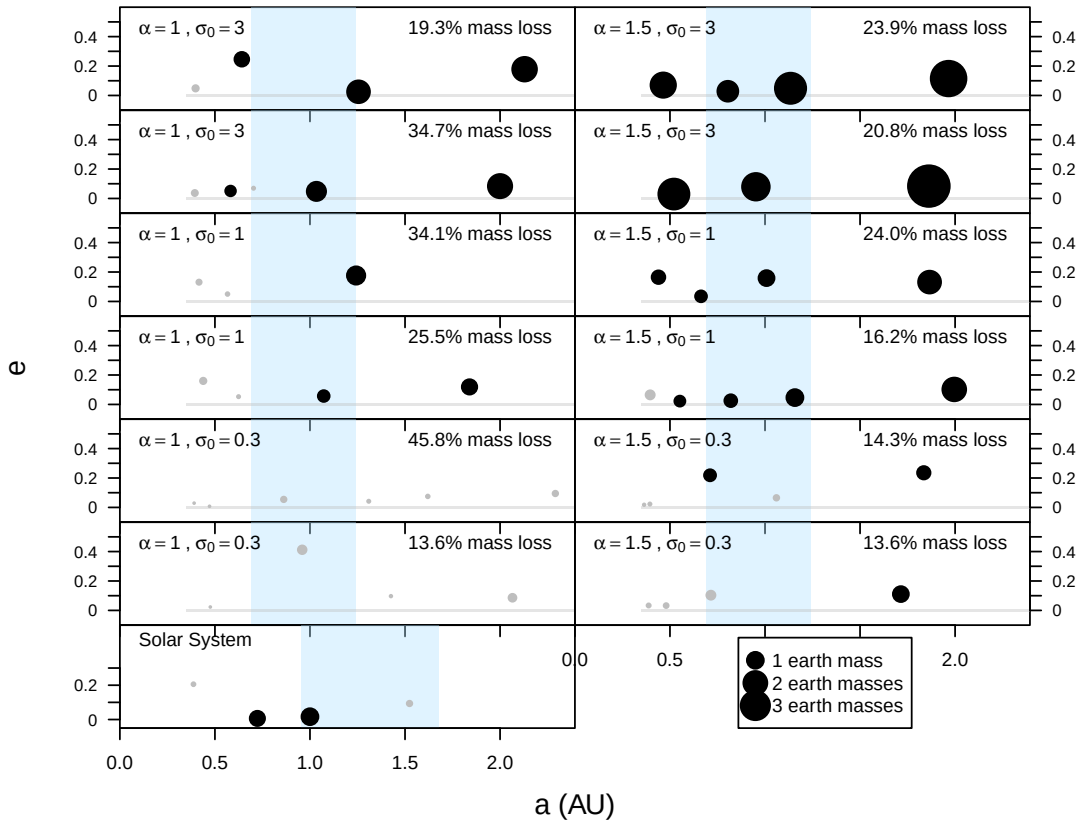

Figure 3.9: Same as Fig. 3.9 but for $r_{tr} = 3.1$ AU. The similarity to Fig. 3.8 in planets formed and the higher ejection rates confirm that material placed beyond the truncation radius of 2.77 AU is quickly removed.

Chapter 4
Audumbla: A Semi-Numerical Planet Formation Algorithm

We present a semi-numeric code to mimic the output of numerical planet formation simulations with as few parameters as possible. As computational power has increased, our ability to simulate planet formation has developed to the point that now we can begin to draw general conclusions about the way a debris disk of planetesimals evolves into planets. This algorithm is a way to codify and test qualitative assumptions about how planet formation works, focused on reproducing the mass and spacing of resulting planets. It is not meant as a replacement for thorough numerical simulations, as such studies still provide the calibration against which my model can be checked. However, using the proper assumptions, it allows one to form a set of planets from a debris disk in a tiny fraction of the time that a full numerical simulation would take. By comparing the results of this code with the output of n-body simulations starting from the same initial parameters, I can identify which aspects of planet formation can be reliably predicted and which are still unrepresented.

4.1 Introduction

By the 1990s, galactic astronomers had used N-body simulations to develop a significant body of knowledge about galactic evolution through hierarchical mergers. This approach built up a needed corpus about the physics of galactic structure, but was prohibitively slow and computationally demanding. In addition, some aspects of physics were not fully captured by N-body simulations. By developing a semi-

analytic approach that built on the knowledge gained from numerical simulations, scientists had a shortcut to the information they wanted (see Cole et al. (1994); Kauffmann et al. (1993); Lacey & Silk (1991); Somerville et al. (1997); White & Frenk (1991)). We seek to usher in a similar era in planetary formation.

At a high level, the process for both the galactic merger methods and my planetary formation method are the same: they take a population of small bodies and successively merge them with each other into a few larger bodies, walking through a tree-like structure as in Fig. 4.1 by starting at the leaves and proceeding down the branches. At each node, an interaction takes place which represents a complicated physical interaction, but simplifies it down to a single outcome based on statistical likelihoods: each time two planetesimals interact, they can either collide or scatter off one another. In a traditional N-body simulation the outcome is determined by a complex interaction of the physical parameters at the outset, and would be determined by integrating the motions of each one throughout a close encounter. We can generalize, however, to simply say that two objects interact, and have some percentage of merging, otherwise they scatter. As long as we choose a probability that accurately represents the physical system and correctly identify any systematic biases in the probabilities, this method will produce equally valid results with significantly less effort.

I present a prototype algorithm to recreate the most interesting output of planet formation simulations – the planets formed – as simply and quickly as possible. Of course, as our understanding of planet formation is still incomplete, this approach does not yet cover all possible parameter ranges, and the excellent, detailed numerical planet formation simulations being done by many research groups today are still absolutely essential to pushing forward the boundaries of our understanding. We aim merely to simplify and codify the knowledge generated by such work.

This project has much room for growth and would benefit from the input of the many esteemed planetary formation experts in our community to improve its accuracy and expand the range of scenarios it can handle. To that end, the algorithm is encoded in Python and available on GitHub (`https://github.com/RJWorth/Audumbla`) under the Creative Commons License. Users can also submit pull requests to the Git repository to suggest modifications for incorporation into the distributed code.

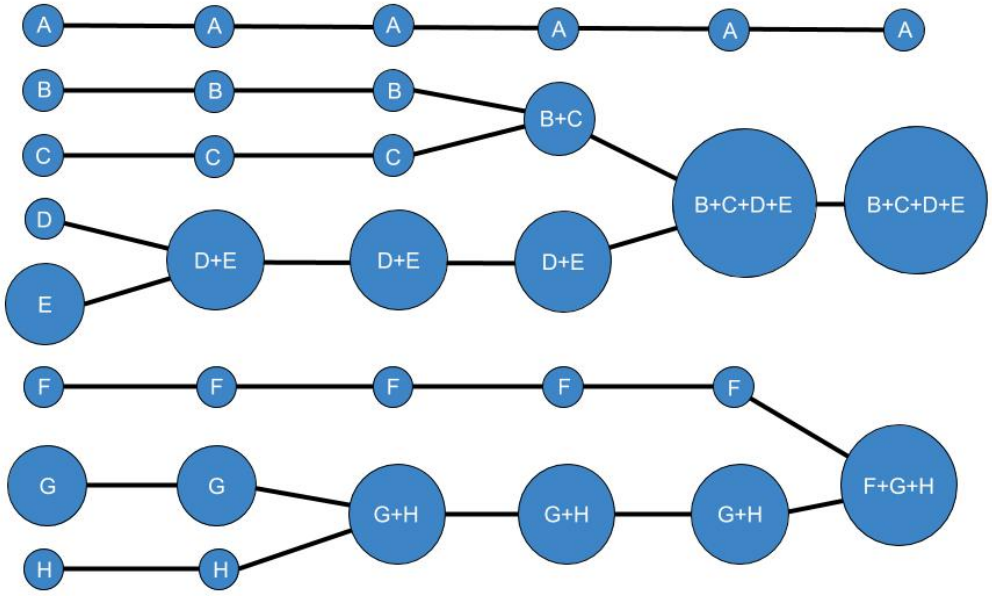

Figure 4.1: Graph tree representation of hierarachical merging algorithm, with the circles representing objects in the simulation. The leftmost column shows the initial disk, and each interaction moves us one column to the right, as objects are merged.

4.2 Current algorithm

Audumbla is a work in progress, meant to be developed further to more accurately capture the true behavior of systems. Here I describe the code as it currently stands, and also indicate areas in which further improvements are planned.

The algorithm generates a disk of coplanar objects from an underlying power-law density profile. This profile is based on Hayashi (1981), and is of the form

$$\rho(r) = \int_{r_i}^{r_o} \rho(r) r^{\alpha} \mathrm{dr} \tag{4.1}$$

where $\rho(r) = \rho_0 \times 7.1 \mathrm{g/cm}^3$ inside the ice line and $\rho_0 \times 30 \mathrm{g/cm}^3$ beyond it.

Currently, the user can choose an exponent $\alpha = 3/2$ or 1, though eventually this will be adapted to accept any reasonable value. The other disk variables are the radii of the inner edge, outer edge, and ice line (r_i, r_o, r_{ice}); a MMSN-density scaling factor (ρ_0); and a list of debris masses with a corresponding list of the

Parameter	Description	Default
r_i	Inner disk radius	0.35 AU
r_o	Outer disk radius	5.0 AU
r_{ice}	Ice line	2.7 AU
ρ_0	Scaling factor, where density = MMSN$\times\rho_0$	3
α	Density profile exponent (can be 3/2 or 1)	3/2
N_{R_H}	Maximum interaction separation in R_H	10
m	List of planetesimal masses	(M_{Mars}, M_{Moon}) in $M_\odot$
f_m	Target fraction of total dust mass in each of the masses in m	(0.5, 0.5)
f_{ej}	Fraction of interactions resulting in scattering and ejection	0
r_{dr}	Maximum particle drift allowed per interaction (inward, outward)	(0, 0) AU

Table 4.1: Definitions of the algorithm's input parameters, their default values, and units.

fraction of the disk that should be in each mass level.

Initially, each object only has a mass and semimajor axis, though eccentricity and inclination will be incorporated eventually. The probability of interaction between each pair of objects in the disk is calculated by taking the inverse of their separation in mutual Hill radii

$$R_H = \left(\frac{m_i + m_j}{3M}\right)^{1/3} \frac{a_i + a_j}{2} \tag{4.2}$$

$$P_{ij} = \frac{1}{\Delta a / R_H} = \frac{R_H}{a_i - a_j} \tag{4.3}$$

where m_i and a_i are the mass and semimajor axis of disk object i, and M is the mass of the central body of the disk. This results in interactions happening primarily between objects that are adjacent or nearly adjacent in the disk, as is typical in numerical simulations. The exact formulation of the probability of interaction is somewhat arbitrary at present, chosen to achieve the goal of favoring interactions between objects which are near each other, and also weighted more heavily toward larger objects. This is also the most computationally expensive part of the algorithm, as calculating this value between every pair of objects scales as $\mathcal{O}(n^2)$.

During each interaction, there is a user-specified probability that the smaller of the two objects will be scattered and removed from the disk. Eventually, the scattering step could involve more sophisticated interactions such as moving an object to the outer part of the disk without ejecting it completely, which may help more accurately reflect the movement of material within an evolving disk.

If scattering does not occur, the two objects are merged into a new object with their combined masses, and a new a which is chosen to conserve the kinetic energy of the original objects' orbits. When eccentricity has been implemented, the eccentricities will be determined by conserving the angular momenta of the merged objects. Between interactions, a random drift in a, r_{dr}, is calculated for each disk object, with maximum values inward or outward given by the user. This randomized drift does not strictly conserve energy, but allows for a simple computational procedure because all of the values are assigned independent of one another. Solving this problem correctly will complicate and slow the computation, but it should not scale worse than the current $\mathcal{O}(n^2)$.

The algorithm repeatedly calculates interactions as above until all objects in the disk are well separated. This is defined as when each object is separated from each other object by at least $n_{R_H} R_H$, where n_{R_H} is a user-specified constant. The choice of n_{R_H} essentially determines the stop time of the disk, and choosing too small a value will result in a disk which has not fully evolved. However, too large a value may result in a disk which forms only a few large objects containing most of the mass, which is not necessarily representative of reality. In typical simulations, a stopping separation of approximately $10R_H$ results in a reasonable final system, but further exploration should be done to determine the most appropriate value.

4.3 Evaluation

The program outputs a list of planets formed and the masses and semimajor axes of each of the bodies. We examine how the various input parameters affect the resulting output system, as well as how they interact with one another. We also discuss the range of parameter space that balances physical plausibility and agreement with comparison numerical simulations.

The final number of planets and their spacing is primarily dependent on the parameter N_{R_H}, which defines the separation at which objects no longer interact

and therefore determines when the algorithm stops. The total mass in the disk is determined by the density scaling factor ρ_0, which influences the resulting planetary masses, and the inner and outer radii of the disk r_i and r_o. The disk extent also strongly influences the extent of the resulting planetary system, as does the amount of drift allowed, r_{dr}. The drift can be set to zero, but numerical simulations of an annulus of debris result in planets that are spread significantly beyond the initial boundaries, and the drift parameter is necessary to mimic this behavior. Currently this parameter is simply a range bounded by two constants value in AU. The lower and upper limits, $r_{dr,in}$ and $r_{dr,out}$, determine how quickly objects can drift inward or outward within the system, and each object's drift is drawn from a uniform distribution between $r_{dr,in}$ and $r_{dr,out}$. The drift has also been scaled with the inverse of the object's mass, so lighter objects move around more than heavier ones. In the future, this parameter will also allow for drift limits which scale with the object's location in the disk and how much the surrounding disk has been cleared out. This is important in capturing the eventual stability of parts of the disk in which the remaining objects are well-separated, as seen in the inner part of the disk during the latter portion of the MERCURY simulation in Fig. 4.2b.

4.3.1 Comparison with MERCURY planet formation

For the very first versions of the algorithm, a simple "by-eye" comparison has been used to evaluate the qualitative similarities of the results. As *Audumbla* is refined, however, quantitative metrics become important. The relevant quantities we aim to reproduce are the number of planets in a system, their masses, and their separations. The planned evaluation techniques for subsequent improvements will require simulating a batch of systems with each method, using the same initial conditions as one another. The most appropriate test for consistency would be to determine whether the system parameters appear to have been drawn from the same underlying population, such as with a Kolmogorov-Smirnov test.

In order to calibrate the model against existing knowledge, I ran simulations in MERCURY (Chambers, 1999) starting from the same initial protoplanetary disk in order to compare results and performance. The disk parameters used for both were mostly the same as the defaults in Table 4.1, with the exception of r_o, which was reduced to 3.1 AU. In the *Audumbla* run, a value of $f_{ej} = 0.003$ was chosen to

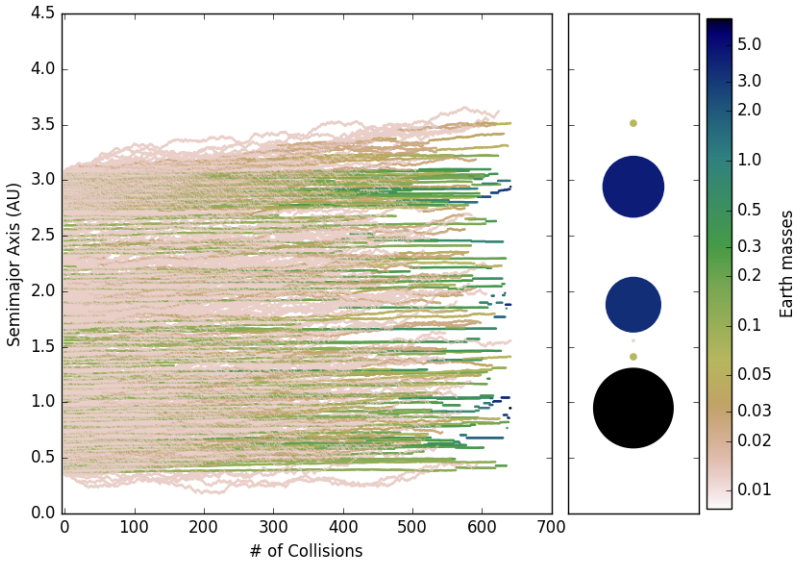

(a) *Audumbla*

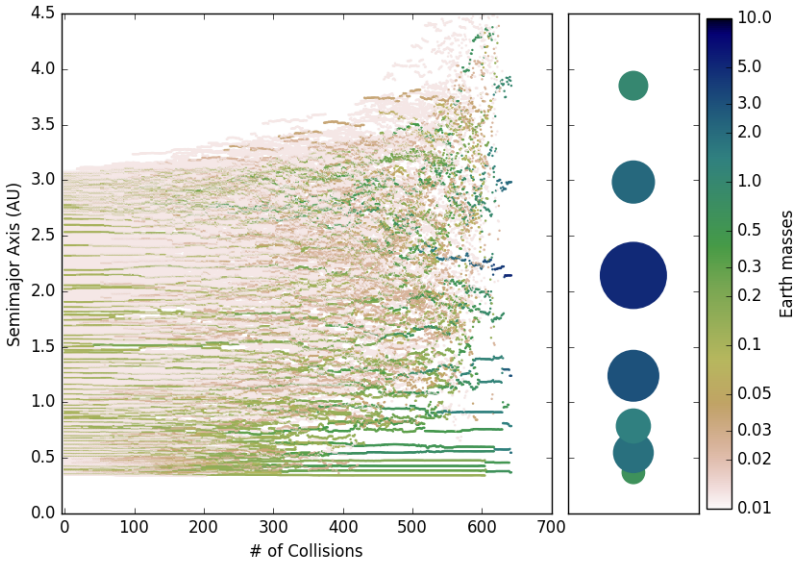

(b) MERCURY

Figure 4.2: Direct comparison of output of *Audumbla* with MERCURY on systems with the same initial conditions. Note that the x axis is not a measure of time, but number of interactions. The time metric used by the algorithm would result in more horizontal space between interactions on the right side of the plot, as later interactions take place between increasingly widely-separated bodies.

match the number of ejections in the MERCURY simulation, and the f_{dr} values used were (4×10^{-10}, 4.5×10^{-10}), chosen because they gave visually similar rates of disk expansion in the first two thirds of the simulation. Matching the much more rapid expansion seen in the latter part of the MERCURY simulation will require more sophisticated drift calculations.

Viewing the output of *Audumbla* and MERCURY side by side (Fig. 4.2), we see that both systems have similar numbers of surviving objects (six in *Audumbla*, seven in MERCURY), and in both cases the most massive planets are several $M_\oplus$. However, in the MERCURY simulation all of the surviving objects are planets with at least 0.5 $M_\oplus$ of mass, whereas in the *Audumbla* simulation, three of the surviving objects are smaller than the initial planetary embryos. The distribution of mass between surviving objects is skewed towards a few large bodies and some remaining unprocessed ones, indicating the probability function being used to choose interactions is weighted too heavily toward selecting large bodies. In addition, the pattern of movement of objects in the disk is very uniform throughout the simulation in *Audumbla*, while in MERCURY there are many complex behaviors seen at different times and locations. The algorithm must be updated to assign drift based on an object's surroundings and the amount of time represented by a given interaction.

The two plots show many discrepancies, certainly, but there is also a rough similarity overall, and this was achieved in less than ten minutes of wall time for *Audumbla* whereas the MERCURY simulation took thirteen hours. Many of the discrepancies can be addressed by adding new lines to the algorithm and tuning them appropriately. Although this will also add to the computational burden, it will almost certainly still be far faster than the MERCURY approach.

4.3.2 Annulus test case

One test cased being used to tune the behavior of the algorithm is that of a narrow annulus as in Hansen (2009), which used MERCURY to simulate an annulus extending from 0.7 to 1.0 AU, containing 2 $M_\oplus$ distributed equally between 400 planetesimals. In the original study, planetesimals are distributed either randomly or with equal spacing within the annulus. *Audumbla* assumes a power law distribution, for which I have used an exponent $\alpha = 1$ and a density coefficient of 13.15, which results

in the same number of objects in the annulus. In order to match the spreading of material inward from the initial annulus, the parameter $r_{dr,in}$ was raised to 4.45×10^{-10} AU per interaction.

The simulations in Hansen (2009) typically produced between three and five surviving objects, commonly two planets near the inner and outer edges of the annulus, similar to Earth and Venus, and some smaller bodies further outward or inward of the original ring, similar in mass and location to Mercury and Mars. My simulations produced a larger variation in the properties of the final system, with a tendency for smaller, more numerous planets. Systems typically consisted of a single large mass near the center of the original disk with progressively smaller bodies to either side. Migration away from the original ring can be roughly matched with random drifts (in AU per interaction for each object) between -4.45×10^{-10} and 4.5×10^{-10}, respectively. See Fig. 4.3 for examples of different types of systems formed by *Audumbla*, and Fig. 4.4 for the distributions of the planet parameters from MERCURY and *Audumbla* simulations.

The *Audumbla* simulations exhibit a peak in the center of the original ring because the mass tends to form one large mass near the center. In Hansen (2009) the mass tends to result in two large planets, one near either edge of the ring, which they state is an effect of conservation of angular momentum – the planned improvements to this area may help improve consistency between these results. In addition, the planets formed outward and inward of the rings are typically lower in mass than expected – improved angular momentum conervation and drift parameters should also help transport more mass into these regions. However, getting all the masses up to the expected range will require systems with fewer planets in the end, and it is unclear whether these modifications will affect that parameter.

4.3.3 Areas for Further Refinement

Audumbla currently conserves energy when choosing the semimajor axis for a new object after a merger. However, because there is no eccentricity parameter at this time, there is not yet a conception of angular momentum. This is one of the next planned improvements to the code. Including eccentricity will also allow for a more sophisticated process for selecting objects to interact, as we can determine which

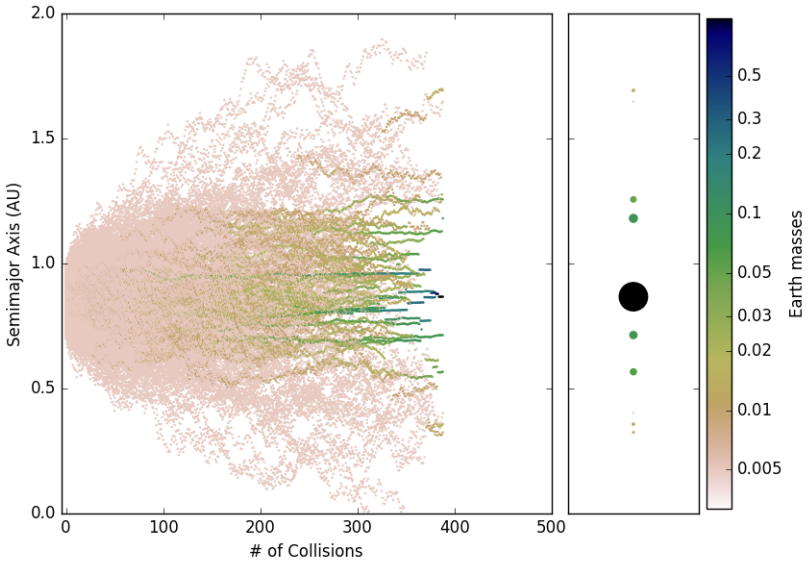

(a)

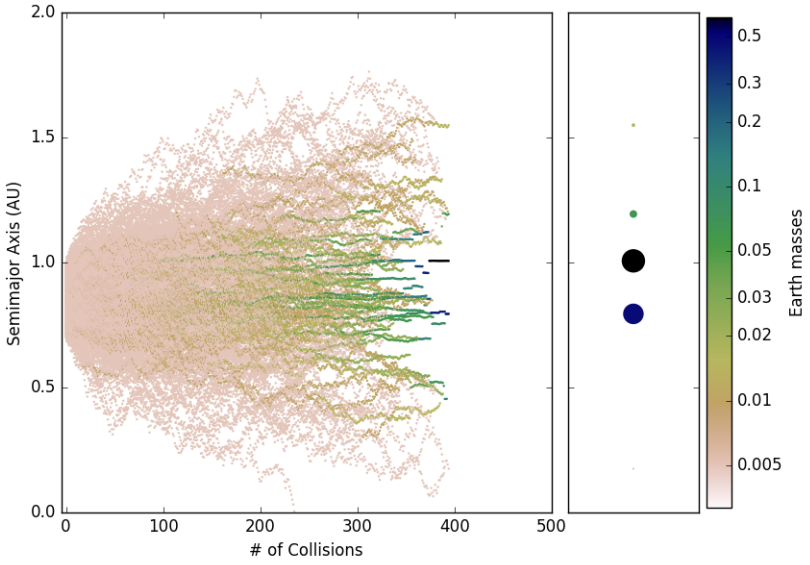

(b)

Figure 4.3: Two examples of systems formed by integrating an annulus of planetesimals: (top) one with a single large central planet and several smaller ones to either side, and (bottom) one with two larger planets and fewer small ones.

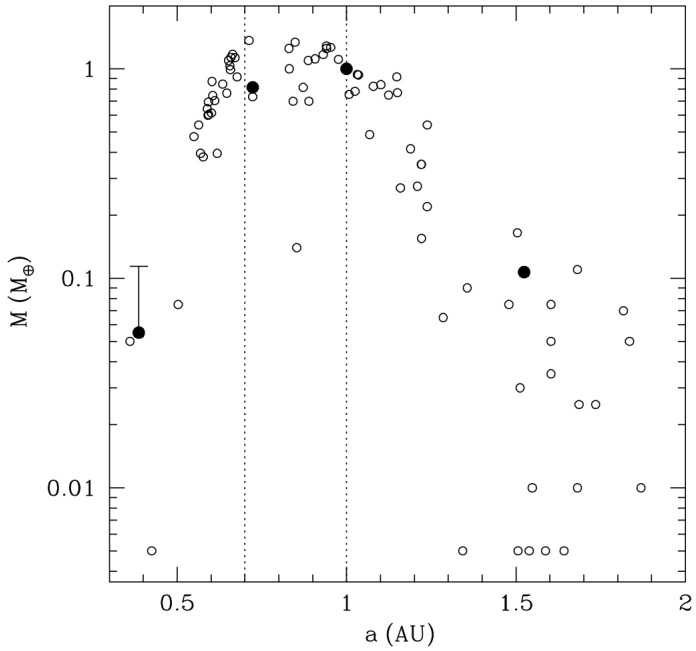

(a) Fig 1 from Hansen (2009). All planets formed from 23 simulations. Solid circles are Solar System planets, open circles are from their simulations.

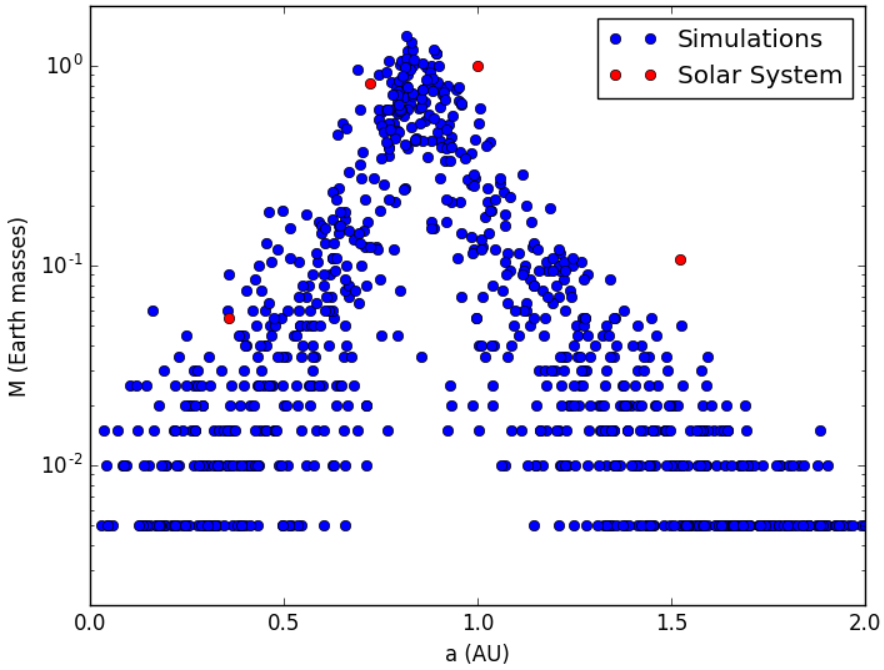

(b) Planets formed in 100 *Audumbla* simulations of a similar annulus.

Figure 4.4: The distributions of mass and semimajor axis of planets produced from an annulus of planetesimals in MERCURY and *Audumbla*, as described in Sect. 4.3.2.

orbits are actually crossing.

Currently in *Audumbla*, the radial movements of objects within a disk are simply random, but in reality they are determined by complex gravitational interactions with nearby objects. The current random motion serves as a first-order approximation in the aggregate, but there are several ways in which it should be improved. Limiting the magnitude of the drift by making it inversely proportional to the object's mass was the first refinement. The next steps will be to include dependencies on the object's surroundings. As a portion of the disk clears out, leaving a few large, stable bodies with sufficient space between them to prevent interactions, the drift should be reduced accordingly. In N-body simulations, this occurs sooner in the inner portion of the disk than beyond the ice line. The magnitude of drift per interaction should also change over the course of the simulation. As the disk clears, interactions become less frequent, so each interaction step represents a larger passage of time, allowing for more drift between interactions. An accurate representation of particle drift should reproduce larger drifts between interactions at later stages in a simulation, while simultaneously showing less drift in particles which are well-separated from their neighbors, as shown in the MERCURY simulation in Fig. 4.2b.

One of the major discrepancies in the final planetary systems produced is that *Audumbla* tends to group the mass together into a few large bodies and several tiny ones, compared to MERCURY simulations in which the mass is distributed more equitably. The above changes to how mass is moved throughout the simulation will alter this tendency, but if the trend continues after these adaptations, the calculation for probability of interaction should be adjusted to increase more slowly with object mass.

4.4 Conclusions

We believe a semi-analytic approach to planet formation, while currently in an early form and of limited practical applications, presents a new way to conceptualize the formation of planetary systems, and thus holds great potential. With the right choice of inputs, this algorithm allows for the generation of a system of planets from a debris disk in a few minutes – two orders of magnitude less time than that required by a fully numeric simulation. With further refinement to the way the

algorithm makes decisions, it should be possible to generate planetary systems from disks with a useful level of accuracy, in a fraction of the computaitonal time of current methods, hopefully allowing for future advances in scientific progress.

Chapter 5
Conclusion

This dissertation has addressed the intersection between dynamics and astrobiology, specifically examining it in two areas: planet formation and lithopanspermia. Both are important in understanding the likelihood or prevalence of life in the Universe. Through dynamic simulations of planet formation we can establish how habitable planets come into being, establishing how common worlds capable of supporting life are. Through studies of lithopanspermia, we learn how life can spread and be dispersed between habitable worlds, influencing the likelihood that a given habitable world will actually have life.

5.1 Lithopanspermia

In Chapter 2, I discuss the evidence that material is exchanged between planets in the Solar System. We know with certainty that material from Mars has been transferred to Earth with relative frequency, and that the conditions the rock fragments were subjected to might be survivable by some of the hardier known microorganisms. Models indicate that material from Mars should also have reached the other terrestrial planets, as well as Jupiter and its moons. We also expect such transfer has happened from Earth to all those locations as well as Saturn and Titan.

This transfer means that it is possible life from Earth has made it to other habitable environments, and may have taken root there. It also raises the question of whether Earth's life originated here, or was transferred from elsewhere. Mars, in particular, was habitable early in its history, and likely became habitable earlier than Earth did, thanks to its smaller size and faster cooling. Given how quickly

life arose on Earth, and the higher rates of impacts in the young Solar System, it is plausible that life first arose on Mars and was transferred here, then died out on its origin planet as the atmosphere evaporated.

Europa, with its subsurface oceans of liquid water and active interior due to tidal friction, is one of the strongest Solar System candidates for a habitable environment beyond Earth. We found it very likely that material from Earth has reached Europa, with a probability of 0.996. Whether that material contained viable life, whether that life survived the impact with Europa, and whether it would then be able to get through the ice shell on the surface, remain uncertain. However, the surface does not appear to be completely static. It features chaos regions where the ice appears to have broken up somewhat and then refrozen, which could have allowed surface material through to the open water in the process. There have also been recent detections of water erupting into space (Roth et al., 2014), which may allow us to directly examine the water of Europa's interior in the near future, without needing a mission capable of drilling through the ice. This will likely accelerate the search for life in Europa, making it all the more important for us to know whether any life found is "native" to Europa or may have been transferred there from elsewhere.

An area of interest to future lithopanspermia studies is that of transfer to dwarf planets such as Ceres. The recent Dawn mission, currently in orbit around Ceres, is conveying a large wealth of information about conditions on this class of objects. Earlier in its history, Ceres was likely warmer and may have contained a liquid water ocean similar to Europa's, which could have hosted life, though without a continuing heat source it has become considerably colder in more recent times.

A side-effect of studying transfer within the Solar System is the simulation of a large number of fragments being ejected from the system entirely. Whether such fragments could carry life between separate planetary systems is a question of special interest with the recent discovery of Proxima Centauri b (Anglada-Escudé et al., 2016). As a habitable-zone planet orbiting the closest star to our own, this represents the most likely known case for interstellar transfer.

5.2 Planet Formation

5.2.1 Planets in Alpha Centauri

The Alpha Centauri binary lies near the boundary for stars which are too close to form circumstellar planets. In its current orbit, the final stages of planet formation can proceed for the closest few AU to the star, allowing for terrestrial planets in the habitable zone; but the earlier stage in which planetesimals accrete to form planetary embryos may be impeded significantly by the companion star's influence (Thébault et al., 2009). However, the extremely distant orbit of Proxima Centauri suggests the system may not always have had this spacing. If the outer star initially formed in a close orbit and was thrown out to its current one via interactions with the inner two stars, the binary's orbit would likely have been shrunk in the process (Reipurth & Mikkola, 2012). By simulating hundreds of interactions of this type, we quantify the typical change in parameters that could be expected – most simulations show a small decrease in semimajor axis and a significant increase in eccentricity, resulting in a much smaller pericenter after the interaction. In addition, we study the effects on the disk during these interactions, and find that material near the star remains most undisturbed as long as it lies inward of the truncation radius, which is a slightly-nonlinear function of the binary's pericenter.

As most stars are members of multistellar systems, understanding the relationship between stellar companions and circumstellar disk stability across all parameters will be important in understanding the planetary population. I studied binaries with equal or nearly-equal mass ratios, and with pericenters of no more than a few tens of AU. In this range, the truncation radius r_{tr} followed the minimum pericenter to the power of ~ 1.2, rather than as a simple linear relationship, meaning the fraction of the orbit that allows stable disk material grows as the orbit widens. However, whether this continues for even larger orbits should be studied in depth as well. It seems unlikely that this relationship could continue indefinitely, as eventually the truncation radius would overtake the pericenter and predict disks in regions the stars actually pass through, which is physically implausible.

The Alpha Centauri star system is an interesting case, both because it is our nearest neighbor and thus of special interest for observations and far-future space missions, and because its unusually wide hierarchical structure may give us insight

into stellar formation more generally. Reipurth & Mikkola (2012) propose that many, possibly most, stars form in groups which are dynamically disbanded as the nascent gas cloud core dissipates. In the majority of both their simulations and ours, the three-body systems broke apart into a binary and a single star. If this type of turbulent history is the norm, it may imply that most stars we look at have gone through interactions which have a chance at altering their protoplanetary disks. With our growing body of information on planetary systems around stars of all types, there may be signatures of such interactions left in seemingly-quiet systems.

5.2.2 Proxima Centauri b

The recent detection of a planet in orbit around Proxima Centauri (Anglada-Escudé et al., 2016) brings the question of Proxima's planetary formation environment into the spotlight. Although it was not the focus of my work, I can extrapolate from what I do know.

Because of M stars' very low luminosity, their habitable zones are extremely close to the star. The conservative Habitable Zone (Kopparapu et al., 2014, 2013) for Proxima lies between 0.043 to 0.085 AU. Proxima Centauri b lies in this range currently, but because the protoplanetary disk mass is expected to scale down with the stellar mass, there is probably not enough mass in the inner part of the disk to form an Earth-mass planet. The planet likely formed further out and migrated in to its current position. Let us assume the disk must remain untruncated to at least 10 AU (a somewhat arbitrary benchmark). At the upper end of the range I explored in Chapter 3, I found that $r_{tr} \approx 0.3 p_{min}$. If we apply this rule to Proxima, then it must never have had a pericenter below 33.3 AU.

In my simulations, I explored pericenter values up to ~ 27 AU, not far below this value. However, given Proxima's current distance of $\sim 15,000$ AU, its semimajor axis and eccentricity must lie well outside the range I examined. If we assume it is currently at apocenter with a very high eccentricity, then the semimajor axis $a = 15,000/(1+e) \approx 15,000/2$, for a minimum a of about $7,500$ AU. A pericenter of 33 AU would imply an eccentricity of about $1 - 33/7,500 = 0.996$, which is extremely high. However, due to the nature of the interactions, this is not as uncommon as might be expected. In fact, Proxima's pericenter dips below 33 AU

in about 30% of my simulations of the three stars' interactions.

5.2.3 *Audumbla*

The new *Audumbla* planetary formation algorithm presented here represents a new way of looking at simulating the creation of planetary systems. It can create a system of planets from a debris disk in a tiny fraction of the time required by traditional simulations. The algorithm is still very much in development to improve the accuracy of results, but with further refinement it could become a useful tool for the future of exoplanet research.

5.3 Final Thoughts

Through these various projects, I have explored the intersection of dynamics and astrobiology. I believe astrobiology is of fundamental interest to our species in the long run, and though the immediate, practical benefits may be minimal, it is critical to our understanding of the Universe and our place in it. In addition, such understanding should be grounded in the interactions of gravity and other fundamental laws of physics which shape our cosmos, making dynamics a crucial underpinning to human advancement.

Bibliography

Anglada-Escudé, G., Amado, P. J., Barnes, J., et al. 2016, Nature, 536, 437

Anosova, J., Orlov, V. V., & Pavlova, N. A. 1994, A&A, 292, 115

Anosova, J. P. 1986, Ap&SS, 124, 217

Artymowicz, P., & Lubow, S. H. 1994, ApJ, 421, 651

Barbieri, M., Marzari, F., & Scholl, H. 2002, A&A, 396, 219

Barnes, R., Deitrick, R., Luger, R., et al. 2016, ArXiv e-prints, arXiv:1608.06919

Beech, M. 2012, Astronomy and Geophysics, 53, 6.10

Bekker, A., Holland, H. D., Wang, P.-L., et al. 2004, Nature, 427, 117

Benedict, G. F., McArthur, B., Chappell, D. W., et al. 1999, AJ, 118, 1086

Benest, D. 1988, A&A, 206, 143

Benzerara, K., Menguy, N., Guyot, F., Dominici, C., & Gillet, P. 2003, Proceedings of the National Academy of Science, 100, 7438

Bogard, D. D., & Johnson, P. 1983, Science, 221, 651

Boss, A. P. 1997, Science, 276, 1836

Bottke, Jr., W. F., Vokrouhlický, D., Rubincam, D. P., & Nesvorný, D. 2006, Annual Review of Earth and Planetary Sciences, 34, 157

Brown, M. E., & Hand, K. P. 2013, AJ, 145, 110

Brugger, B., Mousis, O., Deleuil, M., & Lunine, J. I. 2016, ApJL, 831, L16

Butler, R. P., Marcy, G. W., Williams, E., Hauser, H., & Shirts, P. 1997, ApJL, 474, L115

Carr, R. H., Grady, M. M., Wright, I. P., & Pillinger, C. T. 1985, Nature, 314, 248

Chambers, J. E. 1999, MNRAS, 304, 793

—. 2012, Mercury: A software package for orbital dynamics, Astrophysics Source Code Library, ascl:1201.008

Chambers, J. E., & Murison, M. A. 2000, AJ, 119, 425

Chambers, J. E., Quintana, E. V., Duncan, M. J., & Lissauer, J. J. 2002, AJ, 123, 2884

Chapman, C. R., Cohen, B. A., & Grinspoon, D. H. 2007, *Icarus*, 189, 233

Chatterjee, S., & Tan, J. C. 2014, ApJ, 780, 53

Chiang, E., & Laughlin, G. 2013, MNRAS, 431, 3444

Cisar, J. O., Xu, D.-Q., Thompson, J., et al. 2000, Proceedings of the National Academy of Science, 97, 11511

Clark, B. C. 2001, Origins of Life and Evolution of the Biosphere, 31, 185

Cochran, W. D., Hatzes, A. P., Butler, R. P., & Marcy, G. W. 1997, ApJ, 483, 457

Cole, S., Aragon-Salamanca, A., Frenk, C. S., Navarro, J. F., & Zepf, S. E. 1994, MNRAS, 271, 781

Coleman, G. A. L., Nelson, R. P., Paardekooper, S.-J., et al. 2016, ArXiv e-prints, arXiv:1608.06908

Demory, B.-O., Ehrenreich, D., Queloz, D., et al. 2015, MNRAS, 450, 2043

Desidera, S., & Barbieri, M. 2007, A&A, 462, 345

DeWarf, L. E., Datin, K. M., & Guinan, E. F. 2010, ApJ, 722, 343

Dones, L., Gladman, B., Melosh, H. J., et al. 1999, *Icarus*, 142, 509

Dumusque, X., Pepe, F., Lovis, C., et al. 2012, Nature, 491, 207

Duncan, M. J., Levison, H. F., & Lee, M. H. 1998, AJ, 116, 2067

Eggenberger, A., & Udry, S. 2010, in Astrophysics and Space Science Library, Vol. 366, Planets in Binary Star Systems, ed. N. Haghighipour, 19

Eggl, S., Haghighipour, N., & Pilat-Lohinger, E. 2013, ApJ, 764, 130

Endl, M., Kürster, M., Els, S., Hatzes, A. P., & Cochran, W. D. 2001, A&A, 374, 675

Endl, M., Bergmann, C., Hearnshaw, J., et al. 2015, International Journal of Astrobiology, 14, 305

Fabrycky, D. C., Lissauer, J. J., Ragozzine, D., et al. 2014, ApJ, 790, 146

Faivre, D., & Zuddas, P. 2006, Earth and Planetary Science Letters, 243, 53

Fischer, D. A., Marcy, G. W., Butler, R. P., et al. 2008, ApJ, 675, 790

Forgan, D. 2012, MNRAS, 422, 1241

Gladman, B. 1997, *Icarus*, 130, 228

Gladman, B., Dones, L., Levison, H., Burns, J., & Gallant, J. 2006, in Lunar and Planetary Science Conference, Vol. 37, 37th Annual Lunar and Planetary Science Conference, ed. S. Mackwell & E. Stansbery

Gladman, B., Dones, L., Levison, H. F., & Burns, J. A. 2005, Astrobiology, 5, 483

Gladman, B. J., & Burns, J. A. 1996, Science, 274, 161

Gladman, B. J., Burns, J. A., Duncan, M., Lee, P., & Levison, H. F. 1996, Science, 271, 1387

Golden, D., Ming, D., Morris, R., et al. 2004, American Mineralogist, 89, 681

Goodwin, S. P., Kroupa, P., Goodman, A., & Burkert, A. 2007, Protostars and Planets V, 133

Guedes, J. M., Rivera, E. J., Davis, E., et al. 2008, ApJ, 679, 1582

Haghighipour, N., & Raymond, S. N. 2007, ApJ, 666, 436

Hale, A. 1994, AJ, 107, 306

Halevy, I., Fischer, W. W., & Eiler, J. M. 2011, Proceedings of the National Academy of Science, 108, 16895

Hansen, B. M. S. 2009, ApJ, 703, 1131

Hatzes, A. P. 2013, ApJ, 770, 133

Hayashi, C. 1981, Progress of Theoretical Physics Supplement, 70, 35

Hoffman, P. F., Kaufman, A. J., Halverson, G. P., & Schrag, D. P. 1998, Science, 281, 1342

Holman, M. J., & Wiegert, P. A. 1999, AJ, 117, 621

Hut, P., & Bahcall, J. N. 1983, ApJ, 268, 319

Ivanov, B., & Hartmann, W. 2007, Treatise on Geophysics, 10, 207

Jang-Condell, H. 2007, ApJ, 654, 641

—. 2015, ApJ, 799, 147

Jang-Condell, H., Mugrauer, M., & Schmidt, T. 2008, ApJL, 683, L191

Jiang, Y.-F., & Tremaine, S. 2010, MNRAS, 401, 977

Kasting, J. F., Whitmire, D. P., & Reynolds, R. T. 1993, *Icarus*, 101, 108

Kauffmann, G., White, S. D. M., & Guiderdoni, B. 1993, MNRAS, 264, 201

Kepler, J. 1619, Harmonices Mundi

Khurana, K. K., Kivelson, M. G., Stevenson, D. J., et al. 1998, Nature, 395, 777

Kokubo, E., & Ida, S. 1998, *Icarus*, 131, 171

Kopparapu, R. K., Ramirez, R. M., SchottelKotte, J., et al. 2014, ApJL, 787, L29

Kopparapu, R. K., Ramirez, R., Kasting, J. F., et al. 2013, ApJ, 765, 131

Kraus, A. L., Ireland, M. J., Huber, D., Mann, A. W., & Dupuy, T. J. 2016, AJ, 152, 8

Lacey, C., & Silk, J. 1991, ApJ, 381, 14

Lada, C. J., & Lada, E. A. 2003, Annual Review of Astronomy and Astrophysics, 41, 57

Leinhardt, Z. M., & Stewart, S. T. 2012, ApJ, 745, 79

Levison, H. F., & Duncan, M. J. 1994, *Icarus*, 108, 18

—. 2013, SWIFT: A solar system integration software package, Astrophysics Source Code Library, ascl:1303.001

Li, G., & Adams, F. C. 2015, MNRAS, 448, 344

Lissauer, J. J. 1987, *Icarus*, 69, 249

—. 1993, Annual Review of Astronomy and Astrophysics, 31, 129

Loeb, A., Batista, R. A., & Sloan, D. 2016, *Journal of Cosmology and Astroparticle Physics*, 8, 040

Lorenz, R. D., Stiles, B. W., Kirk, R. L., et al. 2008, Science, 319, 1649

Lovis, C., Snellen, I., Mouillet, D., et al. 2016, ArXiv e-prints, arXiv:1609.03082

Maher, K. A., & Stevenson, D. J. 1988, Nature, 331, 612

Marcy, G., Butler, R. P., Fischer, D., et al. 2005, Progress of Theoretical Physics Supplement, 158, 24

Martel, J., Young, D., Peng, H.-H., Wu, C.-Y., & Young, J. D. 2012, Annual Review of Earth and Planetary Sciences, 40, 167

Marzari, F., & Scholl, H. 2000, ApJ, 543, 328

Matthews, R., & Gilmore, G. 1993, MNRAS, 261, L5

Mayor, M., & Queloz, D. 1995, Nature, 378, 355

McKay, C. P., Mancinelli, R. L., Stoker, C. R., & Wharton, Jr., R. A. 1992, The possibility of life on Mars during a water-rich past., ed. H. H. Kieffer, B. M. Jakosky, C. W. Snyder, & M. S. Matthews, 1234–1245

McKay, D. S., Gibson, Jr., E. K., Thomas-Keprta, K. L., et al. 1996, Science, 273, 924

Meadows, V. S., Arney, G. N., Schwieterman, E. W., et al. 2016, ArXiv e-prints, arXiv:1608.08620

Melosh, H. J. 1988, Nature, 332, 687

—. 2003, Astrobiology, 3, 207

Melosh, H. J., & Tonks, W. B. 1993, Meteoritics, 28

Mileikowsky, C., Cucinotta, F. A., Wilson, J. W., et al. 2000, *Icarus*, 145, 391

Mugrauer, M., & Neuhäuser, R. 2009, A&A, 494, 373

Müller, T. W. A., & Kley, W. 2012, A&A, 539, A18

Newton, I. 1687, Philosophiae Naturalis Principia Mathematica

Nyquist, L. E., Bogard, D. D., Shih, C.-Y., et al. 2001, *Space Sci Rev*, 96, 105

Payne, M. J., Wyatt, M. C., & Thébault, P. 2009, MNRAS, 400, 1936

Perryman, M. A. C., Lindegren, L., Kovalevsky, J., et al. 1997, A&A, 323, L49

Popova, E. A., & Shevchenko, I. I. 2012a, in IAU Symposium, Vol. 282, From Interacting Binaries to Exoplanets: Essential Modeling Tools, ed. M. T. Richards & I. Hubeny, 450–451

Popova, E. A., & Shevchenko, I. I. 2012b, Astronomy Letters, 38, 581

Porras, A., Christopher, M., Allen, L., et al. 2003, AJ, 126, 1916

Pourbaix, D., Neuforge-Verheecke, C., & Noels, A. 1999, A&A, 344, 172

Pourbaix, D., Nidever, D., McCarthy, C., et al. 2002, A&A, 386, 280

Quintana, E. V., Adams, F. C., Lissauer, J. J., & Chambers, J. E. 2007, ApJ, 660, 807

Quintana, E. V., Lissauer, J. J., Chambers, J. E., & Duncan, M. J. 2002, ApJ, 576, 982

Rabl, G., & Dvorak, R. 1988, A&A, 191, 385

Rafikov, R. R., & Silsbee, K. 2015a, ApJ, 798, 69

—. 2015b, ApJ, 798, 70

Rajpaul, V., Aigrain, S., & Roberts, S. 2016, MNRAS, 456, L6

Raymond, S. N., & Cossou, C. 2014, MNRAS, 440, L11

Reipurth, B., Clarke, C. J., Boss, A. P., et al. 2014, Protostars and Planets VI, 267

Reipurth, B., & Mikkola, S. 2012, Nature, 492, 221

Reipurth, B., Mikkola, S., Connelley, M., & Valtonen, M. 2010, ApJL, 725, L56

Reyes-Ruiz, M., Chavez, C. E., Aceves, H., et al. 2012, *Icarus*, 220, 777

Ribas, I., Bolmont, E., Selsis, F., et al. 2016, ArXiv e-prints, arXiv:1608.06813

Roth, L., Saur, J., Retherford, K. D., et al. 2014, Science, 343, 171

Sanz-Serna, J. M. 1992, Acta Numerica, 1, 243

Schulte, P., Alegret, L., Arenillas, I., et al. 2010, Science, 327, 1214

Sleep, N. H., & Zahnle, K. 1998, *J Geophys Res Planets*, 103, 28529

Somerville, R. S., Primack, J., & Nolthenius, R. 1997, ApJ, 479, 606

Stassun, K. G. 2012, Nature, 492, 191

Steffen, J. H., & Li, G. 2016, ApJ, 816, 97

Stoer, J., & Bulirsch, R. 1980, Numerical analysis

Team, R. C., et al. 2013

Thebault, P., & Haghighipour, N. 2014, ArXiv e-prints, arXiv:1406.1357

Thébault, P., Marzari, F., & Scholl, H. 2006, *Icarus*, 183, 193

—. 2008, MNRAS, 388, 1528

—. 2009, MNRAS, 393, L21

Thomas-Keprta, K. L., Bazylinski, D. A., Kirschvink, J. L., et al. 2000, *Geochimica et Cosmochimia Acta*, 64, 4049

Tobias, C., & Todd, P. 1974, Space radiation biology and related topics.(A 74-42829 22-04) New York, Academic Press, Inc., 1974„ 197

Tobie, G., Lunine, J. I., & Sotin, C. 2006, Nature, 440, 61

Treiman, A. 2000, in Astronomical Society of the Pacific Conference Series, Vol. 213, Bioastronomy 99, ed. G. Lemarchand & K. Meech

Turbet, M., Leconte, J., Selsis, F., et al. 2016, ArXiv e-prints, arXiv:1608.06827

Veras, D., Crepp, J. R., & Ford, E. B. 2009, ApJ, 696, 1600

Veras, D., & Evans, N. W. 2013, MNRAS, 430, 403

Way, M. J., Del Genio, A. D., Kiang, N. Y., et al. 2016, *Geophysical Research Letters*, 43, 8376

Wells, L. E., Armstrong, J. C., & Gonzalez, G. 2003, *Icarus*, 162, 38

Wertheimer, J. G., & Laughlin, G. 2006, AJ, 132, 1995

White, S. D. M., & Frenk, C. S. 1991, ApJ, 379, 52

Wiegert, J., Liseau, R., Thébault, P., et al. 2014, A&A, 563, A102

Wiegert, P. A., & Holman, M. J. 1997, AJ, 113, 1445

Wisdom, J., & Holman, M. 1991, AJ, 102, 1528

Worth, R., & Sigurdsson, S. 2016, arXiv preprint arXiv:1607.03090

Worth, R. J., Sigurdsson, S., & House, C. H. 2013, Astrobiology, 13, 1155

Xie, J.-W., Zhou, J.-L., & Ge, J. 2010, ApJ, 708, 1566

Zuluaga, J. I., & Bustamante, S. 2016, ArXiv e-prints, arXiv:1609.00707

Vita

Rachel J. Worth

Education

Ph.D.	Pennsylvania State University	December 2016
M.S.	Pennsylvania State University	December 2014
B.S.	University of Wisconsin–Madison	August 2009

Experience

2016	Data Science Fellow, Insight Data Science
2010–2016	Research Assistant, Pennsylvania State University
2009–2010	Teaching Assistant, Pennsylvania State University

Fellowships and Awards

2014–2016	Academic Computing Fellow
2012–2014	Pennsylvania Space Grant Consortium Fellowship
2015	CEHW Travel Grant
2010–2016	Zaccheus Daniel Awards
2009	Braddock Fellowship
2009	Fay Ajzenberg-Selove Award
2008	Hilldale Undergraduate Fellowship Award
2008	Wisconsin Space Grant Consortium Research Award